UNIVERSITÀ DEGLI STUDI DI PADOVA

DIPARTIMENTO DI INGEGNERIA INDUSTRIALE

CORSO DI LAUREA MAGISTRALE IN INGEGNERIA CHIMICA E DEI PROCESSI INDUSTRIALI

**Tesi di Laurea Magistrale in
Ingegneria Chimica e dei Processi Industriali**

FLASH PROCESSING OF COPPER ELECTRODES PRINTED FROM COPPER OXIDE NANOPARTICLE INK

Relatore: Prof. Alessandro Martucci
Correlatori: Dr. Jacek Jasieniak
Ing. Enrico Della Gaspera

Laureando: FRANCESCO PAGLIA

ANNO ACCADEMICO 2014 – 2015

Abstract

The Integrated Systems and Devices Group of the Manufacturing Flagship at the Commonwealth Scientific and Industrial Research Organization (CSIRO) among other achievements pioneered the use of nanomaterials for solution-processed optoelectronic devices, such as printed organic solar cells and OLEDs. However, in such applications the metal electrodes were still deposited through thermal evaporation, a vacuum-based expensive technique.

This thesis tries to fill the gap investigating the possibility to fabricate flexible and printed copper electrodes based on the deposition of copper oxide nanoparticles. For this reason, two different techniques, slot-die and inkjet printing, are used in order to compare their different benefits and disadvantages in the deposition process, as well as to understand the influence on the electrode's properties. However, due to their non-conducting nature, the copper oxide nanoparticles must be processed: because of the plastic substrates relative low processing conditions, an innovative technology is applied to convert the CuO to Cu: the intense pulsed light sintering.

In addition to a fine control of the copper nanoparticles transformation, high-performance electrodes are fabricated, achieving a great conductivity, as well as an optimal mechanical stability. A good stability against oxidation has been achieved also without encapsulation. However, the best results are obtained with slot-die coating, which is a quick and fast technique, but does not achieve the resolution of inkjet.

In this work, ~27% of the conductivity of the bulk copper was achieved processing the electrodes at room temperature, in addition to optimal resistance to oxidation without encapsulation, as well as to mechanical stress, reaching a resistance variation of only 18% when bent.

Riassunto

Questa Tesi é stata svolta nell'ambito di ricerca dell'*Integrated Systems and Devices Group*. Questo team, facente parte della divisione *Manufacturing* del *Commnwealth Scientific and Industrail Research Organization* (CSIRO), é specializzato nello sviluppo di applicazioni optoelettroniche flessibili ed é sempre stato all'avanguardia nell'utilizzo delle piú recenti tecniche di deposizione di materiali nanocompositi.

D'altra parte, negli ultimi anni gli sforzi maggiori sono stati concentrati nella fabbricazione dei *devices* prinipicali, quali *organic light-emitting diodes* (OLEDs) o celle solari flessibili, tralasciando lo sviluppo concernente la deposizione di elettrodi metallici. Infatti, per la loro creazione si fa tutt'ora uso di tecniche che operano al di sopra delle condizioni ambientali: un processo termico sotto vuoto permette la deposizione della maggior parte dei materiali utilizzati, ma operando in condizioni "spinte", esso risulta essere alquanto dispendioso e poco adatto ad un approccio su larga scala.

Questo lavoro cerca di colmare la lacuna che si é venuta a creare, focalizzandosi sulla creazione di elettrodi di rame flessibili e quindi la possibilitá di fabbricare un'unica applicazione che racchiuda in sé alcuni dei device principali e che ne rispecchi le loro peculiaritá. Inoltre, tale fabbricazione coinvolge un processo che opera a temperatura ambiente, riducendo cosi le condizioni operative tipiche dei processi convenzionali.

Piú in dettaglio, due differenti tecniche sono state utilizzate per la deposizione di una soluzione di nanoparticelle di ossido di rame (II) (CuO) su substrato plastico caratterizzato da PET, ed uno strato poroso per aumentare l'adesione dell'elettrodo finale: slot-die e inkjet printing. La prima é una tecnologia molto semplice, facilmente applicabile ad una vasta gamma di soluzioni: non a caso in questa Tesi viene sperimentata per la prima volta la deposizione di un inchiostro di nanoparticelle tramite slot-die, in precedenza prerogativa di altre metodologie. Il concetto basilare é la formazione di una struttura stabile, il menisco, che possa dare continuitá materiale tra la testina della slot-die e il substrato dove la soluzione viene depositata. D'altra parte, essa é caratterizzata anche da importanti limitazioni, riguardanti soprattutto la complessitá del design che si puó ottenere. Ció é dovuto proprio alla semplicitá del meccanismo sul quale si basa.

La seconda é la tecnica per *printed electronics* per antonomasia: svariati studi sono stati condotti sulla deposizione di nanoparticelle metalliche e non, con tale tecnologia sviluppandola ad un livello mai visto prima. Molti sono i vantaggi che derivano dal suo utilizzo: primo fra tutti la possibilitá di digitalizzare il design e modificarlo a piacimento senza dover sostituire alcuna parte meccanica. La qualitá e l'uniformitá del risultato sono

molto al di sopra di quelle che si possono ottenere con altre tecniche, cosí come la complessitá del disegno: motivi articolati e deposizioni multistrato sono facilmente realizzabili tramite la tecnologia *drop-on-demand*, capace di dispensare un numero predefinito di gocce per unitá di area. Anche in questo caso peró ci sono alcuni limiti d'applicazione. La soluzione deve rispettare severi requisiti circa le proprietá chimico-fisiche, in modo da facilitare la deposizione del materiale. Inoltre, problemi di intasamento degli orifizi sono molto frequenti, dovuti soprattutto alla loro grandezza, normalmente dell'ordine di alcuni micron. Una parte consistente del lavoro é stata dunque dedicata all'ottimizzazione di queste due tecniche di deposizione.

Al fine di conseguire elettrodi conduttivi, si é reso necessario processare i film depositati, in modo da ottenere la transizione dallo stato ossido a quello metallico: la reazione si basa su un meccanismo termico che prevede la riduzione del rame da parte di agenti riducenti presenti in soluzione. D'altra parte, la temperatura necessaria per tale riduzione risulta essere molto maggiore se paragonata alla temperatura di transizione vetrosa del substrato plastico. Per tale motivo é stato utilizzata una tecnologia innovativa: processando i campioni con luce pulsata ad alta intensitá, si é in grado di raggiungere le condizioni necessarie per la reazione, solo nei film depositati ma non interessando il substrato. Questo é dovuto al fatto che la maggior parte dei materiali plastici sono trasparenti nel visibile e quindi non vengono coinvolti nel processo di assorbimento della luce, a differenza, in questo caso, delle nanoparticelle di ossido di rame. Tale processo comporta quindi l'assorbimento di luce localmente, l'innalzamento della temperatura e quindi la transizione allo stato metallico finale.

Investigando le condizioni ottimali di "flash" e, quindi, variando la quantitá di energia erogata al sistema, si é scoperto che la reazione di riduzione é caratterizzata da un processo multi-step che coinvolge uno stadio intermedio definito dal rame ossido (I) (Cu_2O). Diverse analisi sono state effettuate in modo da comprendere in maniera approfondita di che tipo di transizione si tratti e in che modo essa avvenga, raggiungendo un controllo eccellente del processo di trasformazione a rame metallico. In questo modo, ulteriori considerazioni potranno essere effettuate, soprattutto circa processi di ottimizzazione, quali ad esempio evaporazione, totale o parziale, del contenuto di solvente in soluzione per migliorare le proprietá fisico-elettriche del film.

Con l'obiettivo di migliorare le perfomance degli elettrodi di rame, é stato investigato anche un approccio multistrato. I risultati ottenuti sono stati eccellenti, con un miglioramento sostanziale delle proprieta meccanico-elettriche dei film metallici. D'altra parte, é stato possibile ottenere questo risultato solo per una particolare formulazione, la sola che é risultata stabile durante il trattamento a luce pulsata ad alta intensitá.

Gli elettrodi cosí ottenuti sono stati ulteriormente analizzati: un costante confronto tra singolo e doppio strato é stato affrontato in modo da determinare il reale incremento delle

performance. Inizialmente si é testata la stabilitá in presenza di ossigeno e non: il rame, infatti, tende ad ossidare facilmente, compromettendo specialmente le proprietá elettriche e comportando una riduzione complessiva dell'efficienza. Ottima stabilitá é stata riscontrata non solo in ambiente condizionato con azoto, ma anche in presenza di ossigeno, rilevando dopo 20 giorni un incremento di solo il 20% per ogni tipo di elettrodo.

Una delle caratteristiche principali di un device flessibile é la capacitá di curvare senza veder diminuire la propria efficienza. Per questo motivo gli elettrodi sono stati sottoposti anche a dei test di curvatura: la superiore stabilitá meccanica del doppio strato rispetto al singolo ha influenzato notevolmente la risposta ad uno stress meccanico, comportando una minima variazione della resistenza elettrica. Il test effettuato in assenza di ossigeno, riproducendo le condizioni ottenibili con un incapsulamento dell'elettrodo, hanno dato il miglior risultato, con una variazione della resistenza del 18% rispetto a quella iniziale. É stata dunque dimostrata la necessitá di una barriera per prevenire l'attacco dell'ossigeno e la conseguente diminuzione dell'efficienza.

In questa Tesi sono stati raggiunti eccellenti risultati: operando in condizioni ambientali, si é ottenuto un ottimo controllo della reazione di riduzione; inoltre, le proprietá meccanico-elettriche degli elettrodi di rame cosí ottenuti si sono rivelate sopra ogni aspettativa. É stata infatti raggiunta una conducibilitá pari al ~27% della conducibilitá del rame bulk, con un'ottima stabilitá, non solo alle reazioni di ossidazione, ma anche in situazioni di stress meccanico.

Index

Table of Figures

Introduction

Flexible and Printed Electronics (FPEs) are transforming the way people consider electronic device. The introduction of the microchip into daily life decades ago has enabled countless portable applications to emerge (e.g. mobile phone, television, etc...), this innovative technology is having a massive impact in the way we live and interact with the surrounding world. Moreover, integrated electronics are not conceived anymore to be only smaller and faster than the predecessors, but other important properties have become essential in order to enhance the user experience: large area, improved lifetime, low-weight, high-power, low-cost and green/clean manufacturing are new aspects that are now related with the current electronic devices design. This revolutionary approach is sustained by several projects that are trying to develop and consolidate flexible and printed devices in many areas as possible, offering know-how and support where necessary. For example, *FlexTech Alliance* gathers everyone who believes that advancements in flexible electronics can make the difference for a healthier, safer and simpler world, managing technical programs for advanced flexible electronics from the R&D stage through to commercialization ([1]).

The fact that FPEs are quickly expanding is also proven by several market statistics: if today the world FPEs market is estimated in \$1.2B ([2]), in the next future it will grow so fast to reach \$73B in 2025 ([3]), led by flexible organic light-emitting diodes (OLEDs).

Part of Flexible and Printed Electronics is represented by Flexible Printed Circuits (FPCs), known as well as flexible printed circuit boards (Flexible PCBs). As a matter of fact, FPCs replace what the rigid boards were for the traditional electronics: they support the main devices, for example flexible displays or flexible transistors, by providing the necessary interconnections between them and allowing the exchange of electrical information. However, they must reflect the overall ideology on which FPEs are based, in terms of design and manufacturing. This would lead not only to smaller applications, but also to an overall device that involves all the characteristics described so far. Thus, many advancements are necessary in order to keep up Flexible Printed Circuits with the innovations reached in the many devices, such as solar cell, OLEDs and thin film transistors (TFTs), where the research is mostly focused. In this view, copper nanoparticles associated with plastic substrates, could be one of the best solutions in order to create efficient FPEs. This stems from their low-cost and high availability, as well as lightweight and non-toxic nature. However, new fabrication ways have to be considered, joining the

reciprocal benefits: the conventional technologies are hard to apply in order to obtain a sustainable manufacturing process. This must involve a roll-to-roll (R2R) system and a large area production, which define nowadays the standards for the fabrication procedure, due to the higher yields and the possibility to produce new types of devices with respect to the stepwise counterparts.

Therefore, starting from copper oxide nanoparticles and Polyethylene Terephthalate (PET) substrates, this thesis tries to investigate the viability to create copper flexible printed circuits for commercial applications: the aim is to fabricate highly performing metal copper electrodes combining innovative and traditional techniques. Thus, conventional methods are adapted to the nanoparticle deposition, while an intense pulsed light processing is applied in order to create conductive patterns. The combination of these two steps makes it possible to achieve an efficient process, easily scalable to manufacturing level. Moreover, attention is paid towards the performance of the copper electrodes, investigating not only the electrical properties, but also the overall stability, to try and determine an optimal solution between the material, power consumption and the principal major characteristics.

In the first chapter, a general overview of FPEs and FPCs is introduced, defining the limits of this work in the wide range of flexible electronics. The main applications, as well as the principal materials and the deposition techniques adopted for FPEs fabrication are briefly described. The second chapter explains the major advantages that derives by the use of nanoparticle inks and PET substrates. Additionally, the techniques involved in this work for the copper oxide nanoparticles deposition, slot-die and inkjet printing, are described in detail, highlighting their peculiar aspects, which might make the difference in the electrodes fabrication. In the third chapter, an optimal deposition with both coating methods is achieved; however, a higher effort is directed towards the investigation of the flash processing. Different conditions are applied in order to examine the behavior of copper oxide nanoparticle films under an intense pulsed light. In these terms, many analysis are performed evaluating chemical composition as well as the nanoparticle structure of the samples investigated.

As previously introduced, the fourth chapter describe the testing of the environmental and structural stability of the copper electrodes. These measurements ascertain the possibility of applying such electrodes to real world application.

Conclusion are introduced in the last fifth chapter, considering the obtained results and the future investigations.

Chapter 1

Flexible and Printed Electronics

This chapter introduces Flexible and Printed Electronics, defining its meaning and explaining the advantages of Flexible Printed Circuits. Printable materials are then discussed, in addition to the substrates that can be used in flexible devices. The chapter finished with a dissemination of the advantages that come with printing approaches.

1.1 Definition of Flexible and Printed Electronics

Flexible and printed electronics describes a broad range of technologies applicable across a multitude of devices, going from the simple circuit to hi-tech devices, such as smartphone, solar cell and or flexible displays. The common theme of FPEs is that they enable the fabrication of electronic products that can be easily integrated into daily life. Moreover, they show countless advantages in the manufacturing process: the most important is the ability to reduce the production costs. This depends on many factors, but it is recognized that roll-to-roll processing has a main role in this competitive manufacturing system.

In order to obtain flexible printed electronics, some requirements have to be met. Firstly, the device must be flexible. Unlikely the silicon-based circuits, FPEs can be bent and shaped without any damage. This can be achieved by the adoption of different materials with respect the conventional Si, which have flexible properties suitable for the fabrication of such devices. Thus, flexibility is one on the main characteristics that affects Flexible and Printed Electronics.

Furthermore, they must be printed. Printing techniques are very competitive with respect to other types of fabrication methods, such as lithography, materials doping or pattern transferring. United with flexibility, printing technologies have revolutionized the way to create a flexible electronics, due to their low-cost, material saving, easy and fast production and the possibility to obtain complex devices without involving really expensive stepwise processes, and are capable of large area manufacturing. The joined benefits deriving from these properties have enabled printing to replace traditional material, such as germanium with inherently green counterparts, plastic and inks. Moreover, the final product results in

lightweight, shock resistance and produced with a lower energy consumption.

All these characteristics are found in many common electronic devices. Flexible solar cells are the most evident outcome of innovation in flexible and printed technology. The ability to shape and conform the device to an uneven surface is a goal that was unthinkable with the silicon-based conventional panel. Moreover, they can be easily integrated into daily life, as shown in **Figure 1.1a**, where a flexible and printed solar cell is shown integrated in a back bag.

(a) (b)
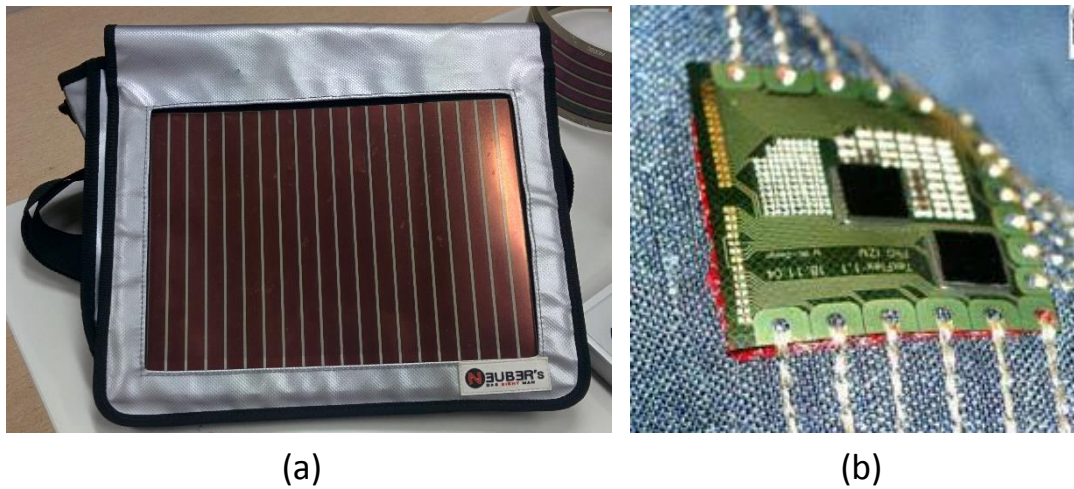
Figure 1.1. *Two examples of Flexible and Printed Electronics: (a) flexible solar cell implemented in a back bag (Courtesy of CSIRO); (b) wearable flexible device. Picture adapted from ([4])*

More recent achievements derive from medical applications, where biochemical sensor are implanted in the human body, for example for monitoring the vital functionalities. The lower cost and the high efficiency have enabled great results in the improvement of the life quality. Squeezing conformable sensors under the skin is a success that has quickly traduced in a multitude of applications. However, wearable sensors (**Figure 1.1b**) ([4]) sector has to be reported as one of the leader fields, which has pushed more than others towards innovative devices: smart T-shirt, Hi-Tech watches and glasses are few of the countless outcomes. The capability to conform themselves to the human skin and to interact with it makes them the technology of the next future. In this field, the capability to create thin and shaped devices is fundamental to fabricate flexible electronics that can reproduce the ability of the body itself: wearable sensor can receive and send information from and towards the skin.

1.1.1 Flexible Printed Circuits

Flexible Printed Circuits is one of the bricks on which FPEs is based on, providing all the functionalities that in the conventional rigid device were supplied by conducting wires. It can be referred to them with different terminologies, such as flex circuits, flex printed circuit board (PCB). However they reflect the common denominator: the capability to be flexible. As FPEs, FPCs takes advantage from the flexibility of the material utilized and the printing techniques that are used as fabrication methods (**Figure 1.2**) ([5]). Thus, they involve countless benefits, as previously reported for flexible printed electronics.
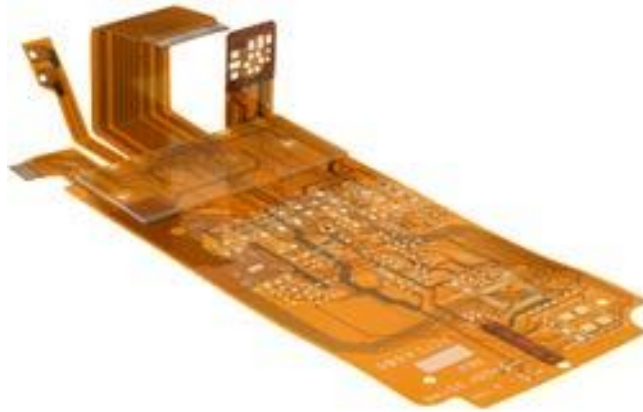
Figure 1.2. *Example of Flexible and Printed Circuit. Image adapted from ([5])*

A flexible printed circuit in a commercial format consists of a metallic layer of traces bonded to a dielectric layer ([6]). Copper is a very common as a conductive material, but other metals can be easily implemented. The thickness can be very thin, less than 0.0001", or very thick, up to 0.1". The dielectric counterpart is usually made by polyimide or polyester, moreover sometimes an adhesive is used to attach the conducting layer to the flexible substrate. Many different advantages have been introduced by FPCs and they can be summarized as following ([5]):

- Assuming all different shapes and thickness necessary for the applications;
- No space limitations;
- Handling and assembly costs considerably reduce with respect the rigid counterpart;
- Lightweight;
- Reducing wiring errors;

- Unparalleled design connectors;
- Elimination of mechanical connectors;
- Higher circuit density;
- More robust temperature range;
- More robust operating temperature range.

Most of them derive from the ability to digitalize the desired pattern for the connection necessary in the application. Therefore, human errors are reduced because of limited human interactions. Moreover, the digital support can considerably improve the device population density per unit of area and the pattern complexity in a way that it unthinkable with other types of circuits board. Furthermore, the performance are enhanced with respect to the traditional counterparts, due to the intrinsic characteristics, such as high surface/volume ratio that leads to an increased heat dissipation. It is easy to understand that these innovations can quickly enhance the application of Flexile Printed Circuits in which is the panorama of FPEs.

1.2 Printable Materials

A consistent manufacturing process is mainly developed by the selection of the right polymer, precursor or colloidal solution. This solution must meet specific rheological properties that are suitable for printed electronics. In order to achieve the aim of a low-cost and lightweight printed device a wide range of materials have been explored, both organic and inorganic. These materials can be easily divided in three main categories: (a) conductors, (b) semiconductor and (c) dielectrics [7] [8]. Beside them, a list of composites having dual nature has been investigated, such as insulator, ferroelectric and photosensitive, piezoelectric and piezoresistive. Moreover, hybrid solutions have also been used, involving organic/inorganic materials [9].

Most of the printable materials are defined as solutions, due to the advantage to be associated to many different printing technique, such as inkjet printing, slot-die or doctor blading. However, they must show optimal properties to be printed in various types of substrates, involving mainly plastic and glass foils. For example, a good ratio of chemical and physical stabilizers with respect to the active materials is necessary in order to assure an optimal balance between Brownian and gravitational motion of the particle. If some sort of solid content is involved, the most important property is a good dispersion in order to avoid agglomeration problems, which can easily degrade the deposition process.

1.2.1 Conducting Materials

Conducting materials are the fundamental part of every electronic device, forming its main layers and interconnections. For this reason, nowadays the confidence in deposition of this kind of materials has reached a high level: a fine control of thickness and resolution is possible obtaining very efficient patterned metal structure. Several printing techniques require an optimization of the solution's properties such as viscosity and surface tension, conductivity and compatibility with the underneath materials, when a multilayer structure is involved. With this in mind, frequent adjustment are necessary by using surfactants and volatile additives. However, because the complexity of several printed electronics, the conducting material has to be chose also considering the properties of the neighboring compounds, in order to exalt the function of each layer and obtain the optimal efficiency of the entire device.

Metal compounds are really common in such applications: silver, carbon and copper have been deeply explored for their optimal performance in terms of electrical and mechanical properties in various types of substrates ([10]). However silver is highly expensive, thus most of the efforts have been directed towards carbon and copper, even if the latter easily oxidize.

With similar conductivity, crystalline organic conducting materials have been also investigated, involving organic compounds, such as polyacetylene, combined with p- and n-dopants ([11]). Furthermore, the chemical structure can be designed in order to enhance the electrical and mechanical properties. The doping process can be carried out with metallic conductors or semiconductors, as in the case of PEDOT:PSS (3, 4-polyethylenedioxythiopene-polystyrene sulfonic acid). However, the low-cost of organic conductors is balanced by the lower conductivity that they can achieve with respect to the conventional metals ([12]).

Beside the organic doped conducting materials, nanocomposite compounds have been developed for flexible and printed electronics. They are obtained for example by mixing metallic nanoparticles with organic elastomers, such as Poly (dimethylsiloxane) (PDMS) ([13]). The most challenging aspect in nanocomposite materials is the proper dispersion of nanofillers in the base polymers, which considerably influences the rheological properties of the mixture to be printed. As a matter of fact, the agglomeration could affect the printability and the uniformity of the layer deposited. Avoiding this issue, the nanofillers are firstly added to a dispersant solution and then mixed with the polymer.

1.2.2 Semiconductors Materials

Semiconductor materials are critical components for developing active electronic and sensing devices. The most important aspect of this compounds that is under development

for electronic devices is the transduction of free carriers within the semiconductor dielectric interphase. As reported for the conducting materials, also the semiconductor ones can be divided into organic and inorganic materials: the former are taken in considerations for their optimal performance and stability, the latter for the low-cost processing at ambient conditions and flexibility.

Examples of an inorganic semiconductor is Si or various oxides of transition metals [14] [15]. While amorphous silicon is used in chemical vapor deposition (CVD) for large area flexible devices, crystalline Si is also used for flexible electronics fabrication by adopting dry printing techniques. It can be processed by using precursor or nanoparticles, but its annealing temperature makes it incompatible with most of the plastic substrate. Oxide of transition metals can be used for flexible electronics fabrication, however most of the times there are deposited under vacuum rather than printing. ZnO and GIZO can be printed but a temperature of 350-500 °C must reached in sintering for optimum charge mobility.

Also in this case, solubility and proper dispersion of organic semiconductors are the main important parameters to be taken into consideration for optimal depositions. However, a reliability problem arises when the organic materials are processed for a long time, because they lose stability due to their high degradability.

1.2.3 Dielectrics Materials

For devices requiring high capacity multilayered printed structures, thin layers of dielectric materials are essential in order to provide an optimal insulation to prevent malfunctions due to leakage currents or low voltage operation. A uniform layer of dielectric material promotes the activation of the carrier caused by an electric field or other transduction phenomena.

While inorganic compounds, such as silica and alumina, are difficult to print, low-cost organic dielectric materials can be easily dissolved in several solvent and solution and so printed, in addition to be characterized by a high availability.

The importance of dielectric layer in electronic devices is proved by the attention given to the interface semiconductor/dielectric, which is the most influential aspect for performance and stability of the device [8].

1.3 Substrates for FPEs

Even if flexibility is one of the most peculiar characteristics of a FPE, it does not mean that a device does not have to meet any other requirement. Obviously, many different qualities have to coexist in a flexible electronic device, without renouncing better functionality, so, all the properties that are required to obtain a functional device, rigid or flexible, have to be kept at high standard. As it is still explained in ([16]), these requirements are different and they can be summarized as the following:

- *Optical properties*: Bottom-emitting or transmissive displays need optically clear substrates. Moreover, substrates for LCDs application must have low birefringence.

- *Surface roughness*: The thinner the device films, the more sensitive their electrical function is to the surface roughness. If the roughness over long distance is acceptable and most the time unavoidable, the one over short area must be avoided. It is useful to underline how if plastic substrates are characterized by only long distance roughness, the metal ones are usually rough on both scales.

- *Thermal and thermo-mechanical properties*: The glass transition temperature T_g must be compatible with the process temperature T_{max}, because if there is any mismatch between the active layers and the substrate, it may incur in a fracture or mechanical stability problems. A good approximation for tolerable mismatch is $|\Delta CTE \cdot \Delta T| \leq 0.1\text{-}0.3\%$, where ΔCTE is the difference in coefficients of thermal expansion between substrate and device's films, and ΔT is the difference in temperature along all the process. High thermal conductivity may be important also for the cooling of current-load circuits.

- *Chemical properties*: The substrate should not release contaminants and should be inert towards the chemicals used in the various deposition process. For specific applications, such as OLEDs, the substrate should be also a good barrier against permeation by atmospheric gases.

- *Mechanical properties*: A high elastic modulus makes the substrate stiff, and a hard surface supports the device layers under impact.

- *Electrical and magnetic properties*: Conductive substrates might be used as a common node and as an electromagnetic shield. Electrically insulating substrates minimize coupling capacitances. Magnetic substrates can be used for temporary mounting of the substrate during fabrication, or for affixing the finished production

Table 1.1. *Properties of different substrates for flexible electronics ([16]).*

Property	Unit	Glass (1737)	Plastics (PEN, PI)	Stainless steel (430)
Thickness	μm	100	100	100
Weight	g/m^2	250	120	800
Safe bending radius	cm	40	4	4
Roll-to-roll processable?	–	Unlikely	Likely	Yes
Visually transparent?	–	Yes	Some	No
Maximum process temperature	°C	600	180, 300	1,000
CTE	ppm/°C	4	16	10
Elastic modulus	GPa	70	5	200
Permeable to oxygen, water vapor		No	Yes	No
Coefficient of hydrolytic expansion	ppm/%RH	None	11, 11	None
Prebake required?	–	Maybe	Yes	No
Planarization required?	–	No	No	Yes
Buffer layer required? Why?	–	Maybe	yes: adhesion, chemical passivation	yes: electrical insulator, chemical passivation
Electrical conductivity	–	None	None	High
Thermal conductivity	W/m·°C	1	0.1–0.2	16
Plastic encapsulation to place electronics in neutral plane	Substrate thickness	5×	1×	8×
Deform after device fabrication	–	No	Yes	No

In **Table 1.1** are reported the main properties for some materials that are suitable for substrate in a flexible devices fabrication, highlighting the compatibility with R2R process.

1.3.1 Thin Glass

Glass substrates are one of the most widespread supports for flexible devices in flat panel display technology. This is due to the fact that glass sheets below 100 μm thickness become flexible ([17]). Nowadays glass substrates can be 30 μm thin and show great properties for the further application. They are characterized by good thermal stability, resisting up to 600°C and have a low coefficient of thermal expansion (CTE) of $\sim4\times10^{-6}$/°C, furthermore, impermeability against oxygen and water and resistance to most process chemicals. Moreover they have a high scratch resistance and electrical insulation. But probably the aspect where glass substrates stand out is their optical properties: high optical transmittance $\geq 90\%$ in the visible, low stress birefringence and smooth surface with RMS roughness of 1 nm or less. However, one of major drawbacks of the glass substrates is their inherent brittleness and difficultly in handling. The strength of glasses depends on the entire product history, which leaves mechanical or chemical traces on their surfaces and their edges: the more evident the traces are, the lower is the strength of the substrate. So to improve mechanical stability, a good strategy is to combine glass with polymers, in fact, laminating the substrate with a plastic foil, applying a thin hard coat or applying a thick

polymer coat can reduce breakage during handling, while preserving the good mechanical and optical properties of glass.

1.3.2 Plastic Film

Organic polymer foils are major substrate candidates for flexible electronics ([18]). They can provide a lot of different advantages as lightweight, transparency, flexibility and even deformability, in addition to low cost and roll-to-roll process. However, the most important disadvantage that affects plastic substrates, as said before, is the low process temperature T_{max}, which must be compatible with the glass transition temperature T_g. On top of this, the low dimensional stability and the high coefficients of thermal expansion CTE must be considered. Such properties might be responsible for the formation of fractures on the device after several cooling-heating cycles and compromise its functionality. Furthermore, because the elastic modulus of polymer foils is a factor 10-50 lower than the lowest inorganic compounds, a small thermal mismatch stress can make the difference and create deformations during the overlay registration of the flattened piece in a step-by-step process. The overlay control is necessary when different patterns are placed on the silicon wafer one over the others and they must be aligned correctly to avoid malfunctions on the final device. Also low permeability against oxygen and other atmospheric gases is another important factor that can influence the performance of the device. Polymer substrates with CTE below 20 ppm/ ˚C are preferred a substrates for silicon-based device materials.

There are several polymers which might be considered valid candidates as substrates for flexible devices, including 1) the thermoplastic noncrystalline polymers such as polycarbonate (PC) and polyethersulphone (PES), 2) the thermoplastic semicrystalline polymers: polyethylene terephthalate (PET) and polyethylene naphthalate (PEN) or 3) high-T_g materials as polyarylates (PAR), poly-cyclic olefin (PCO) and polyimide (PI). PC, PES, PAR and PCO are optically clear and have relatively high T_g, compared to PET and PEN, but they are characterized by a CTE of 50 ppm/ ˚C or higher and poor resistance to process chemicals. PET, PEN and PI are more prominent due to a relatively small CTE, around 15-16 ppm/ ˚C, and high elastic moduli, in addition to good process resistance. PET and PEN are optically clear with a transmittance >85% in the visible, moreover they absorb a little amount of water, around 14%, however they have a process temperature T_{max} of only ~150˚C and 200˚C, even after annealing. Although PI has a high $T_{g,}$ up to 350˚C, it hasn't a good optical property due to the fact it absorbs in the blue range and so it results yellowish. However, no one polymer currently meets the requirements for OLEDs application, because the high oxygen permeation in the plastic substrate. Barrier layer coatings can improve some properties, such as permeability by gas, moisture absorption, strengthen adhesion of device films and reduce surface roughness.

1.3.3 Metal Foil

Other candidates to be considered in flexible electronics applications are metal foil substrates, which become flexible when they are less than ~125μm thick. The first fundamental difference with respect to the other two options, plastic and glass substrates, is the impossibility of them to be transparent. As such, metal foils are commonly utilized for emissive and reflective displays. In some circumstances, the preference for metal substrates derives from their ability to tolerate high temperatures. Specific steel foils can reach up to 1000˚C, avoiding the issue observed with the plastic substrates and allowing to operate at the optimal conditions for fabrication of the device films. Furthermore, they show great resistance against corrosion and chemical attack with no water or oxygen absorption, in addition to magnetic shielding [19]. On the other hand, metal supports have some issues as well, especially related to the surface roughness. Because applications in the electronics field required very flat surfaces, with limited imperfections and inclusions to maintain electrical integrity, it is necessary to apply polishing or planarization processes in order to ensure an optimal device functionality [20]. Planarization can be obtained through the application of a film that could be organic polymers, inorganic, for example methylsiloxane spin-on-glass (spin-on-glass, SOG, is a type of glass that can be applied as liquid and cured to form a layer of glass having characteristics similar to those of SiO_2), or a combination of both, with silicate spin-on-glass. It is important to underline that the higher the organic content in the planarization is, the thicker the film can be applied without causing cracks, obtaining a smoother surface. Obviously, the planarization by organic films introduces again a temperature problem that can be partially solved by applying an inorganic overlayer by pulsed-laser processing. A typical planarization process includes different steps as spin-on, hotplate baking and high-temperature curing. Because metal foils are electrically conducting, they can be utilized also as a back contact in some applications, as solar cells, but for others it is necessary to insulate the substrate to provide circuit isolation, this is made possible by applying SiN_x or SiO_2 layers. Insulation also allows adhesion and barrier formation against process chemicals.

1.4 Deposition Techniques for FPEs

Printed electronics involves conventional printing technologies, associated with new inks that are suitable for flexible device fabrication [21]. Thus, the benefits achieved in the long history of printing techniques can still be applied for flexible electronics. A wide range of different methods have been developed, with the advantages to produce high-quality devices, to be extremely cost-efficient and to have the capability to print from low to high volumes without many issues. The fact is, even if they have been developed for rigid

boards, they can be easily applied for flexible substrates.

Therefore, the roll-to-roll manufacturing concept is available for FPEs fabrication, due to the intrinsic properties of both devices and printing techniques. R2R processing is one of the most prominent techniques due to its capability to reduce the amount of waste material and increase the production yield. This approach is different with respect to the conventional ones because it does not treat a single product per process step, but it is considered as a steady state process, with the consequence of an increased throughput and lower consumption of raw materials. In this terms, the ability of the device to be flexible represents a compulsory criteria for applying a R2R concept in a manufacturing system, where the substrate is unwound from a roll in order to create a single continuous web. Such webs can undergo one single processing step, in which all the active layers are deposited in one step or can be processed multiple times unwinding and rewinding the roll ([22])([23]). This simplifies the traditional step-by-step processes, enabling large-area devices to be created with a much faster process, while conventional techniques are subjected to size limitations and longer processing times. The resulting process is made more flexible as well, because the use of the simpler techniques, which are easily adaptable to different productive lines for different final products.

Moreover, the particular design and technologies of such printing techniques enable the creation of more or less complex patterns, allowing for the fabrication of simple devices through to multilayer and multifunctional structures. Nowadays, mask printing methods, which involve the use of a negative mask designing the desired pattern, are still used and adopted by the simplest techniques; however, the digital support is pushing towards a less problematic choice: the pattern can be digitalized and modified, based on the functionalities and the structure that are wanted to give to the final device.

The most common deposition techniques for Flexible and Printed Electronics are reported as following.

1.4.1 Vacuum Deposition

Vacuum deposition is a family of processes used to deposit layers of material atom-by-atom or molecule-by-molecule on a solid surface. These processes operate under the atmospheric pressure and the deposited layers varies from a thickness of one atom up to millimeters.

If the vapor source is a solid or a liquid the process is called physical vapor deposition (PVD). Instead, when the source is a chemical vapor precursor, the technique is called chemical vapor deposition (CVD). The latter presents different types of deposition: low-pressure chemical vapor deposition (LPCVD), plasma-enhanced CVD (PECVD), and plasma-assisted CVD (PACVD). The vacuum environment may be used for different aims:

- reducing the particle density in order to not let them collide during the deposition;
- providing a low pressure plasma environment;
- reducing the particle density of undesirable atoms and molecules (contaminants);
- providing a means for controlling gas and vapor composition;
- providing a means for mass flow control into the processing chamber.

The particle vapor can be generated by different processes:

- thermal evaporation;
- sputtering;
- cathodic arc vaporization;
- laser ablation;
- decomposition of a chemical vapor precursor, chemical vapor deposition.

The vacuum deposition technique is a stepwise process due to the different operations necessary to allow a suitable deposition of the material. Furthermore, this method requires a huge amount of material, most of which is wasted on the mask that is used to cover the substrate in order to obtain the desired pattern. For these reasons, this technique is not suitable for a R2R system that aims to a single-step process and decreases the amount of material utilized in the fabrication of the device. Moreover, vacuum deposition is a very complex technology, unlikely adaptable to a Roll-to-Roll deposition, characterized by a moving web.

1.4.2 Spin Coating

The most common method in organic flexible devices is spin coating that allows a more homogeneous film formation during drying process than other coating technique. The typical spin coating technology involves application of a solution onto a substrate that is vacuum attached to a rotor. After the solution has spread evenly on the substrate, the base is rotated at high revolutions per minute (rpm), removing the excess of liquid by the rotational acceleration and allowing an optimal thickness control. The thickness, the surface topography and the morphology of the final film for a particular material in a given solvent at a given concentration is highly reproducible. Moreover, these three properties highly depend on the rotational speed, viscosity, volatility, diffusivity, molecular weight and concentration of the solutes, but they are less influenced by amount of the solution deposited, the rate of the deposition and the spinning time. The final thickness after a spin coating process can be estimated by the follow **Equation 1.1**:

$$d = k\omega^{\alpha} \quad . \tag{1.1}$$

Where ω is the angular velocity in m s^{-1} and k and α are empirical constants related to the physical properties of the solvent, solute and substrate.
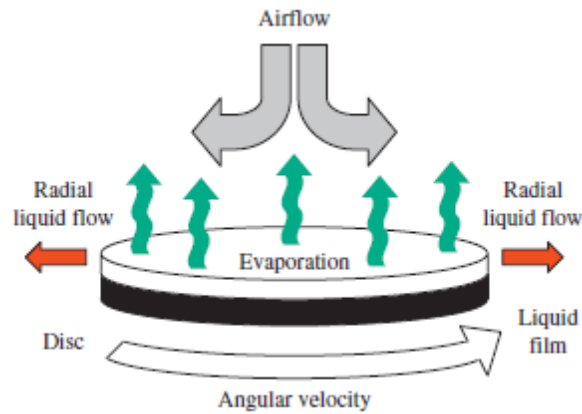
Figure 1.3. *Representation of spin coating deposition method. Image adapted from ([20]).*

It is important to understand that when the excess of solution has been removed by the rotational acceleration, the wet film is characterized by different phenomena, such as solvent evaporation, change in viscosity, radial flow of the solution, and shear thinning and molecular orientation due to the shear field, phase separation of blends and diffusion of molecules in the film. Even if spin coating is largely utilized in lab scale, due to its high reproducibility, the stepwise process and the huge amount of waste material (>90%) make it not compatible with a R2R configuration. Furthermore, this technique is not suitable for patterning, thus more complex devices are difficult to fabricate. The operation of a typical slot-die system is schematically represented in **Figure 1.3**.

1.4.3 Knife-Over-Edge Coating

This technique is a 0-dimensional coating, which means that it possesses an absence of a predefined pattern, so the entire surface is coated with solution. Knife-over-edge coating provides a continuous appliance of ink in a stripe with a define width (defined by the knife) by a stationary knife positioned over a moving web, as showed in **Figure 1.4**, which is unwound from a starting roll and may be unsupported. The ink is also supplied in a bath in front of the knife which is placed very close to the substrate. In this way the fixed blade pushes it in order to create a deposition, determined by only the gap underneath the edge.

The resulting thickness can be roughly calculated by **Equation 1.2**:

$$d = \frac{1}{2}\left(g\frac{c}{\rho}\right) \quad . \tag{1.2}$$

Where g is the gap distance between the blade and the substrate in cm, c is the concentration of the solid material in the ink in g/cm^3 and ρ is the density of the material in the final film in g/cm^3, when the blade is flat and parallel with the surface of the substrate. There is no waste of ink in this process because the amount of ink required can be set and will be coated all onto the substrate. It's a very simple technique where the only variable is the ink flow feed to the reservoir and the gap between web and knife, allowing the coating on uneven surface and levelling with smooth films. Moreover, it's suitable for large-area deposition without any patterning, due to the fact that the only pattern that can be obtained is a film with the width of the blade.
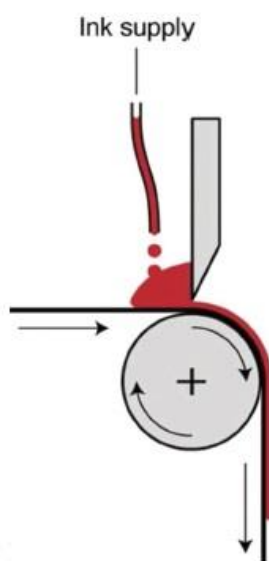
Figure 1.4. *Representation of knife-over-edge methods. Picture adapted from (*[23]*).*

Knife-over-edge is a simple technique that can be easily used in lab-scale, but it is hard to applied in manufacturing systems, due to its mainly characteristics.

1.4.4 Slot-Die Coating

Slot-Die coating is a 1-dimensional technique, characterized by the coating of stripes of different material along only one direction that can be well suited for a multilayer flexible device, where the materials are deposited on top of each other. It is very similar with respect to the previous technique, because it involves the use of a blade and a moving web, furthermore there isn't waste of ink due to the fact that it can be supply in order to be all coated at the end of the process, as it is schematically represented in **Figure 1.5**. However Slot-Die coating shows some critical differences. First of all, the head is more complex if compared with the knife-over-edge equipment, showing different parts including a shim that carries the coating blade, and a mask, which allows the ink to flow through the head. The mask is usually 10-100 μm thick and a viscosity in the range of 1-20 cP characterizes the ink. In fact, the constant supply of ink forms a standing meniscus between the moving substrate and the head that creates a continuous coat of pretty even thickness over a large area. By modulating the ink flow with a suitable pump and by controlling the speed of the underneath substrate and the free gap for the coating, it is possible to obtain different thicknesses, which are also dependent on the ink viscosity and the solid content.
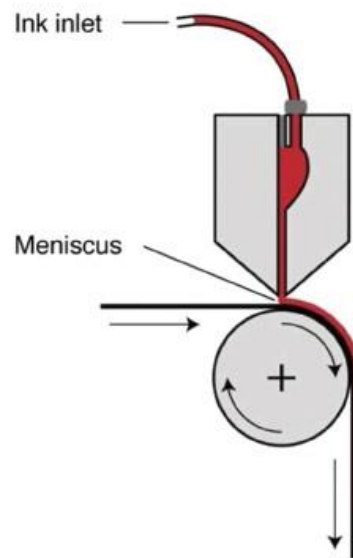
Figure 1.5. *Schematic illustration of a slot-die technology. Image taken from ([23]).*

For a given web, ink flow rate, coating width and solid concentration, the dry thickness

can be estimated by **Equation 1.3**:

$$d = \frac{f}{Sw} \cdot \frac{c}{\rho} \quad .$$

(1.3)

Where d is the thickness in cm, f is the flow rate in cm^3/min, S is the web speed in cm min^{-1}, w is the coated width in cm, c is the solid content in the ink in g/cm^3 and ρ is the density of the dried ink material in g/cm^3. Being a 1-dimensional technique, it creates a 1-dimensional pattern that is suitable for electrical interconnections between different layers, making possible flexible devices fabrication at large scale. However, there is a limitations range, in term of web speed, ink composition and ink flow rate, beyond which coating is no longer possible.

1.4.5 Screen Printing

Screen printing is a very versatile printing technique that allows for full 2-dimensional patterning of the printed layer. Its main requirements, as opposite to other methods, are a high ink viscosity and a low volatility for coating solution, keeping the distance from other techniques also for the presence of a large wet film thickness. The process involves a screen of woven material (synthetic fiber or steel mash) that has been glued to a frame under tension. The pattern is obtained by filling the screen with an emulsion that prevent the coating solution to reach the areas where no print should appear. The area of printed pattern is kept open (without emulsion). The screen is then filled with coating solution and brought into proximity of the substrate. A so-called squeegee is forced into the screen bringing it into contact with the substrate and then drawn linearly across the screen thus forcing coating solution through the open areas onto the substrate and in that manner reproducing the pattern. One of the most important parameters about screen printing is the theoretical paste volume of the screen, V_{screen}, normally measured in cm^3/m^2, which gives the thickness of the coated film. Other factors that can influence the printing process are the force with which the squeegee is pushed, its speed and the snap-off distance, in addition to the solution viscosity. The final thickness of the dried film can be evaluated by the follow **Equation 1.4**:

$$d = V_{screen} k_p \frac{c}{\rho} \quad .$$

(1.4)

Where V_{screen} is the theoretical paste volume of the screen in cm^3/m^2, k_p the pick-out ratio that described the partially deposited material, c is the concentration of the solid material in the ink in g cm^{-3}, and ρ is the density of the final dried film in g cm^{-3}.

There are two types of screen printing, flat bed and rotary screen printing (see **Figure 1.6***a* and **1.6***b*).
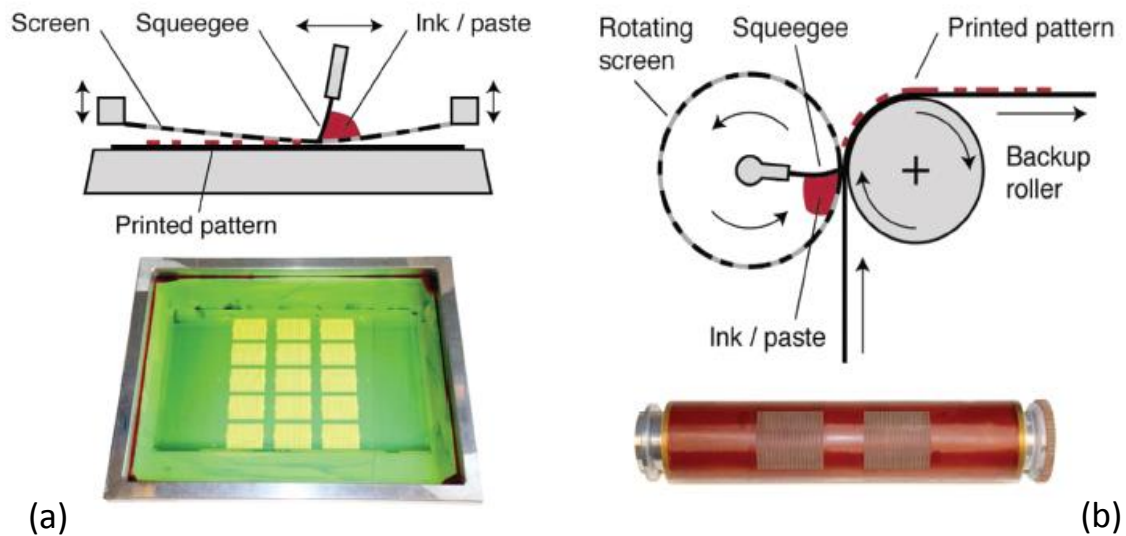
Figure 1.6. *Schematic representation of a flat bed screen printing (a) and a rotary screen printing (b). Pictures adapted from ([23]).*

The former is the conventional technique, where the squeegee is swiped over the screen, transferring the ink on the substrate and obtaining the desirable pattern. Although it is not thought for a R2R system due to the process' time-consuming steps, as for example changing the substrate after every deposition, the flat bed screen printing has been successfully applied to a R2R configuration. The latter is the most suitable for a continuous deposition, characterized by a moving web and using the same concept of the flat bed screen printing. In fact, the stationary squeegee is placed with the ink inside a rotating tube, which presents open areas where the solution is pushed in, allowing the pattern deposition on the substrate, placed in contact with the coating apparatus. Rotary screen printing can achieve very high processing speed, > 100 m/min, if compared with the 0-35 m/min of the flat bed one. However it is much more expensive due to the waste of ink in the initial adjusting phase. Notably, even under steady-state conditions it is a very reliable technique.

1.4.6 Gravure Coating

Another 1-dimensional coating technique is the gravure printing that allows the deposition of pre-etched patterns onto flexible substrates. It is even more complex than knife-over-edge and slot-die deposition but it is based on the same concept of not wasting of ink during deposition. **Figure 1.7** shows how the simplest form it comprises a 2-roller system, where the coating roller has an engraved pattern that is partially inserted in an ink bath. The excess of ink is eliminated by a doctor blade just before the contact between the coating roller and the moving web, which is supported by another roller, avoiding ink
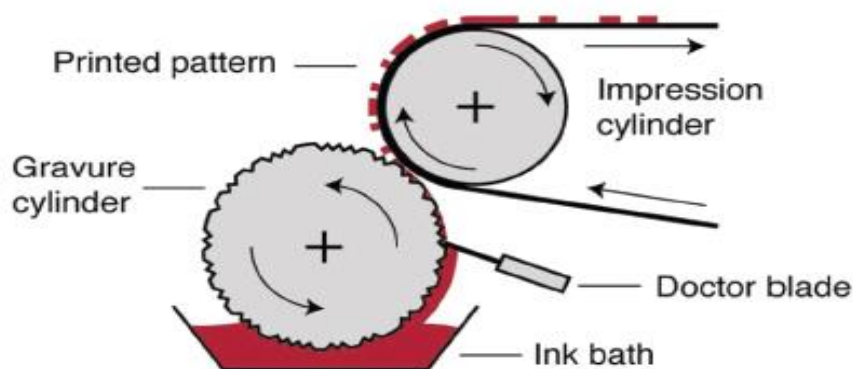
Figure 1.7. *Representation of the simplest gravure coating technique. Image taken from ([23]).*

losses and pattern's imperfections due to the excess of ink. This is transferred onto the substrate in the desired pattern by the tight touch between the coating roller and the substrate, allowing the movement from the roller cavities to the web. Obviously, when a new kind of pattern is required, it is necessary change the engraved roller.

This technique results suitable for low viscosity inks and for very high web speed. However, the quality of the pattern is not suitable for high performing devices.

1.4.7 Flexography Printing

The basilar concept of flexography is similar to that of gravure printing's one: the ink is transferred to the moving web by a soft printing cylinder, typically made by rubber or photopolymer. The flexography system is traditionally composed by four rollers, where a fountain rotor supplies the ink to a ceramic anilox roller, characterized by micro-cavities

in the surface, which is made in contact with proper printing cylinder that is engraved with the desired pattern. Finally, the ink is deposited onto the substrate that is supported by another cylinder that rotates in the same directions of the printing one. Similar to the gravure printing, the excess of ink is removed by a doctor blade positioned in contact with the anilox cylinder. In **Figure 1.8** it is schematically showed the flexographic deposition concept.
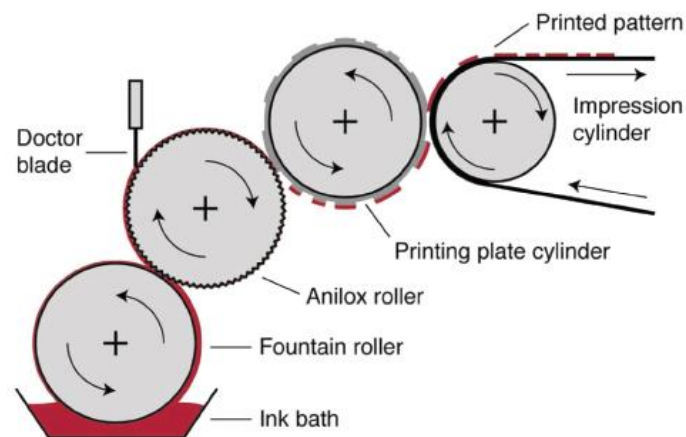
Figure 1.8. *Flexographic method adapted for a flexible device fabrication. Picture taken from (*[23]*).*

The flexographic deposition is an evolution of the gravure printing and so it is wider used than the predecessor in coating of printed devices.

1.4.8 Inkjet Printing

Inkjet printing allows a 2-dimensional patterning obtained by a pixelated pre-pattern with a defined resolution unlike the techniques described so far, which present the same pattern for every deposition if it has not previously been changed. Inkjet printing is based on two main technologies, thermal and piezoelectric, which permit a drop-on-demand deposition for a high resolution printing. The former is typically utilized in low-cost inkjet printers, but the lat ter has successfully settled as a reliable roll-to-roll technique. In the piezoelectric inkjet printing process, the droplet is mechanical compresses by a piezoelectric crystal and electrostatically charged by an electric field. At this point, it is pushed out from the nozzle in the position defined by digital software. In order to obtain high resolution depositions

(up to 600 dpi), the printing head requires many nozzles, which also decrease the amount of time necessary for the complete deposition. Specific limitations are required in inkjet printing as well: for example ink with a low viscosity (4-30 cP) are required, often achieved with a mix of 5-8 different solvent, as well as the capability to be electrostatically charged, in addition to a high surface tension, typically >35 m m^{-1}, necessary to easily create a stream of droplets.
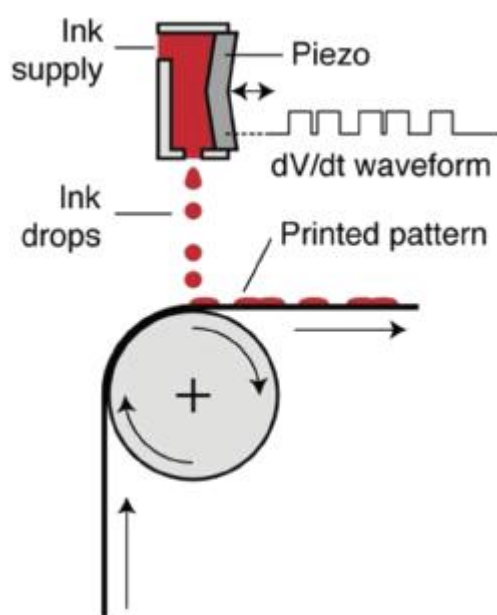
The dry thickness resulting from the inkjet deposition is given by the number of droplets

Figure 1.9. *Schematic illustration of an inkjet printing deposition adapted from ([23]).*

delivered per area, the volume of each droplet and the concentration of the material in the ink and it can be estimated by the follow relation, **Equation 1.5**:

$$d = N_d V_d \frac{c}{\rho} \quad . \tag{1.5}$$

Where N_d is the number of the droplets delivered per area in cm^{-2}, V_d the volume of the droplet in cm^3, c the concentration of the material in the ink in g/cm^3 and ρ the ink density in g/cm^3.

The inkjet printing is suitable for a R2R approach, allowing a high pattern resolution not achievable with other type of printing technique. Moreover, it results more practical and flexible due to the possibility to adjust the pattern through a software and prevent the change of the entire roller manually. Substrate can be coated with a resolution of 600 dpi with a web speed of 75 m/min.

The techniques described so far are summarized in **Table 1.2**, enabling to compare the several deposition methods by different characteristics. Attention is paid to the possibility

Table 1.2. *Description of the main characteristics of the principal deposition techniques. L=low; M=medium; H=high; VH=very high.*

Technique	Scalability	Speed	Ink Waste	Film Quality	Pattern	R2R Compatible
Thermal Evaporation (vacuum)	M	L	M	H	2D	Y
Spin-Coating	L	L	H	M	0D	N
Doctor-Blading	M	L	L	L	0D	Y
Knife-Over-Edge	H	H	L	M	0D	Y
Screen	H	H	L	M	2D	Y
Slot-Die	H	VH	L	M	1D	Y
Gravure	H	VH	L	M	2D	Y
Spray	H	H	M	L	1D	Y
Inkjet	H	M	L	M	2D	Y

to scale-up the technique from the laboratory application to the manufacturing process: it is probably the main characteristic required from a printing technique. Moreover, the process speed and the material waste are underlined. Eventually, an indication of the complexity of the pattern and the R2R compatibility are reported.

In this work slot-die coating and inkjet printing will be explored, trying to understand the possibility to obtain high performing electrodes. From **Table 1.2**, it is possible to observe that they are characterized by the more interesting properties, in terms of process speed and ink waste (slot-die) and pattern dimensionality (inkjet).

Summary

In this chapter the technological information necessary to understand this work have been explained. It has been explained the meaning of a Flexible and Printed Electronics and the material which it is based on, as well as the deposition techniques developed for it fabrication. In the next section, slot-die coating and inkjet printing will be deeply investigated: the procedures used in both methods will be outlined.

Chapter 2

Materials and Methods

The fabrication of copper electrodes was based on the deposition of a copper oxide nanoparticle ink on a flexible plastic substrate and post-processing using flash photosintering. In this chapter, their most important properties are introduced, in relation to the printing techniques involved. Moreover, the printing methods that were utilized are explained, with a focus on the main operative parameters that have been tuned, in order to optimize the electrodes deposition.

2.1 Copper Ink and Substrate Description

An ink of copper (II) oxide (CuO) nanoparticles suspended in an aqueous solution and a plastic foil were the materials used for the copper electrode deposition described in this work. They show optimal properties for this type of application, as reported in the following sections.

2.1.1 Metalon® ICI-002HV

The ink used in the deposition of the copper electrodes was supplied by Novacentrix™, as an aqueous solution containing copper (II) oxide nanoparticles, called Metalon® ICI-002HV. It contains approximately 16% in weight of copper oxide, which average particles size is around 130 nm in diameter, as shown in **Figure 2.1**, where the particles size distribution for a typical batch is reported. It has to be taken into account that this result is obtained using a dynamic light scattering measurement (Malvern Instruments Zetasizer) and therefore it measures the clusters in solution (single particles or aggregates of particles) with their hydrodynamic diameter. For these reasons, the actual nanoparticles size might be slightly smaller ([24]).

The solution is specifically made for inkjet printing. As previously discussed, there are limitations about the specifics of the inks suitable for inkjet technology, in this case for the piezoelectric printing system. One of the most important parameter to consider is the viscosity, which for the copper oxide solution is between 9-15 cP at room temperature.

Additionally, a quite high surface tension is required, estimated around 27 dynes/cm, in order to avoid any difficulties in droplet creation in the inkjet system. The specific gravity of the ink is measured to be in the range of 1.2-1.4, while the ink is neutral to slightly acid, with a pH value of 6.0-7.0. These entire characteristics meet the requirements specified for optimal inkjet deposition.
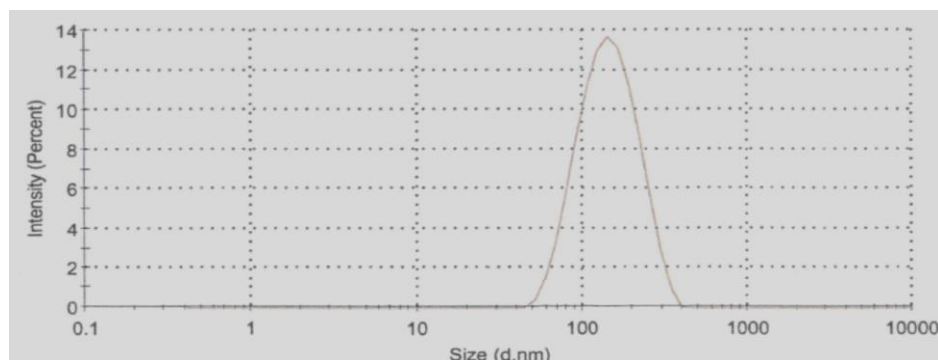
Figure 2.1. *Nanoparticle size distribution for a typical Metalon® batch. Figure taken from ([24])*

This ink showed a high miscibility with different solvents, especially with ethanol. The hydrocarbon has the capability to disperse in an optimal way the copper oxide nanoparticle, obtaining a stable solution without any phase separation or precipitation of solids. This specific affinity between the commercial ink and ethanol was useful in the slot-die deposition, where the ink's properties, specifically obtained for an inkjet printing, were not suitable due to the high viscosity. With a proper dilution, different solutions were produced. Based on the volumetric percentage of the solvent content, the ink properties changed towards a lower viscosity and a lower surface tension, showing a higher evaporation rate. These changes were not studied in depth, but further details will be discussed in the next chapter.

The choice of the copper nanoparticle ink for the deposition of conductive electrodes was not accidental. Because flexible electronics are designed to be bendable, rollable and stretchable, the use of proper solutions in coating techniques in order to maintain a high conductivity has become fundamental. The right ink option can considerably improve the chemical and mechanical stability of the final device to deliver better performance. In this view, many different options for the preparation of flexible electrodes have been studied, such as conductive polymers, molten metals, organo-metallic compounds, metal precursors and metallic nanoparticle suspensions ([25]).

Among these classes of materials, conductive polymers should be the most advantageous

for flexible devices, given their mechanical properties. However, their relatively low conductivity plays a major role in reducing their allure. Considering the other options, the operating temperature of molten metals is too high with respect to the maximum process temperature for a roll-to-roll manufacturing, which is limited by the glass transition temperature of the plastic substrate. Organo-metallic compounds require a chemical reaction, which typically involves more than one chemical and/or additional heat treatment to drive a reduction process. Moreover, the final electrodes from such methods show a large amount of organic compounds that can affect the electrical properties.

Nanoparticle dispersions can bridge the very high conductivity of metals with the low process temperature akin to polymer processing. Because of their small size, nanoparticles offer a reduction of melting temperature compared to that of the bulk material ([26]). However, sintering has to be achieved in order to enhance the electrical conductivity towards the value of the bulk materials. This is one of the main goals of this thesis.

In addition to a reduced melting temperature, the nano-scale size of the particles can modify other physical properties, such as electronic, magnetic, catalytic, optic and thermodynamic ones, compared to bulk material. These unique characteristics are related to the fact that by decreasing the size, the surface of the particles becomes prevalent compared to their volume, thus changing their chemical and physical behavior. The low melting temperature, and by extension the sintering temperature, enables milder processing conditions to be suitable for fabricating metal electrodes.

Several metallic compounds have been proposed in the form of a nanoparticle ink, such as gold (Au), silver (Ag) ([27]), copper (Cu) and nickel (Ni) ([28]). Ideally metallic features for conductivity would be sufficiently conductive, stable and cheap. Considering these factors, despite gold and silver nanoparticles showing a lower melting temperature and suitable electrical properties, they are cost prohibitive for large area application. Their current prices per ounce are $1200 for Au and $17 for Ag. Instead, copper and nickel cost are more suitable for large area applications because they cost $0.17 and $0.36 per ounce, respectively. Unfortunately, they are easily oxidized, which degrades their electrical properties and forms the scientific challenge. Metalon® ICI-002HV contains copper oxide nanoparticles, which are converted to a bulk copper films with photo-reduction. Therefore, they are naturally stable in dispersion, but do require encapsulation to avoid oxidation for practical use.

2.1.2 Novele™ IJ-220

The substrate on which the Metalon® was deposited was produced by the same company, Novacentrix™. It is developed particularly for nanoparticle inks. Novele™ IJ-220 is a PET-based substrate for low-cost and low-temperature applications where transparent

films are desired. It is not a simple PET support, because it presents an over-layer that is extremely porous and around 30 μm thick. This enhances the mechanical stability of the deposited electrodes. When the solution is coated on Novele™ IJ-220, it permeates the porous structure and after sintering a continuous network is created. This deeper interconnection between solution and substrate enables for an improved mechanical stability, avoiding easy delamination of the deposited layer. Different possibilities have been considered as flexible plastic substrate, for example polyetherimide (PEI), polycarbonate (PC), polyarylate (PAR), polyimide (PI) and polyehtylene terephthalate (PET), in addition to photographic paper. Although each plastic substrate may be suitable for flexible application, it has been demonstrated how PET shows a better predisposition for room temperature sintering processes, such as intense pulse light annealing ([29]).

The flash sintering mechanism involves a photothermal effect that leads to heat generation, which is confined within the individual nanostructure. The substrate should not take part in the formation of the conductive film, but for the above case it is certainly involved in structuring the sintering process. In fact, **Figure 2.2** shows that flash sintering with the same solution of Ag nanoparticle ink, at 14% in weight in solution with ethanol, which is printed with the same inkjet printing parameters onto different plastic substrates has drastic differences.
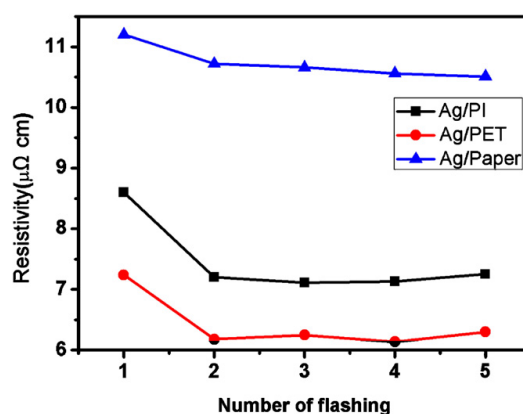
Figure 2.2. *Resistivity variations as a function of number of pulses for different types of substrate. Figure taken from ([29]).*

The evaporation rate of the solvent from the ink following ink deposition affects the formation of a continuous structure, due to the fact that the generated heat is dissipated before vaporization of the organic compounds and melting of the nanoparticles. In these

terms, a plastic substrate with low thermal conductivity should be optimal to prevent the heat dissipation in the surroundings and to confine more heat in the nanostructure. However, reaching very higher temperatures in the top layers is not advised, because it has been demonstrated how it can lead to surface defects that decrease the electrical properties of the conductive film. On the other hand, a higher thermal conductivity implies a faster heat dissipation, which prevents the formation of a uniform film structure due to the difficulty in reaching the perfect conditions in the layer.

Table 2.1. *Thermal conductivity for some of the plastic substrates.*

Substrate	Thermal conductivity ($Wm^{-1}K^{-1}$)
PI	0.52
PET	0.19
Photo paper	0.04

With this in mind, PET shows an intermediate thermal conductivity, as shown in **Table 2.1**, enabling an optimal heat transfer during flash and also sintering of the nanoparticle into a uniform framework whilst avoiding the formation of surface defects.

The plastic foil used in the applications shows a basis weight of 175 ± 10 g/m^2 and a thickness of 140 ± 12 μm, measured with a caliper.

2.2 Slot-Die Printing Apparatus

A 3-Dimensional (3D) printer featuring a slot-die printing head is one of the two deposition instruments that were used for the copper electrodes fabrication. This choice has to be attributed to the outstanding characteristic, which have made it one of the largely technologies studied for flexible electronics fabrication. Slot-die technique is a 1-dimensional (1D) coating, which means that is not suitable for creating complex patterns except stripes that can be narrow or wide depending on the shape of the printing head ([22]). The 1D patterning is more involved in the fabrication of simple multilayer devices, such as solar cells, or for the interconnections between different layers. Several investigations have been performed in order to analyze the behavior of such technology in the manufacturing of flexible devices, especially for organic photovoltaic inks ([30]).

This work varies from the conventional slot-die applications, because it does not involve a polymeric solution, but a nanoparticle ink. At the present, there are limited studies discussing the deposition of a nanoparticle mixture by slot-die for flash sintering, and this work is partly devoted to filling this technological gap. The main aim of this study is to

optimize the deposition of copper oxide nanoparticle, in order to investigate the suitability of this solution in a slot-die system and create performing copper electrodes. In fact, by coupling the unique properties of a nanoparticle solution with this proven technique, several advantages can be introduced in the fabrication of flexible electronics.

Slot-die 1-dimesional patterning may be thought as a limitation if compared to other printing technique, such as inkjet printing, which will be treated as a reference methods. However, the lower resolutions of the slot-die printing is counterbalanced by the very simple apparatus that can lead to important advantages. First of all, an elementary system involves an easier control of the coating process, because of the less variables that characterize the solution deposition. It is translated in a faster and deeper comprehension of the parameters that can influence the phenomenon. Moreover, a simpler printing head enables more accessible changes: different configurations are available and they are easily interchangeable, without creating profound variations on the entire coating system. This even means that slot-die can be easily adapted to several solutions, which show different properties. On the other hand, an elementary apparatus can be easily checked in presence of malfunctions and quickly repaired if necessary. The maintenance becomes immediate, without involving expensive spare parts. In fact, the cost of a slot-die system is much cheaper with respect to other techniques. With this in mind, the scale-up of such system for industrial application is achievable with small adjustments, without changing the nature of the method. Thus, the effortless scale-up is the strength that leads slot-die to be one of the most prominent techniques for a roll-to-roll process.

Additionally, a 3D printer platform is associated to the slot-die printing head as a fabrication tool for the electrodes deposition ([31]). This combination gives to the entire system a further degree of freedom, with respect to the convention slot-die technology. Traditional designs are based on a fixed printing head that is put in contact with a moving web: the ink is pumped through it and deposited onto the flexible substrate that is wound from one end and rewound to the other. In this case instead, the printer is an extruder that can move automatically along the x, y and z axis with a precise position control, varying the head acceleration/deceleration/speed for an accurate ink's deposition. Furthermore, additional parameters can be introduced, for example the temperature of the printing head as well as the plate temperature. A software controls the movements and the positioning of the 3D coater head, enabling more accuracy in the solution deposition.

2.2.1 Slot-Die Coating Head

In order to deposit thin and uniform copper film onto the flexible substrate, a slot-die coating head was used as end of the 3D coater. The common design for a slot-die print-head involves several components, each one with a specific function. The parts can be

easily assembled together by screws, and they are fabricated in order to exhibit an inner channel where the ink is pumped through, creating a solution flow that is deposited onto the underneath substrate. The equipment that was used for the copper electrodes deposition is shown in **Figure 2.3**, where the components are arranged in the sequence in which they were assembled.
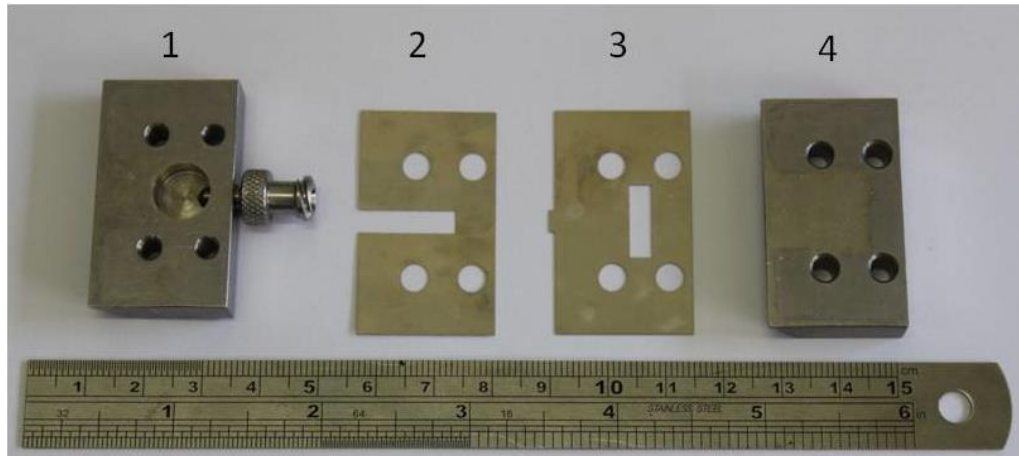
Figure 2.3. *The slot-die coating head in the disassembled version in order to show the different components.*

The front and the rear pieces, numbered as (1) and (4), are thicker than the central masks, because their function is to give stability with their weight to the entire apparatus, which has to avoid sudden movements due to possible contacts with the flexible substrate or vibration coming from the motor of the coating system. Their thickness is wider than the other parts also because it has to allow the screws to have a sufficient stroke giving to the print-head the solidity necessary to contrast the pressure created by the pumping of the ink inside it. The front piece, the part that faces the coating direction, shows a different design with respect the rear part. An extension can be observed going inside the component, ending at the beginning of a circular cavity: it is the connection the coating head and the syringe that can be screwed in it for a better grip. The recess at the center of the front piece is the reservoir for the ink: if it is pumped inside the coating head directly into the slot for the deposition, the pressure that could be generated may create some instability in the ink flow, influencing the deposition. The cavity disconnects the pumping process with the ink flowing, allowing the suppression of possible flow instability during the coating process. The inner parts represent two masks, whose main functions are to create the slot through

which the ink can flow just before the deposition and, the most important, to generate the meniscus necessary for defining the desired pattern. It can be seen, in fact, how the mask (2) shows a channel starting at the same height of the reservoir and ending at the same level of the front and rear components, creating a free path where the solution can go through. The shim, as the component (3) is designated, is probably the most important piece of the coating head. The blade that characterized one of its ends enables for the formation of the ink meniscus, which is the basilar concepts for the deposition by slot-die. Due to the solution properties, such as viscosity and surface tension, the liquid creates a curved surface that makes in contact the coating head with the underneath flexible substrate. This structure is continuously refilled by the ink flow and it enables the deposition of the ink by the head motion.

The meniscus has a really unstable nature and it depends from different factors, both solution properties and coater parameters, and it may be disappear due to some instabilities. This is the main issue for a slot-die coating and it can become really challenging to find the right settings and properties in order to create and stabilize the convex lens for a proper deposition. The blade can't determine the type of deposition, which is characterized by only stripes, but it can define its width. For the copper electrodes a 4 mm blade was utilized that ensured the deposition of valid samples for the subsequent characterizations. The amount of ink that is coated onto the substrate can be adjusted by the thicknesses of the mask and the shim, as well as by coater parameters, such as the volume of ink pumped or the head speed. In this case, a 50 μm thick shim and a 200 μm thick mask were adopted.

Particular attention was given to the sequence in which the different parts were assembled. As everyone can notice, there isn't a predefined way to set up the coating head, which may differ for the position that the mask and the shim can assume. However, even if for the organic solutions it is usually chosen an inverse sequence with the respect to the one illustrated in **Figure 2.3**, for a nanoparticle ink an arrangement that involve front piece, mask, shim and rear piece in this order was preferred. The main reason for this choice is related to the nature of the ink, which is an aqueous/ethanolic solution where the nanoparticles are suspended in order to create an apparently one liquid phase. However, it is possible that those nanoparticle may create clogging problems, for example due to the solvent evaporation or aggregation, influencing the normal ink flow and so the deposition. Thus, a configuration that can minimize the possibility to incur in that problem was opted. In fact, placing the mask between the reservoir and the shim enables the ink to flow through the head more easily due to the larger free volume allowed. On the contrary, if the shim is placed before the mask, the solution has access to the slot only through a very tight window, which may lead to clogging-related problems.

To complete the coating head apparatus, a syringe filled with the solution is connected to

the front piece. For the copper electrode deposition, a plastic syringe of 6 ml was utilized, although different alternatives could have been used based on the necessary coating volume.

2.2.2 Felix-Coater-*3D Printer*

The deposition of copper electrodes was achieved using a (3D) coater, partially modified from a commercial 3D printer. This equipment had been previously assembled by a Commonwealth Scientific and Industrial Research Organization (CSIRO) team, in order to deposit the active layers used in bulk heterojunction (BHJ) solar cells, as presented by Vak *et al*. ([31]). In the fabrication of copper electrodes, a similar approach was adopted, replacing the organic polymers used in solar cells with a copper oxide nanoparticle solution.
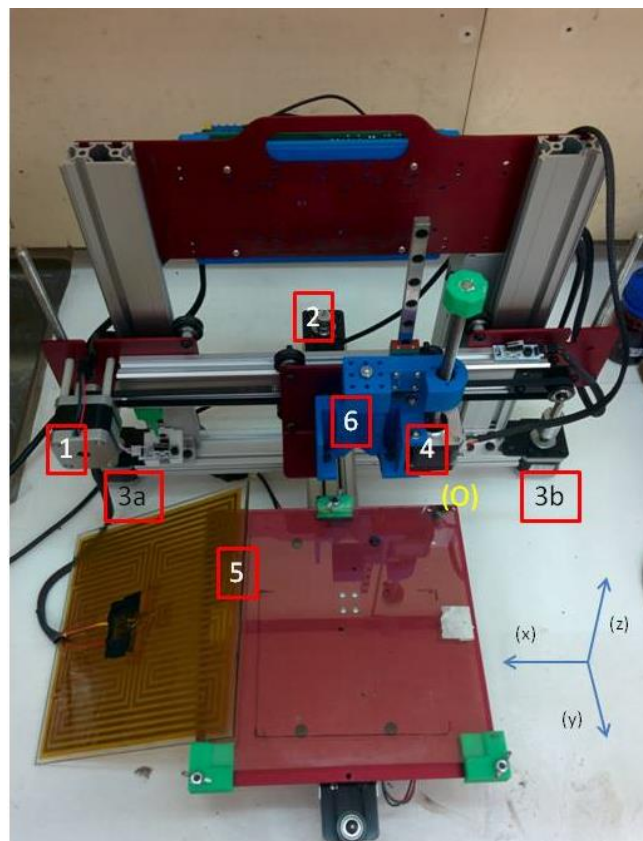
Figure 2.4. *The* Felix Coater-*3D printer, illustrated highlighting the main components.*

With the idea of reducing the coater's complexity, minimizing the cross-contamination in

the solution feed line and decreasing the waste materials by reducing the dead volume, additional modification were made. In details, an integrated syringe pump had been designed to feed the solution directly from the syringe to the slot-die head without any tubes, as shows in **Figure 2.4**, where the *Felix Coater*-3D printer is illustrated.

The basilar concept of the 3D printer is to convert the rotation in linear translation, in order to move the different components along the three *x*, *y* and *z* axes. The independent movements of each part give the desired deposition. The motor (1) allows the coating head (6) to move along the *x*-axis, while motor (2) allows the plate (5) to move along the *y*-axis: the revolution of the rotors is translated in linear motion by a rubber belt. Differently, the motors (3a) and (3b) are connected to ribbed supports that rotate, enabling the variation of the printing head along the *z*-axis. In a similar way, motor (4) operates the pumping system: during its rotation, it varies the level of the piston that pushes the syringe plunger and controls the ink deposition. As it can be observed in **Figure 2.4**, different plates are available, also with temperature control for a faster evaporation of the solvent in the application where a higher heat transfer is required. The three screws that support the plate are responsible for the plate leveling with respect to the coating head. This action enables to obtain uniformity in the thickness layers.

Regardless of what type of solution is utilized for the deposition, the coating procedure is performed always in the same way and involves the following sequence of steps:

1. The system dispenses a small amount of ink in order to fill the void in the coating head and to wet its end with fresh ink at home position.
2. The printing head moves from the home position to the starting point for the deposition at a safe *z*-axis height.
3. To create a solid meniscus and avoid problems related to the stripes' uniformity, a "kiss" action has been implemented. Practically, the coating head is lowered to a predefined height in order to touch the underneath substrate and make mechanical contact. At this point a small amount of ink is dispensed to form the meniscus.
4. The coating head lifts up until the deposition height determined by a Feeler Gauge.
5. The head moves along the substrate characterized by a constant velocity and a constant ink feed rate.
6. If the deposition requires more than one stripe, at the end of each one the head lifts up and repositions itself to the new starting point, reiterating from the step (1).

It is important to underline that the meniscus formation must happen instantly when the coating head touches the substrate, in order to avoid depositions starting at different positions. For this reason, step (3) has been implemented, creating a solid meniscus due to the physical contact between coating head and substrate. This additional action has had the

consequence to considerably improve the reliability of this coating technique.
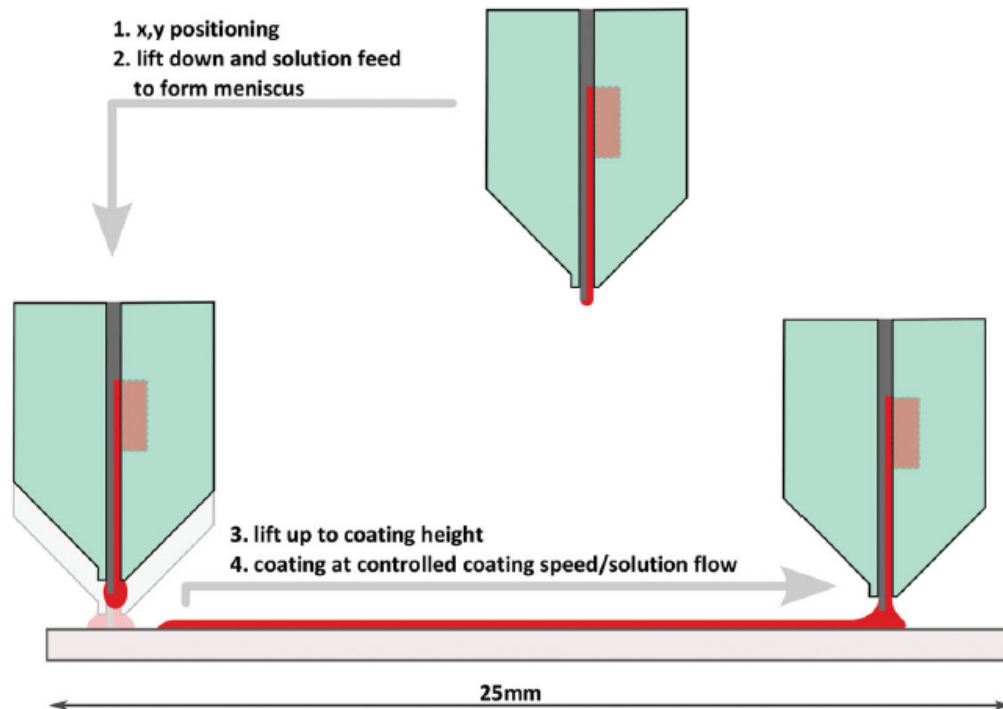
Figure 2.5. *Schematic representation of the stepwise sequence performed by the slot-die coating head during a typical deposition. Figure adopted from ([31]).*

A schematic illustration of the stepwise procedure for a single stripe deposition is reported in **Figure 2.5**, where the principal steps to perform a coating process are highlighted. It can be observed how the maximum coating length may be 25 cm, due to the maximum translation the supports can perform.

At the end, it is a lab scale apparatus, but it can be easily associated to a roll-to-roll concept without any difficulties. Furthermore, the implementation of 3 directions movements may make the difference with respect to a conventional slot-die system in a large area production.

2.2.2.1 *Felix Coater* Software Control

The 3D coater functions are controlled by a digital code. The most important advantage of a digital control is the capability to vary the deposition features without changing any physical part. For example, different patterns, speeds and solution feed rates are possible,

so different results can be obtained with the same solution. Furthermore, this feature strongly reduces the set-up time, which is one of the aspects that is more desired in manufacturing scale. Moreover, less material is wasted and the probability of cross-contamination is reduced with the advantage to obtain different results without replacing mechanical components.

The protocol associated with the machine was developed as reported by Vak *et al* ([*31*]) using a G-code formalism: it is a machine-independent standard, which means that the optimized printing conditions for a specific deposition can be transferred from lab to lab, from machine to machine, by a simple text file `.txt`. This can improve reproducibility and transferability of the results, by simply sharing the protocol's information. For fast processing, a script had been developed in order to easily convert the printing parameters in G-code format. The G-code generator interface is shown **in Figure 2.6**.
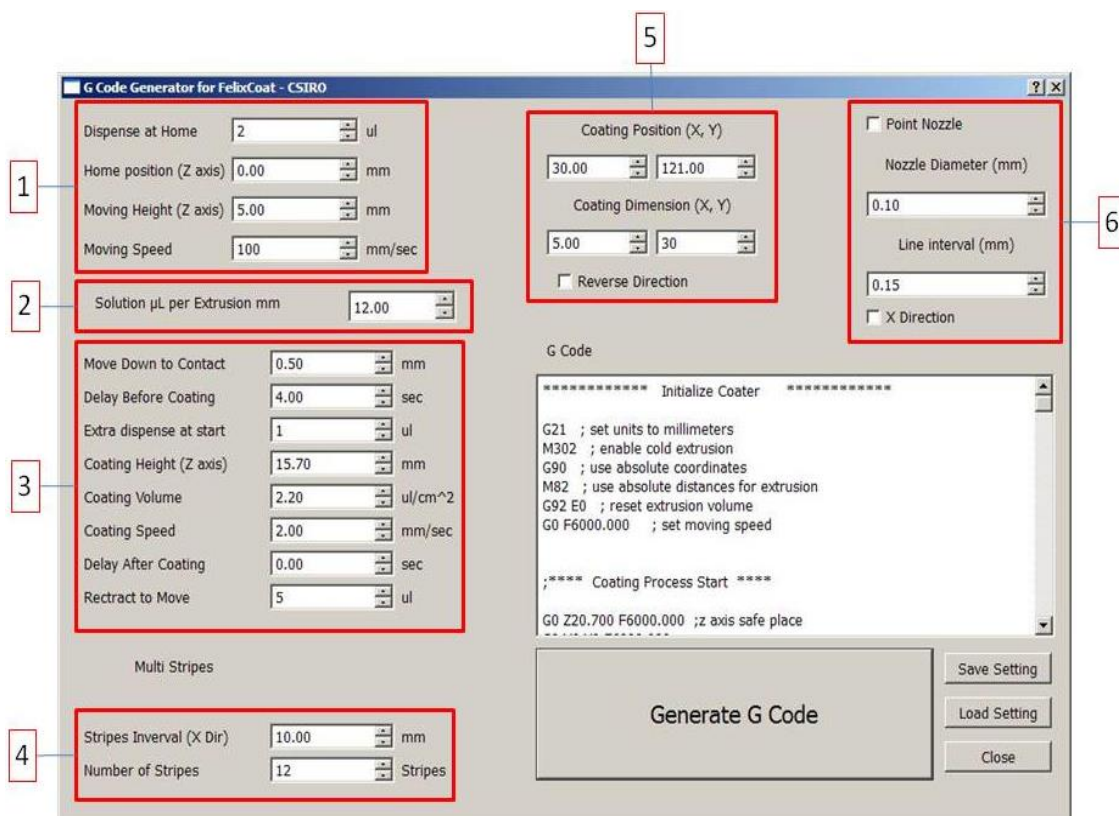
Figure 2.6. *The G-code generator software interface where it is possible to vary the printing parameters, in order to optimize the deposition.*

Many different options are available. In the first box (1), the values of the functions related to the main movements can be changed, for example moving speed, moving *z*-axis and home positions *z*-axis values, as well as the amount of ink dispensed at home position to refill the blade with fresh ink. The second, frame (2), refers to the ink feed rate. It can be easily calculated considering the height's variation of the piston, integrating part of the pumping system. It will be explained further on, when the coater interface will be introduced.

In the box (3), other coating options can be changed, based on the own first trials. Synthetically, the "kiss" step and the deposition's properties can be adjusted: for example, the coating speed and the coating height, two of the most important parameters for a uniform deposition, as well as the extra ink that is dispensed at the starting point in order to create the meniscus. It is fundamental to explain how these options are always customized after a first deposition experience: they are very sensitive to the solution properties and a repetitive adjusting process is necessary to find the optimal values for each set of experiments.

One of the abilities of the 3D coater is to move the coating head not only along one direction, but also on the perpendicular axis. In this way, many different stripes can be deposited, achieving a patterning characterized by parallel lines. This is useful in order to create more complex patterns or increasing the production rate of a single one, enabling a large-area deposition. Thus, the number of the stripes can be decided in the box (4), as well as the distance between each other. The details required for a typical coating process are completed by inserting the coordinates where the deposition starts and the characteristic of each line, so length and width. In fact, the coating plate is thought of as a Cartesian plane where the origin is placed at the coating head home position, which is situated in top-right corner of the plate as marked in **Figure 2.5** with (O). Box (6) is related to the use of a nozzle instead of a slot-die head, which was not utilized in this work.

In the code generator, the entire G code for the relative deposition is also reported in a smaller window. This involves a fast copy-paste of the protocol in the printing software interface, enabling to implement different G code sets: stripes with different parameters can be coated and a multilayer approach is made possible. The printing software has a Repetier-Host interface, as shown in **Figure 2.7**, by which it is possible to move manually the coating head, checking some parameters such as coating height or the starting point for the deposition. Specific controllers are highlighted in box (1). Under the commands for the *x-y-z* axis, the interface for the piston control is placed, as shown by box (2). With this functionality, it is possible to move up and down the support that pushes the syringe plunger during the deposition.
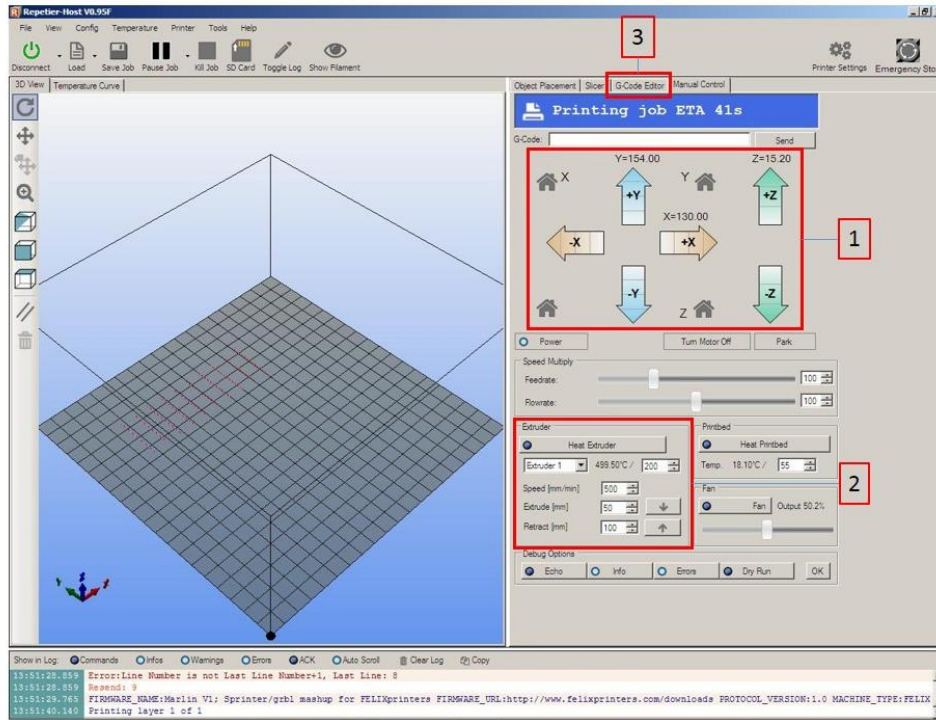
Figure 2.7. *The Repetier-Host interface, which allows to move manually the coating head and to implement the G-code sequence.*

The relation between the input data inserted in the software and the real height mutation can be calculated manually: it was found a proportionality factor (f_p) of 10. Thus, 100 mm in input correspond to a piston's movement of 10 mm. This enables to calculate the amount of ink dispense for each millimeter of variation required by the G code: the value must be reported in code generator, in order to obtain a higher accuracy in the quantity of solution dispensed in the coating process. If it is considered a 6000 µl syringe volume V_0, with a stroke (ℓ_0) of 50 mm, the corresponding variation ℓ_s for the printing software due to the proportionality factor will be (**Equation 2.1**):

$$\ell_0 \cdot f_p = \ell_s \ ; \tag{2.1}$$

so the amount of ink in µl dispensed for each "software" millimeter (*P*) is given by **Equation 2.2**:

$$V_0 \div \ell_s = P \ . \tag{2.2}$$

For the case considered in copper oxide deposition, ℓ_s is calculated as 500 mm and the relative amount of ink per "software" millimeter is estimated as 12 µl/mm.

This procedure is useful when a new type of syringe is used and a new relation must be defined: it enables to get the same results with different tools, improving the reproducibility and the transferability of the technique. In the box (3), the editor for G-code can be found.

2.3 Inkjet Printer

In many different coating techniques it is impossible to precisely define the right amount of solution necessary for each deposition, which translates into a huge quantity of waste materials. Moreover, several problems are related to the impossibility to create an on demand supply of ink. So a constant ink flow characterizes the deposition, limiting the maximum resolution that it can be obtained. With this in mind, inkjet printing tries to avoid such inconveniences. Its basilar concept is to dispense the ink in a "standardized" way, through a high frequency droplets formation of precise volume. In this way, more complex patterns are available, due to the capability to deliver the droplets in specific positions and only when it is required, with a fine control of the solution volume. Several advantages can be introduced by this technology ([32]): a higher resolution is now possible, enabling the fabrication of more complex devices, which allow to reach a further step in device functionality. Furthermore, the process is maskless, not requiring the presence of a physical shadow mask, in order to create the desired pattern. Moreover, the patterning can be easily digitalized: several different depositions may be made without changing any physical components, but only operating by a software interface.

The most important advantage that has been introduced by inkjet printing is the capability to deposit a wide range of different compounds without any issue. The formation of droplets requires some standard about ink properties (especially surface tension and viscosity), but it is an obstacle that can be easily avoided with a right formulation. In addition, the drop-on-demand (DOD) technology has grown up really quickly in the last decades, enabling to reach a pattern resolution and uniformity that had been never thought with conventional techniques. Additionally, because it can be easily implemented in a large-area R2R manufacturing process, inkjet printing is defined as a low-cost technology that can be scaled-up in an easy way.

2.3.1 Thermal and Piezoelectric Systems

Droplets formation can be obtained by different processes, but the most popular are the thermal and piezoelectric approaches. In the former, small air bubbles are created by ink

evaporation in a small chamber on the surface of a heating resistor. During the heating process, the amount of bubbles in the chamber increased, raising the pressure and enabling the ejection of a tiny drop when this reaches a threshold value. When the droplet is pushed out, the system suddenly drops the temperature, enabling the formation of a regular droplet. The ejection process lasts a few microseconds and temperatures up to 300°C can be achieved in the drops formation chamber [33] [34]. This process is very simple and can be easily implemented; however some limitations affect the ink choice. For example, the solvent must evaporate in the range of the temperature that characterizes the printing system; moreover, temperature-sensitive compound can't be printed due to the degradation process that occurs in the droplet's formation. For these restrictions, thermal inkjet printing is limited to commercial printers.

The latter is based on the effect of piezoelectric materials, such as ceramic crystals, which undergo a physical deformation, such as expansion or shrinkage, when subjected to an electric field. The nozzles system from which the droplets are ejected is designed as an ink reservoir and a small chamber separated by the piezoelectric material. When a precise electric charge is applied, the piezoelectric disk shrinks, enabling the solution to flow in the small chamber. After, by the expansion of the piezoelectric crystal due to the application of a specific voltage, the droplet is ejected. The electric field returns so to the starting condition avoiding the loss of more ink through the nozzles by restricting the chamber volume [35]. Piezoelectric systems have the advantage of operating at room temperature, as opposite the thermal technology, so several different compounds can be used in inkjet printing deposition without degrading their properties. The room temperature process is the aspect that has made piezoelectric systems very popular not only at the lab scale, but also in the large-area manufacturing.

An overall issue for inkjet printing systems derives from the micro-size of the nozzles utilized for droplet ejection. To reach a very high resolution, easily up to hundred dpi (droplets per inch), the volume of the droplets is usually around 10 pl. With this order of magnitude, clogging problems become very frequent. For example, aggregation of solid material may be incurred when a nanoparticle suspension is used or the solvent evaporation rate is very high. Sedimentation of the solid fraction of the ink may take place if stabilizing compounds are not present in the ink formulation.

2.3.2 Fujifulm Dimatix Material Printer 2831-2800 Series

The piezoelectric inkjet printer that was used for in this work is a Fujifilm Dimatix Materials Printer (DMP) 2831-2800 series. A 3D printer and a software control pre-installed in a desktop computer compose the entire system. It is conceived to move along the three axes, where a rubber belt, connected to the motor, allows the translation of the

cartridge carriage along the *x*-axis. Additionally, the plate can move along the *y*-axis by the rotation of a worm gear. The cartridge support, instead, enables the variation on the *z*-axis by lifting up the cartridge. This printer is quite complex, providing different options for an optimized deposition. For example, a cleaning pad is placed at origin position, in order to remove the excess of ink during cleaning cycles or after several deposition sequences. Moreover, the plate shows a vacuum system that enables flattened flexible foils, avoiding printing issues due to uneven substrates. **Figure 2.8** shows the Dimatix Materials Printer 2831 (**Figure 2.8a**) and the relative cartridge support (**Figure 2.8b**).

(a)   (b)
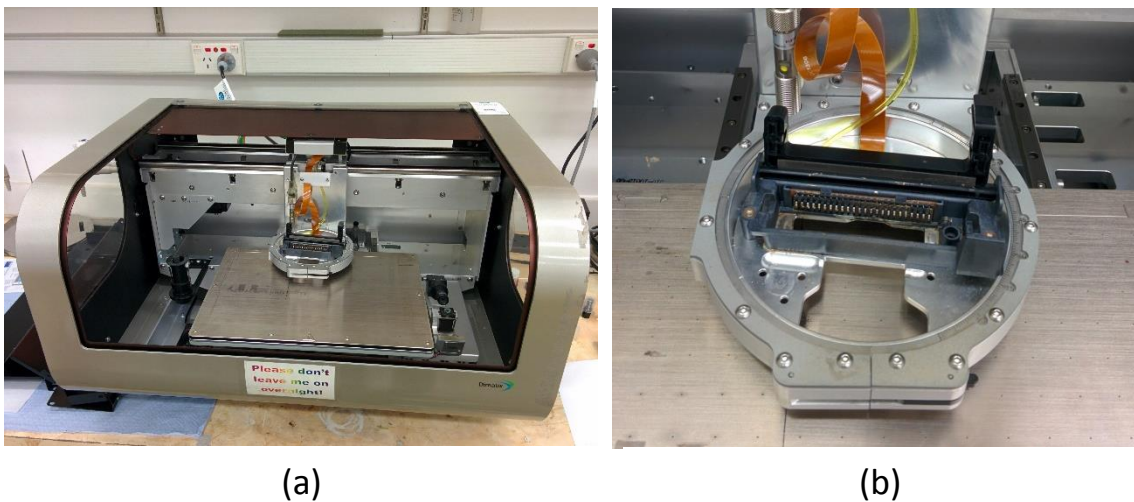
Figure 2.8. *The inkjet printer: (a) the entire system; (b) a particular of the cartridge carrier.*

In order to achieve optimum performance from DMP 2831, some particular characteristics are required. Referring to the jetting conditions, the viscosity must be between 10-12 cP, as well as the surface tension must place in the range of 28-33 dynes. Additionally, low volatility and a density higher than 1 are preferred to avoid clogging problems during printing process.

2.3.3 DMP Cartridges

One of the strengths of DMP 2831 is the capability to disconnect the 3D printing system from the solution apparatus. In fact, the cartridge is completely removable from the printing head carriage, in order to minimize the process steps when removing pre-existing ink and replacing it with another solution is necessary. This concept does not only simplify

the sequence to accommodate the cartridge, but also minimize cross-contamination, when different materials are being printed. For example, different inks may be used because the printing process involves the multilayer deposition of different materials, such as solar cells or OLEDs.

In **Figure 2.9**, a disassembled DMP cartridge is showed: it is composed by an ink reservoir with a volume of 1.5 ml and a printing head characterized by electrical connections, in order to apply the specific voltage to the piezoelectric crystals. The DMP cartridge features 16 nozzles arranged all in a row and it may differ for the volume of the droplet that is created: the one that was used for the electrodes deposition is the DMP Cartridge-16010, which enables the formation of a 10 pl droplets. For higher resolutions, cartridges with 1 pl droplet volume are available.
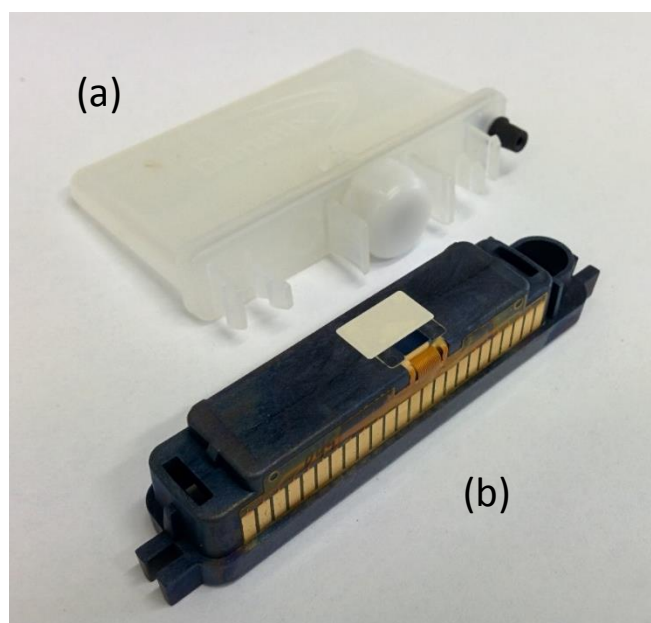
Figure 2.9. *A disassembled DMP cartridge showing the ink reservoir (a) and the printing head characterized by the electrical contact for delivering the specific voltage to the piezoelectric crystals.*

In order to avoid inconveniences during the printing process, the cartridge must be filled following a specific protocol, which avoids micro-bubbles formation that can obstruct the holes from which the droplet is ejected. The ink is sonicated then the cartridge reservoir is filled-up by a syringe with a specific needle provided with the cartridge. During this operation, it is important to filter the solution to remove possible aggregates that may clog-

up the orifices. At this point, the reservoir can be joined with the printing head: it was found really useful putting the cartridge in position that it assumes during the printing process, so with nozzles facing down, for at least half an hour. In this way, even if some bubbles form, they will migrate towards the surface of the ink.

2.3.3.1 Waveform and Cartridge Settings: Software Control

The piezoelectric concept is based on the application of a specific voltage variation in order to get a physical deformation of the piezoelectric crystal. The DPM 2831 software enables to create a customized voltage waveform by a waveform editor: each ink shows different properties and a waveform tool is necessary to vary the jetting conditions. For example, a minimum variation on solution's surface tension and viscosity may require a different behavior in the piezoelectric disk in order to achieve the best printing conditions.

A standard waveform is composed by four phases, as shown in **Figure 2.10**. Starting from a specific constant voltage, which slightly deflects the piezoelectric crystal for standby configuration (1), its reduction in the first segment moves the disk upward allowing the fluid to flows from the reservoir in the jetting chamber. Then, the charge suddenly increases in the second phase deflecting the crystal (2): the pressure in the chamber rises allowing the droplet formation. In the third and four segments (3-4), the voltage is finely decreased in order to easily control the piezoelectric crystal motion during drop breakoff.
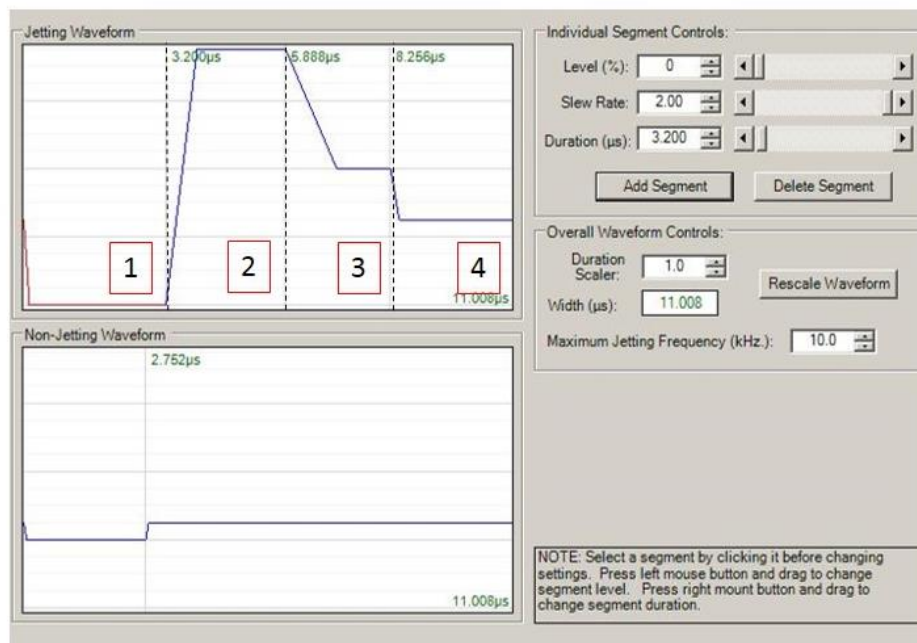
Figure 2.10. *Voltage waveform for jetting nozzles (top) and for non-jetting orifices (down).*

For each segment, amplitude, variation and length of the voltages can be regulated by specific commands, obtaining a depth control of the jetting process. A non-jetting waveform can be modified as well, referring to the standby situation or for the non-jetting nozzles.

The jetting behavior can be also influenced by the cartridge settings, which can be adjusted through the software in specific windows. **Figure 2.11** illustrates the different options that can be modified for every single cartridge, in order to obtain the optimal deposition.

If the customized waveform is applied to every nozzle because it considers the overall solution properties, the jetting process may be different for each nozzle. Due to slight variations of physical characteristic or local properties, the jetting behavior results differ for every orifice and for different cartridges. With this in mind, in **Figure 2.11a** it is showed how the firing voltage, the one that is applied for the droplet ejection, can be modified for each nozzle, defining a specific situation for every hole. Further parameters can be set, such as jetting temperature, in order to get the optimal conditions with temperature-depending properties, or the meniscus set-point. In fact, the printing system operates under pressure, keeping the liquid meniscus at the edge of the nozzle, avoiding ink losses due to some instability. Moreover, the number of the firing nozzles can be decided, eliminating those that are affected by clogging problems.

(a)   (b)   (c)
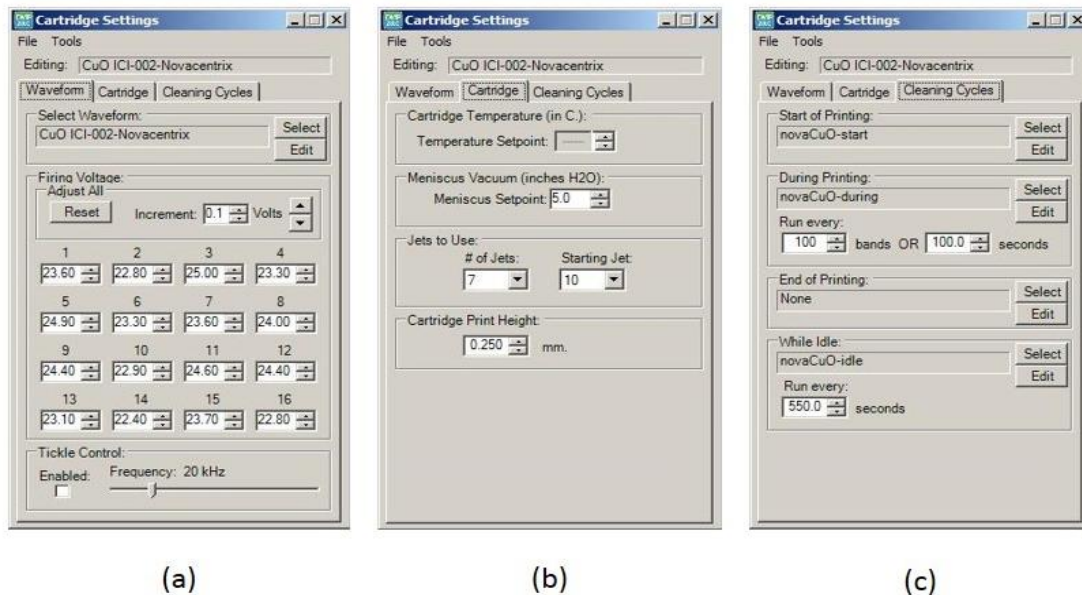
Figure 2.11. *Parameters that influence the deposition process. Firing voltage for each nozzle (a). Meniscus vacuum, temperature and printing height (b). Cleaning cycles settings, where three different actions may be applied: 1) spit, which enables to fire for a predefined time and frequency 2) purge for pushing the fluid through the nozzles at the pressure of 5 psi 3) blot, which means making the cartridge in contact with the cleaning pad (c).*

Other parameters that can be selected are the printing height with respect to the underneath substrate (see **Figure 2.11b**) and an optional cleaning cycle, which can be implemented at various stages of the printing sequence in order to avoid the nozzles clogging (**Figure 2.11c**). A "Drop Watcher" function is implemented in the software interface, enabling to observe the droplets formation and their jetting behavior: this allows to adjust the printing parameters in an on-time view of the jetting process.

For waveform and cleaning cycles' editors and for the cartridge settings, specific files are created in output, respectively with `.csv`, `.clc` and `.jst` file formats. This means that, for each cartridge, a specific configuration can be associated. It is determined by the particular conditions that occur in the use of the specific printing head and it can be uploaded every time the same cartridge is used. Moreover, the capability to refer to external files separates the printing optimization for a specific solution from the equipment that is utilized, enhancing the results' transferability of the same ink in different environments and situations.

2.3.3.2 Pattern Editor

In addition to the features introduced in § 2.3.2.2, a pattern editor is also implemented in the software control, as shown in **Figure 2.12**.
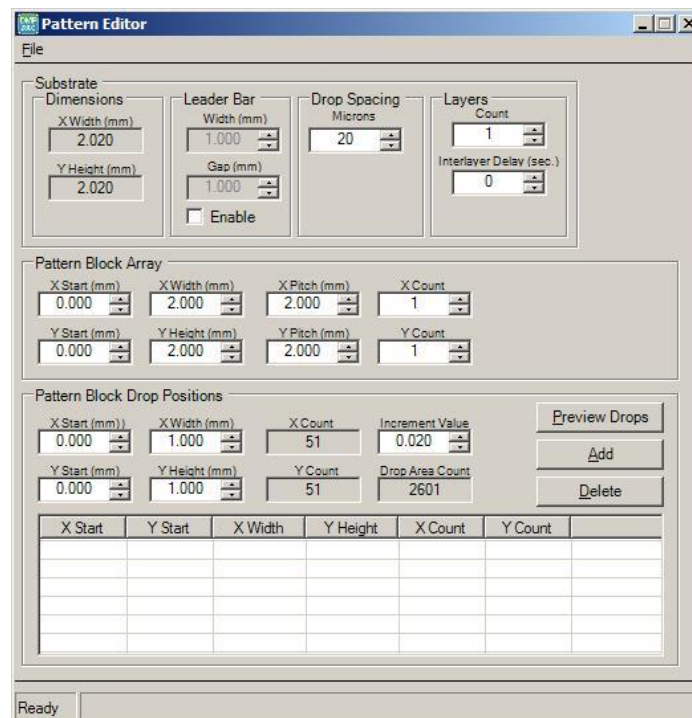
Figure 2.12. *DMP 2831 pattern editor, where it is possible to create a customized design defining the size for each segment, drop spacing and layers' number for the entire deposition.*

This tool operates in two different ways: in one hand, it can digitalize in its code an external image, which can be uploaded in `.png` or `.gbr` file formats. On the other hand, it enables to create its own design by simply creating a pattern conceived on a coordinates system. Thus, starting from the origin, which is place in the top-left corner of the plate, it is possible to decide the droplets positions and create specific patterns.

The patterning creation is based on a block concept, where a single block can be defined and then repeated in order to generate a block array: it is a useful functionality when it is necessary to obtain a multi-device production or when a large-area device shows a repetitive scheme. On top of this, the number of the layers that have to be deposited may be decided, as well as the drop spacing. In fact, the printing head nozzles are arranged in a row with a space between holes of 254 μm. Thus, the longest distance that can be set between each droplet must be the same distance between every nozzle. But for higher resolution, a smaller spacing may be necessary; therefore, a different value can be inserted in the pattern editor. The range in which the drop spacing varies is defined between 5 μm and 254 μm. In order to physically change the nozzle's distance, the software gives in output the angle that the cartridge must be assume with respect to the printing direction (which is along the *x*-axis) for a particular drop spacing.

As all the editors are implemented in the DMP 2831 software, the pattern editor creates in out a specific file, in `.pnt` file format, which may be transferred and uploaded in similar printers, enabling to obtain the same deposition in different laboratories.

2.4 Flash Processing

Nowadays, plastic substrates are the standard for the fabrication of flexible devices in a roll-to-roll process. However, the most important limitation that is related to their use is their maximum process temperature, which must be under their glass transition. Above this value, in fact, the plastic foil softens and eventually melts or decompose, and this is obviously not ideal for a flexible device, where the substrate has to provide support to the active layers. Moreover, if the plastic substrate has some specific functionalities other than supporting, they may be compromised.

Some processes can avoid this problem because they take place at room temperature or under the T_g; however, for other applications, especially for sintering metallic nanoparticle for the fabrication of conductive electrodes, high temperature annealing is required and therefore conventional methods are not applicable anymore ([29]). For example, thermal sintering in a furnace, electrical resistance sintering and microwave sintering are characterized by some disadvantages. Thermal sintering is time-consuming and affects all parts of the flexible device, giving poor results because it is not an area-specific process ([36]). The microwave sintering can reduce the fabrication time, but it shows the same

temperature limitations of the previous one. Electrical sintering could be an alternative, however it can be applied only under certain conditions of the electrical properties of the materials.

In this context, photothermic processes are rapidly emerging as a mean to solve these issue, due to the capability to reach elevated temperature only in confined areas, without involving the plastic substrate. Moreover, they are extremely fast and can be easily applied to a roll-to-roll point of view, enabling to keep under specific value the process variables, for a more affordable device's fabrication.

The basilar principle for photonic curing applications is a selective heat generation within a material caused by the absorption of high energy visible light pulses (0.1-10 ms) by the active material itself ([37]). Materials that do not absorb light in the visible range of the electromagnetic spectrum, are hardly affected by this photo-curing process. In this view, most plastic substrate do not absorb in the visible range, so they are not modified by the process. In contrast, many of the active materials in flexible electronics, especially metal nanoparticles used to deposit the electrodes, show a very strong absorption bands in the visible. When the spectrum of the light source and the absorption one of the conductive material are matched, the energy supplied to the desired area is maximized. The heat generation is achieved through the dissipation of the energy supplied by the very short light pulse by non-radiative energy and exothermic photochemical reactions. Due to the low heat transfer rate involved in the process and the transparency in visible light range, the plastic substrate is affected only partially by this phenomenon, so, it remains practically at room temperature or just above.

In addition to enabling the low temperature curing of active materials on plastic, this technology introduces two other main advantages ([38]). Thin films can be cured in a faster way with respect to the conventional methods, influencing the fabrication process and making photonic annealing suitable for in-line placement with existing printing processes. Moreover, its transient nature enables the formation of new types of films on plastic substrates, through the control of the temperature by photonic energy modulation. In fact, since most of the thermal processes depend on the Arrhenius temperature law, the annealing rate is related to the exponential of the temperature. Thus, a short process can easily replace a time-consuming process. This is the reason why a single fast light pulse, from which derives the denomination of intense pulse light (IPL), can achieve great results in milliseconds, resulting in a "flash" processing.

2.4.1 Process Mechanism

Usually the system involved in the IPL process is characterized by a thin film of thickness x_f, with a thermal equilibration time τ_f, which is deposited over a plastic substrate of

thickness x_s and thermal equilibration time τ_s. The respectively thermal equilibration times can be calculated by the thermal coefficients as in **Equation 2.3**:

$$\tau_i = \frac{c_i \rho_i x_i^2}{4 k_i} \quad . \tag{2.3}$$

Where c_i is the heat capacity in J/K, ρ_i is the density in kg/m^3, x_i is the thickness in m and k_i is the thermal conductivity expressed in W/(m·K).

For an optimal flash processing with duration of t_p, it has been demonstrated that three transient conditions must occur ([38]) as the following **Equations 2.4-2.6** explain:

$$x_f \ll x_s \quad ; \tag{2.4}$$

$$t_p \ll \tau_s \quad ; \tag{2.5}$$

$$\tau_f \ll t_p \quad . \tag{2.6}$$

If these conditions are verified, the surface of the substrate that is in contact with the film reaches a temperature far beyond its maximum working temperature for only a few milliseconds – a time scale that is too short to modify its properties due to the heat generation. This means that the thickness of the film must be much smaller than that of the substrate in order to allow the plastic foil to dissipate the heat generated fast enough due to its higher mass (**Equation 2.4**). Furthermore, **Equation 2.5** imposes process duration much smaller than the thermal equilibration time, not allowing the pulse to heat up the substrate bulk, which has the time to reduce the thermal gradient with its mass. The third condition showed in **Equation 2.6** explains how a little amount of energy is necessary to process the film.

Figure 2.13 represents a numerical simulation that explains the temperature variation as a function of time for a system composed of a 1 μm thick silver film on a 150 μm thick PET substrate. As already said, a high peak of temperature characterizes the film, as opposite the substrate surface in contact with it, which shows a very small temperature change. This is because the plastic support does not absorb in the light spectrum. The relative high mass of the substrate with respect to that of the film is responsible for the negligible variation in the temperature in the bulk of the substrate.
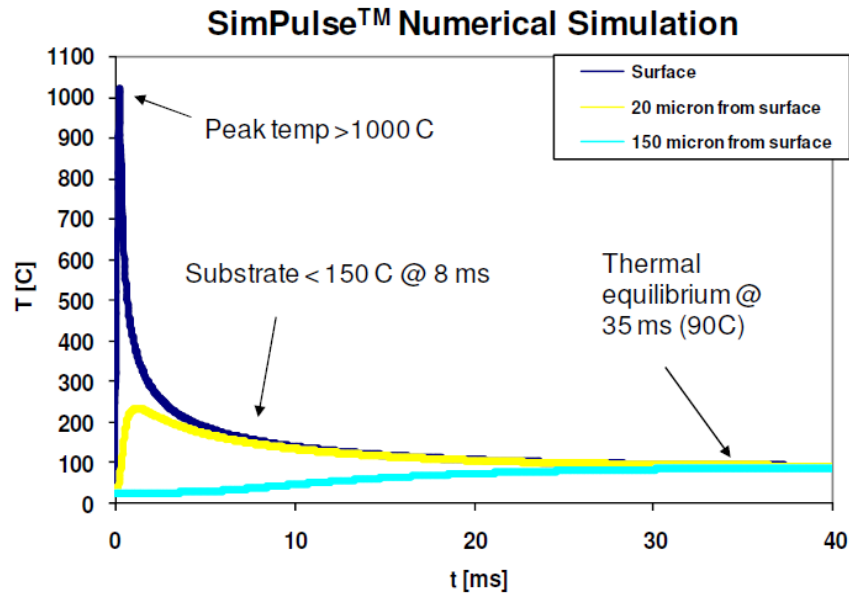
Figure 2.13. *Thermal simulation for an intense pulse light annealing (300 µs, 1 J/cm²) for a 1 µm thick silver film on 150 µm thick PET substrate. This can easily reach temperature beyond 1000 °C without showing any damage. Image taken from ([38]).*

However, flash processing shows some limitations. If the energy supplied to the system is too high, the substrate does overheat at the contact with the absorbing layer and permanently changes its properties, causing inconvenient such as wrinkling of the surface. To avoid this phenomenon conductive and convective heat transfer are beneficial. Furthermore, reducing the time process means that the processing temperature must increase. When energy delivered to the sample is too high, the temperature reaches a value above the gasification temperature of the substrate and the film is lifted off. Supplying too much energy involves another limitation: if the film is too porous, characterized by a huge amount of solvent or has volatile binders, a high radiant power implies a cohesive failure of the film. In order to avoid this problem, a pre-drying process may be necessary, with a lower radiant energy.

2.4.2 Flash Processing Equipment

Xenon Sinteron 2010-S is the equipment that provided the intense light pulse for the copper oxide nanoparticle electrodes processing. It is composed of 2 main parts: the controller, which supplies the electric power and allows to set the flashing parameters, and the lamp box, an enclosed chamber which is divided in two parts: the top parts accommodate the

lamp itself and the bottom is provided with a tray to position the samples, as shown in **Figure 2.14**, where the space to accommodate the samples and the flash lamp are illustrated.

(a)   (b)
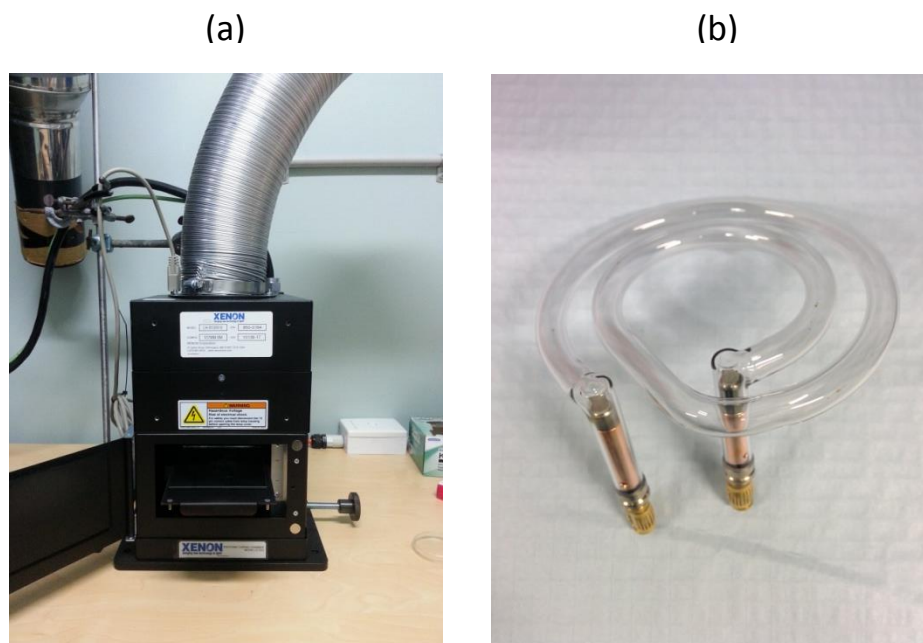
Figure 2.14. *Xenon Sinteron 2010-S lamp box: the samples are place below the xenon lamp in a specific tray (a), while the lamp (b) is installed on top providing the flash pulse on the layer top-face. Characteristic the circular shape in order to keep constant the intensity.*

To complete the entire apparatus, an air cooler is connected to the lamp box, providing the cooling system, and an exhausted collector is placed just above it, in order to aspire all the gases that come out from the sintering processes. It must be taken in consideration the high energy supplied to the system enables oxygen reactions, which may form ozone traces. Moreover, most of the films treated by IPL processing shows high solvent content, with the consequence of elevate hydrocarbon vapors.

The basilar principle is the application of a defined electric field to a xenon lamp: the controller supplies the desired voltage which is released to the lamp for a specific pulse time. The resulting flash spectrum depends on the compound that is excited: the one that characterized Sinterion 2010-S lamp is illustrated in **Figure 2.15**.

It can be observed how the energy released by this process is very high, because not only the visible spectrum is involved, but also the UV range: the smaller is the wavelength, the

higher is the energy associated to the electromagnetic wave, as define in **Equation 2.7**:

$$E = \frac{h}{\lambda} c_l \quad .$$ (2.7)

Where E is the energy associated to a specific wavelength in J, h is the Planck's constant in J·s, c_l is the speed of light in m/s and λ is the wavelength in m. However, the peak emission of the lamp is ~500 nm, so the maximum energy is delivered on samples absorbing broadly in the visible range, as explained before.
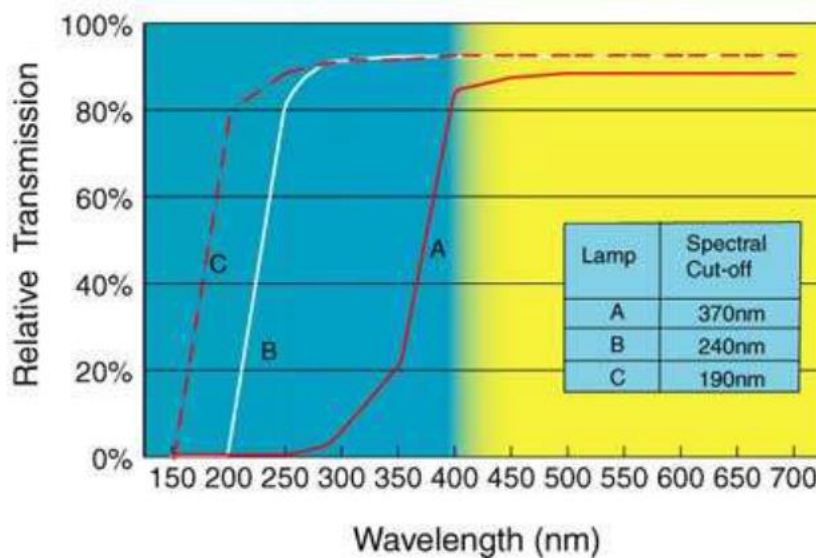
Figure 2.15. *The lamp installed in the Xenon Sinteron 2010-S is the type C, so it can been observed how it spectrum involves not only the visible part but also the UV range, providing more energy with respect to other commercial lamps. Figure taken from Xenon Sinteron 2010-S manual.*

The sample distance from the lamp can be regulated at the desired value, however the energy efficiency, the amount of incidental energy per energy released, is maximum at 1 inch from the lamp window, which correspond to the focal plane of the lamp; as shown in **Figure 2.16**, where the percentage of light intensity in function of the distance (in inches) from the lamp is reported.
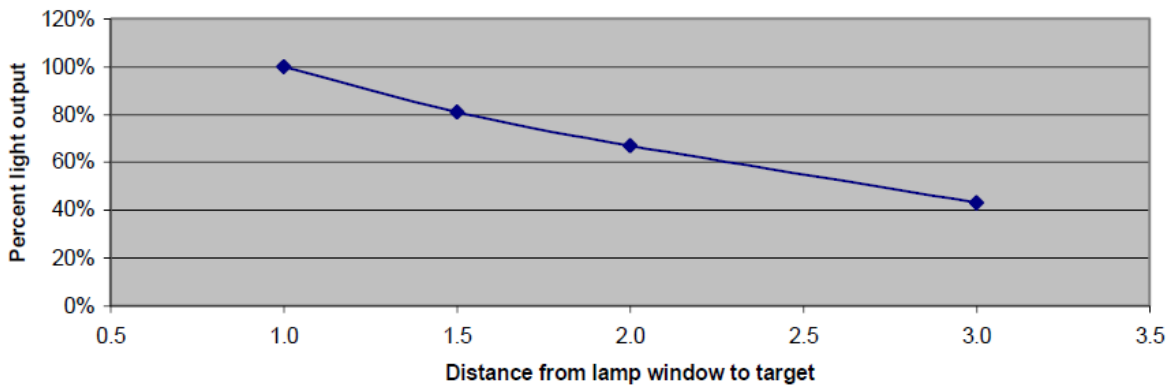
Figure 2.16. *The graphic represents the intensity of light in percentage with respect to that is emitted from the lamp as a function of the distance from the lamp window. The distance is taken in inches. It can been observed a maximum intensity at 1 inch from the lamp. Image taken from Xenon Sinteron 2010-S manual.*

Moreover, the light intensity shows a non-constant distribution on the plane where the sample is placed: even if the xenon lamp has a spiral shape which should provide constant illumination over a circular footprint, there is a radial distribution of the emitted light, with the highest emission delivered at the center (1 inch diameter), and progressively decreasing moving towards the edge of larger footprints.
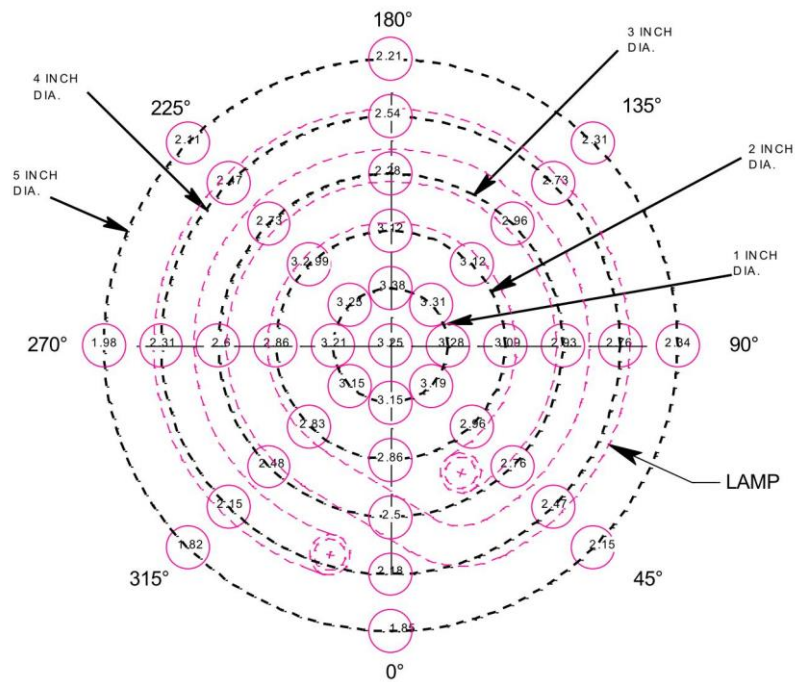
Figure 2.17. *Light intensity distribution over 5 inches surface, for a single pulse at 830 electrical joule delivered and at 1 inch from the lamp window. The maximum intensity reached is 3.38 J/cm².
The result is obtained with a 107 mm spiral lamp. Image taken from instrumentation manual.*

The production company has measured the light intensity distribution over 5 inches diameter, at 1-inch distance from the lamp window, for a single pulse of 830 electrical Joules, as shown in **Figure 2.17**. The light intensity is defined in J/cm^2.

2.4.2.1 Parameters Settings

The Sinteron 2010-S equipment provides an analogic control of the parameters that characterize the process. Many are the variables that are involved in the flash light creation: the voltage V is one of the most important, it is defined in kV and can be set between 1.9 kV and 3.1 kV. In this range, the smallest variation possible is 0.05 kV. The pulse duration may vary from the lowest value of 100 μs to the highest one of 2000 μs with a minimum variation of 5 μs. With these two parameters is possible to calculate the amount of electrical energy is supplied to the lamp apparatus, defined by the following experimental **Equation 2.8**:

$$E = (\frac{V}{3060})^{2.3} \cdot 0.938 \cdot t \quad .$$
(2.8)

Where *E* is the energy in J, *V* is the voltage in Volts and *t* is the time in μs.
Other parameters are related to the capability of the instrumentation to deliver not only one pulse, but also a sequence of flashes. In this case, a period between each pulse can be defined, with a range as well as the number of pulse are necessary for the process. The period may be decided in the range of 1 Hz to 10 Hz, with an increments of 0.001 Hz. The number of pulses can be decided without any limitations. As a matter of fact, different pulse modes can be defined: a SINGLE pulse mode is the standard option, where the only parameters are the voltage and the pulse width. A second mode is the DOUBLE mode: two pulses are automatically implemented and a period must be defined, in addition to the voltage and the width of each pulse. Furthermore, a BURST mode might be chosen, considering the fact more than two flashes can be delivered: in this case an additional parameters is introduced, the number of the pulses that will characterize the process. However, in this mode all pulses have the same width and period. Based on this, a CONTINUOUS solution can be set, where the choice about the number of pulses disappears and a limitation in the period between each pulse is applied. In fact, same flash conditions are repeated infinite times, however the cooling system does not cool the system fast enough when the energy delivered is too high per unit of time.

Summary

In this chapter the details regarding the ink formulations, substrates, printing equipment and flashing equipment used in this work have been outlined. In the following chapters, these materials and concepts will be utilized to better understand how to fabricated printed copper tracks using a photosintering approach.

Chapter 3

Deposition and Flash Processing of Copper Oxide Nanoparticles

This chapter describes the optimization process that led to homogeneous and uniform CuO depositions, and the effect of the exposure of such coatings to intense light pulses, achieving reduction of CuO to Cu and eventually sintering of the metallic deposits to create conductive patterns. Several characterizations techniques have been used to assess the uniformity, quality, morphology, structure and functional properties of the prepared samples in order to obtain an in-depth understanding of both the printing process and the flashing effect.

3.1 General Materials Preparation

The copper oxide nanoparticle ink received from Novacentrix™ is especially made for inkjet printing, in particular is optimized for Dimatix Materials Printer 2831-2800 series. Initially, the ink as received was ultrasonicated with an Ultrasonic Cleaner for 15 minutes: this operation enabled to break the nanoparticle aggregates that could influence the printing process, especially in the case of the inkjet printer. This technology is very sensitive to clogging problems that may occur during the deposition, as reported previously in §2.3.2.1, where sonication and filling cartridge procedure were firstly reported. Such ink preparation may seem very simple and trivial, but it is substantially efficient to reduce most of the blocking problems. Even if the slot-die printing is not as sensitive to clogging, a similar sonication procedure was applied to the ink for slot-die coating as well, mostly to avoid inhomogeneous depositions. Particular attention was paid to the sonication process: it is a high-energy physical treatment that can increase the local temperature very quickly due to the effect of the ultrasounds. If the water bath in which the solution is immersed in not enough to disperse the heat generated, the temperature can reach high values, influencing the ink properties. In fact, it can alter the ink behavior, changing for example viscosity and density, which are temperature functions. Also, the low-boiling components of the ink may evaporate. If it happens, the right conditions for printing may be not satisfied anymore.

As far as the printing substrate is concerned, no information was given about pre-coating procedures: however, a 5 minutes UV-ozone treatment was performed in order to remove any possible surface contaminants. As a rule of thumb, an UV treatment may improve the adhesion of the deposited film to the plastic substrate, but in this case, Novele® already improves it involving a porous layer, where the solution can permeate creating a solid interaction with the plastic foil.

3.2 Inkjet Printing Optimization

For the inkjet printing, it was necessary to define a cartridge setting with a customized waveform, in addition to a sequence of cleaning cycles, in order to get a fine deposition. The Novacentrix™ provided these settings, because they were already defined during ink formulation. However, some changes had to be done in order to optimize the jetting behavior with the DMP 2831 printer and the specific cartridge we adopted. Some adjustments were made for the single nozzles firing voltage, as well as for the cleaning cycles: it was important to keep the right jetting conditions constant. With this in mind, a customized cleaning procedure was useful to avoid solvent evaporation, refilling the nozzles with fresh ink, and to detach some solid particle from orifices, by the purge option. Optimal jetting conditions were found, as demonstrated in the **Figure 3.1**, where it can be seen that part of the firing nozzles have a perfect jetting behavior, without any problems in the droplets formation and in their direction. The image was captured by the Drop Watcher function, which became very useful to monitor real-time changes in the ink's properties. In fact, it allows adjusting the parameters value having a direct comparison with the real effect on the droplet behavior.
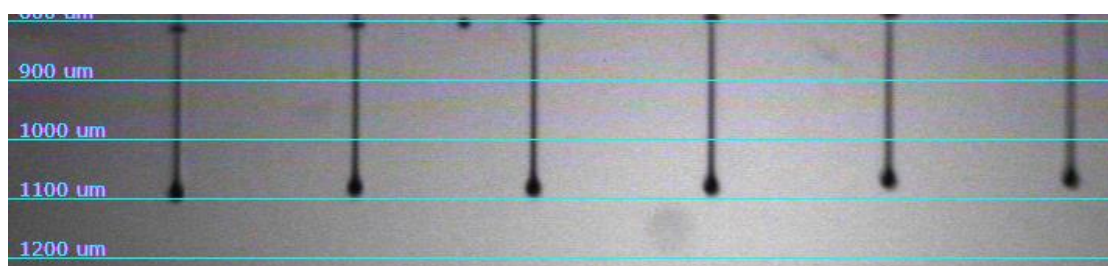
Figure 3.1. *The Drop Watcher snapshot that enables to observed the droplets formation and their jetting behavior. The drops are characterized by similar jetting speed in order to obtain a proper deposition.*

All the cartridge parameters were saved in `ICI-022-master.jst` file, while the cleaning sequence was defined by three components: `start.clc`, `during.clc` and `idle.clc`. They are respectively the settings of the start cleaning cycle, the cleaning cycle operated during the deposition after a predefined time range and the cleaning cycle for the non-firing nozzles or the standby situations. Also a customized waveform was saved as `ICI-022-master.csv`, as shown in **Figure 3.2**.

Figure 3.2. *Characteristic voltage waveform utilized for the inkjet printing deposition. This particular shape enabled to achieve an optimal jetting behavior.*

In order to investigate the best printing conditions, it is clear that the cartridge settings, as well as the cleaning cycle, couldn't be modified further because they were optimized for the best jetting behavior. With this in mind, the best way to modify the printing conditions in order to achieve the highest deposition quality was to change the drop spacing with respect to the same pattern. A 3 cm length and 0.5 cm width single line was drawn through the pattern editor, in order to obtain a suitable sample for further analysis. At this point, the drop spacing was varied between 10 μm and 50 μm with an increment of 5 μm for each different deposition, obtaining a sequence of pattern files named `3x05cmLineXDropSpacing.pnt`, where the X is replaced every time with the relative drop spacing value. **Figure 3.3** shows the different lines deposited with different drop spacing.

It is easy to understand how the different spacing between each droplet can influence the final results. Small drop spacing means a higher concentration of droplets per unit of area (high dpi), resulting in excess of ink and as a result a thick stripe with a lot of trapped

solvent. This is valid for the drop spacing from 10 to 15 μm, the three first lines from the left end of **Figure 3.3**. As opposite, a large distance among the drops leads to a non-continuous film, as showed in the right end stripes of **Figure 3.3**. The samples look uniform along the printing direction, but in the perpendicular one, the droplets are deposited too far from each other. Such conditions are not suitable to achieve a uniform film, especially considering the final purpose of these coatings, which is the production of continuous and conductive copper traces.
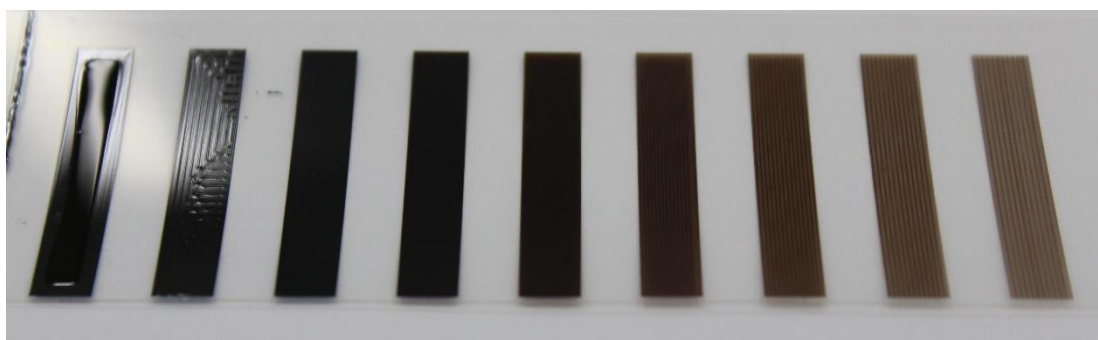
Figure 3.3. *Sequence of inkjet printed lines characterized by equal ink formulation but different drop spacing. It can be observed that for small drop spacing the stripes are still wet (left) because the higher amount of drops dispensed per unit of area. Conversely, for larger drop spacing the lines are not uniform, showing a preferred direction. The optimal conditions are found at 20 μm and 25 μm drop spacing.*

The lines with a drop spacing of 20 and 25 μm, showed the best conditions in terms of droplets uniformity and final homogeneity of the deposited films. The flash processing also confirmed that the coatings prepared with such drop spacing had the best quality: the stripes were flashed all at the same pulse condition in order to obtain a uniform copper film. However, only for the 20 and 25 μm drop spacing lines the resulting film was acceptable, and therefore these drop spacing were the ones chosen for further investigations. For further information about the flashing conditions see §3.4.2.

3.3 Slot-Die Coating Optimization

Samples of similar size were prepared by slot-die deposition. The blade is 0.5 cm long, fixing the coating width. Furthermore, the stripes' length was designed to be 3 cm, in order to obtain samples of suitable sizes for further characterizations.

3.3.1 General Coating Conditions

The most difficult part in slot-die coating is the absence of theoretical principles and experimental studies for the deposition of nanoparticle inks by a slot-die technology. Some investigations have been performed using polymers or small molecules for organic optoelectronic devices, but in this work a complete different system (colloidal nanoparticle ink) was employed. The different nature in terms of inorganic compound, the different behavior by a fluid dynamic point of view due to the two phases involved (solid and liquid), the different stability of nanoparticle in a mixture of stabilizers, the different viscosity and density, all impose unlike different approach with respect to the one assumed with organic materials for organic electronics.

Therefore, the deposition optimization is based on a constant optimization process: all the different parameters were varied in order to obtain an optimal deposition. This involves analysis of different steps during deposition. One of the most important part is the meniscus formation, which can be assured by dispensing a small amount of ink at the moment in which the blade is in physical contact with the substrate. Upon lifting the coating blade to initiate the deposition (see §2.2.2), if the blade is not supplied with enough solution, the meniscus does not form because the surface tension of the ink promotes the separation of the liquid phase between the blade and the substrate. Conversely, if the ink is much more than the amount needed, the excess will influence the first part of the film, which would result thicker and wider respect the rest of the line.

The contact time is also important in the meniscus creation: the longer the blade stays in contact with the plastic foil through the "kiss" action, the better it is for the meniscus to stabilize, avoiding its disappearance when the coating head lifts up starting the deposition. Obviously, this time must be coherent with the production time, which has to be as short as possible.

During the deposition the meniscus must be kept stable for all the distance required. With this in mind, the coating speed and the coating ink volume feed to the blade are of particular importance. At high coating speeds the meniscus suffers from instability and often "disappears", not allowing a complete deposition. Similarly, at low coating speeds the solid particles dragged by the motion of the coating head generate a sort of friction with the substrate, dissipating the surface energy necessary to keep stable the meniscus. For the conditions involved in the copper oxide nanoparticle ink deposition, a speed of 2 mm/sec was found adequate in order to perform an optimal coating process.

Analyzing the coating volume, the relation that gives the amount of ink to be fed in order to get the desired film thickness was hard to find. However, it was observed that the ink feed rate must be above a certain value to assure a uniform deposition: it seemed that other phenomena were involved during the coating, so not all the solution dispensed by the

coating head was deposited on the substrate. For example, solvent evaporation certainly takes place, decreasing the solution flow that can reach the substrate: the solvent must evaporate anyway after the deposition, but during the coating it has the important function to stabilize the solid particle and keep them suspended, and also to maintain the fluid dynamic properties of the ink. As a first approximation, the ink flow rate dispensed through the coating head must be equal to the rate of the deposition of the ink on the substrate, but also considering the action of the solvent evaporation. Therefore, a threshold value where the input ink is equal to the deposited ink plus the dissipations terms must be reached. Theoretically, this is also the condition when the minimum thickness is reached: above this value the ink mass balance presents an accumulation term. The excess of ink that is feed to the system is deposited, creating a thicker film. So it does not only influence the system behavior during the deposition, but also the final results.

Another aspect that may be affected by ink feed regulation is the excess of solution that characterizes the final part of every stripe. As a matter of fact, when the coating head reaches the end of the deposition, the ink keeps flowing through the head, accumulating solution and causing a backflow effect. This is characterized by an ink back motion due to gravity along the film already deposited, varying a lot its final thickness. In order to minimize this problem, the function that enables the coating head to wait at the end of the deposition was set to a zero value.

An in-depth knowledge of all the phenomena that occur in this process, such as meniscus creation and solvent evaporation, would give the capability to finely control the ink deposition. This may lead in one hand to optimize the film properties as a function of its thickness, making them constant along the stripe by uniform process. On the other, it may reduce the amount of waste material, decrease the production time and increase the overall process efficiency. Additionally, the role of the parameters, the reservoir and the pumping system must be fully understood in order to be able to predict and model the behavior of the slot-die printed coatings.

However, every deposition showed the same principal characteristics: the film results uneven, due to the excess of ink dispensed at the starting point and at the end of the stripe. Moreover, the meniscus becomes stable only after one or two depositions, maybe due to transient starting conditions. So, every time the coating head returned to home positions and started a new deposition, an unstable process affected the initial lines.

3.3.2 Ink Dilutions

Differently from the inkjet printing, in slot-die coating there aren't specific limitations to the ink properties. They can vary within a wider range with respect to the small windows that characterizes the inkjet process, in which viscosity and surface tension have a

fundamental role. This means that the solution formulation can be modified, without affecting the stability of the coating behavior. As a matter of fact, when the solution properties change, some adjustments have to be made, but a proper deposition can be obtained anyway. This is in direct contrast with the inkjet printing, where a slight variation of the solution can prevent the droplets formation.

This is an advantage for the user, which can optimize the deposition and the film properties not only changing the coating parameters, but also trying different solutions. For example, decreasing the density means less solid particle per unit of volume, leading to a thinner film, due to the evaporation of most of the solvent after deposition. For this reason, three different formulations were created, obtaining different outcomes. Considering ethanol as a solvent for its high affinity with Metalon®, the original ink was diluted respectively at 50% and the 75% in volume of the solvent. The mixtures that were obtained showed less density and viscosity, as expected. However, the coating conditions optimized for the concentrated solution can be suitable also for the diluted ones. This allowed comparing stripes deposited with different solvent contents but with the same coating parameters.

In order to always create the same coating conditions, they were reorganized in a G-code file, named as `3x0.5cmLines.txt`, and uploaded in the software interface for each deposition. The values for the optimal setting were saved, as well as the number of lines to coat in a single process: it was decided to create a twelve line pattern. This quantity of samples were recognized as a good distribution in order to evaluate the coating stability and, most important, its reliability. The process was fairly reproducible, showing almost the same behavior in every occasion. However, there are few points that deviate from the average result as in every experimental situation.

Figure 3.4. *The comparison between the slot-die deposition of three different formulation: original ink (left); Ink diluted at 50% in volume of ink (middle); ink diluted at 75% in volume of ethanol (right). It can be observed an increase of light-brown coloration with the increase of solvent content and reduction of solid particles.*

Figure 3.4 shows the stripes obtained by the three different solutions. It can be observed that the original ink leaded to a thicker line, resulting in a dark-black color. Furthermore, the lines characterized by diluted ink tend to a lighter color. This depends on the nanoparticle contents: the lower the nanoparticle concentration is, the thinner the film is, causing lower light absorption.

Similarly to what was done for inkjet printed lines, the flash processing can give an idea about which samples can be suitable as copper electrodes, showing a good mechanical stability and good electrical properties. The flashing parameters were assumed the same with respect to the ones chosen for the inkjet printing samples, as reported in §3.2. The flash processing determined that the original, non-diluted ink leaded to coatings too thick for the fabrication of copper electrodes with good conductivity (see §3.4.2).

3.4 Preliminary Flash Processing

During the initial optimization of the flashing conditions, the printed lines were processed with the Xenon Sinteron 2010-S, in order to understand the best parameters that would give a uniform and sintered copper films.

3.4.1 First Considerations

The intense light pulse process is based on the light absorption by the active layer but not by the plastic substrate, which is almost fully transparent in the visible range. Thus, it is fundamental that the copper oxide nanoparticle ink film shows an absorption spectrum at least partially superimposed to the emission spectrum of the flash lamp. In this way, the film can absorb part of the energy delivered by the equipment, causing the heat generation. Demonstrating this, the light emission spectrum and the copper (II) oxide spectrum are compared, as shown in **Figure 3.5**. As observed, the copper oxide nanoparticle can partially absorb the light emitted by the lamp, enabling the heat generation. The matching is not complete, so the energy that the lamp can provide is not totally utilized by the deposited film in its transformation. However, it is sufficient to carry out the reaction from copper oxide (II) to metal copper, as well as the sintering.

In order to keep the energy supplied to the sample as high as possible, some standards were adopted: the film were positioned at 1 inch distance from the lamp window, where the focal plane of the lamp emission is as provided by the manufacturing company. Furthermore, the pulse width was set at the maximum value possible, 2000 µs.

At this point, the last variable that could be changed was the voltage: it was varied within its range in order to get a first impression of the behavior of the copper oxide nanoparticle films under the flash processing. For every value that the voltage assumed, the lamp

delivered a different amount of energy, enabling for a rapid screening of the changes occurring on the samples.
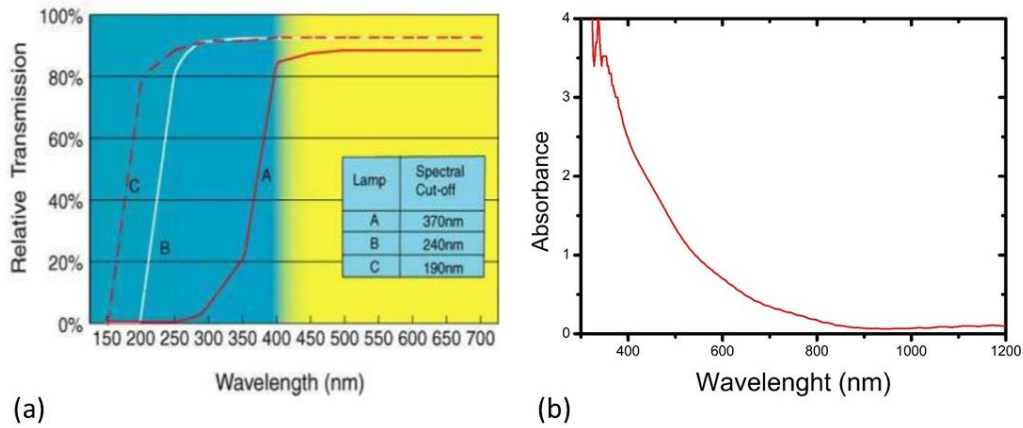
Figure 3.5. *The emission spectrum of the xenon flash lamp (a) and the absorption spectrum of the film coated with the ink diluted at 75% in volume of ethanol (b) are compared. It is possible to observe that the sample absorbs part of the light emitted by the lamp, enabling further transformations for the formation of a copper layer. Figure (a) taken from Xenon Sinteron manual.*

Another aspect to be considered is the different outcome that was observed in stripes flashed at different times after deposition. Casually, it was observed that stripes flashed after a few days from the deposition required more energy to form a homogeneous copper film. This reflects what was demonstrated in a previous study ([39]), where a time-effect on the sintering process had been identified: if the lines are processed after a short time, the ink carrier is not completely evaporated and this influences the photothermic reaction. However, if the delay increases considerably, the reducing agents present in the ink start to either penetrate into the PET film or evaporate, thus becoming less accessible to the CuO nanoparticle and reducing the reaction scale. For this reason, all the films were processed within 2 hours from the deposition, finding this delay an optimal balance between the two phenomena.

3.4.2 From Copper Oxide to Metallic Copper Film

The aim of the first flash processing investigation was to find the conditions that enable the transition from copper (II) oxide nanoparticle to pure metal copper, also providing sufficient energy for the sintering process. As explained previously, the conversion from

copper 2 to metallic copper is a chemical reduction, but this alone is not sufficient to produce a good conductive film. In order to achieve this, sintering of Cu particles, i.e. necking and coalescence, of neighboring particles and eventual formation of a continuous film has to be achieved. Theoretically, the reaction involved is a redox reaction, where the Cu^{2+} is reduced by a photothermic mechanism, enhanced by the presence of redox agents that can accelerate the reaction be providing electrons to the system that are necessary for the chemical reaction. The energy provided also raises the local temperature, reaching the conditions for nanoparticle sintering, as illustrated in **Figure 3.6**. Initially, the nanoparticles are surrounded by residual solvent and any additional stabilizers. Exposure to the flash causes heat generation, which modified the system to metal copper, evaporating the solvent and removing most of the stabilizers. This temperature is high enough to neck the nanoparticles and create a uniform film, characterized by electrical properties similar to those of bulk copper ([40]).
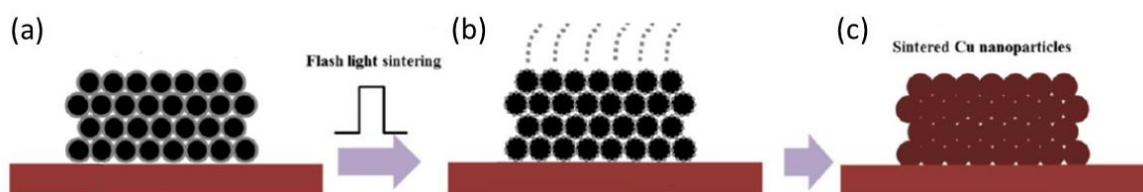
Figure 3.6. *Schematic representation of the mechanism involved in the copper electrodes fabrication. The film as deposited (a) is processed with an intense pulse light, leading to solvent evaporation and nanoparticle reaction (b). The heat generated enables to sinter the solid particle creating a continuous structure (c). Image adapted ([40]).*

The investigation started delivering the highest amount of energy to the sample: this condition is achieved using a voltage of 3kV, corresponding to an electrical energy of ~1700 J, which is the upper limit for the Sinteron system. However, the energy supplied to the film was too high and this led to delamination.

The optimal setting was found at 2.7 kV (~ 1400 electric Joules): films exposed to a light pulse of this energy appeared highly reflective and with an orange color typical of copper. All the films resulted uniform, excluding the edges of each line deposited with slot-die coating process because of the high solvent content at the beginning and at the end of the deposition, typical of slot-die processes.

This flashing condition was applied to each sample deposited with both coating techniques,

but with different coating settings. Their uniformity and electrical properties were evaluated in order to identify the best overall conditions. In **Table 3.1** the different cases are reported. It is interesting to observe that the thicker samples only partially reacted, leading to non-uniform copper electrodes. Furthermore, the films obtained by a lower inkjet printing resolution do not show a material continuity and therefore they are not conductive after sintering. For an intermediate dpi, the films are materially continuous; however, the properties are not optimal for copper electrodes fabrication.

Table 3.1. *The significant process settings for each type of deposition, referring to both coating and flashing conditions, in addition to the sheet resistance and optical aspect are reported. For optical aspect it is referred to Delaminated=partially damaged, Uniform=completely sintered and even film, Continuous=completely sintered but uneven structure Non Continuous=missing material integrity.*

Flash Parameters	Deposition Technique	Reference Printing Condition	Optical Aspect	Average Sheet Resistance (mΩ/□)
2.7 kV 2000 μs	Inkjet Printing	10 μm	Delaminated	n.a.
		15 μm	Delaminated	n.a.
		20 μm	Uniform	138
		25 μm	Uniform	182
		30 μm	Continuous	640
		35 μm	Continuous	950
		40 μm	Not continuous	n.a.
		45 μm	Not continuous	n.a.
		50 μm	Not continuous	n.a.
	Slot-Die	Commercial Ink	Damaged Not reacted	n.a.
		50% v/v solvent	Uniform	171
		75% v/v solvent	Uniform	368

Analyzing the results shown in **Table 3.1**, only few of the total depositions were considered for further characterizations. As a matter of fact, only the inkjet printed films with drop spacing of 20 μm and 25 μm showed a good mechanical stability and an optimal sheet resistance, as well as the slot -die deposition with a diluted solution, respectively at 50% and 75% in volume of solvent.
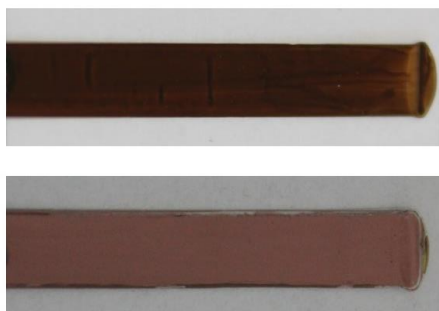
Figure 3.7. *Considering the solution at 75% in volume of ethanol, the comparison between the film as deposited and the uniform copper electrodes obtained after flash processing.*

Figure 3.7 shows an illustrative sample before and after deposition, highlighting the reaction from copper oxide (II) to metal copper, as well as the sintering process.

It is possible to observe the change in sample color, the most visible difference, from the dark-brown of the copper oxide film to the "orange" of the metal copper electrode. The nanoparticle have clearly reacted and sintered, creating a continuous structure.

3.5 Equipment Calibration

The DMP 2831-2800 series is a commercial inkjet printer, so high standards about uniform deposition and coating behavior over the printing plate are assured. However, the 3D coater is a customized 3D printer and the coating process may be not uniform along all the printing area. Slightly variations on the coating head supporting bar, some vibrations caused by the action of the motor or just because the plate support is not even, may vary the gap between the slot-die and the substrate or the amount of volume locally dispensed. This could influence the properties of each electrode, not only as copper oxide but also as metal film, after flash processing. For example, the resistance may vary from stripe to stripe because of the difference in thickness: the thicker the layer is, the easier it is to achieve a percolated coating and therefore a more conductive film. With this in mind, before all the investigations, a 3D coater calibration was carried out in order to understand the coating behavior over the whole plate, and to optimize the slot-die deposition or, if necessary, to limit the deposition in a restricted area where the samples could result be more uniform.

Moreover, even if the deposition is uniform all over the printing area, different

characteristics may occur after flash processing, because the light intensity decreases from the center to the edges of the incidental area. The reaction and the sintering process might occur in a different scale, leading to electrodes with different properties

Therefore, before obtaining any sort of outcome from the characterization of the copper electrodes, quick investigations about slot-die coating and flashing uniformity were conducted. Moreover, in order to reduce the amount of samples to characterize, only the solution with 75% in volume of solvent was deposited and analyzed.

3.5.1 3D Coater Uniformity

In order to understand the coating uniformity over the available area, a patterning characterized by three rows with nine lines each was obtained. The same pattern given by `3x0.5cmLines.txt` G code sequence was repeated for three times at different y-axis level: in this way the coating process covered most of the plate, giving an idea about the uniformity along the x and y-axes. The first row starting point was placed at 18 cm far from the home position, giving 0.5 cm spacing between each row; moreover, the first three exceeding stripes were cut and not analyzed because not complete due to the meniscus instability. After the deposition, significant samples were investigated: for each line, only the first, the fifth and the ninth position were evaluated.
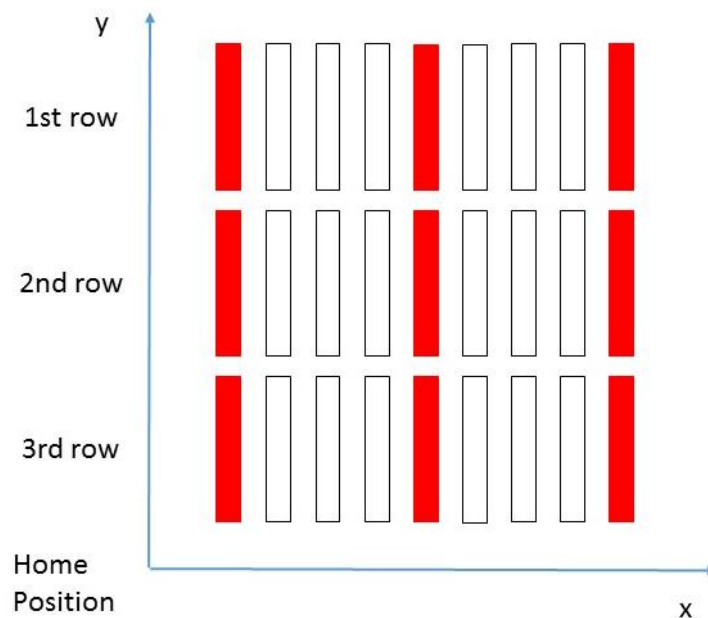
Figure 3.8. *Schematic representation of the pattern obtained with slot-die technique. Highlighted the lines further investigated.*

Figure 3.8 shows a schematic illustration of the overall patterning obtained, highlighting the samples that were used to estimate the uniformity over the coating area. For each row significant lines were chosen in order to obtain information about the coating behavior These significant lines were cut and characterized. In order to evaluate the difference in thickness, a transmission analysis was performed using optical spectroscopy in the range of 300-1200 nm: thicker films will absorb more light with respect to thinner coatings because the larger CuO nanoparticles content, and this can be easily monitored using optical spectroscopy.

Figure 3.9 shows how the coating process is not uniform over all the available area, where the third row, the one in proximity of the home position, resulted thinner than the others.
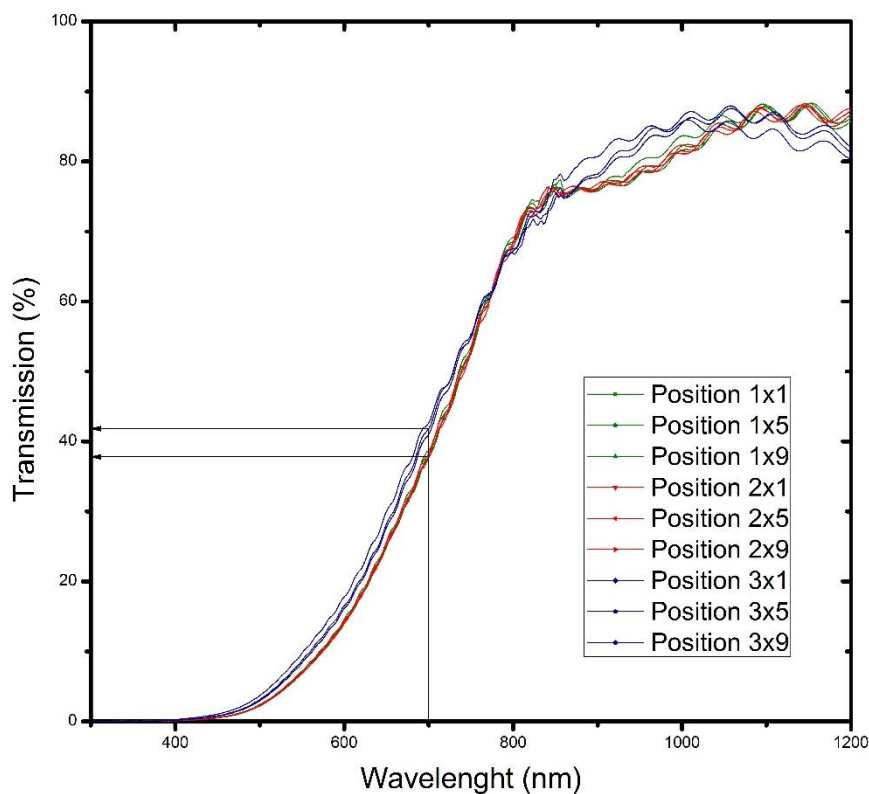
Figure 3.9. *Transmission spectra of the samples placed in position 1, 5, 9, (referring to Figure 3.8) for each row.*

Its spectrum shows a higher transmission over the range evaluated, indicating a lower nanoparticle concentration, due to a less amount of solution deposited.

This may be explained by a variation of the gap between the head's blade and the substrate: a shorter distance decreases the meniscus size with the consequence to reduce the ink deposition rate. The excess of ink that flows to the edge is dragged until the end of the line, enhancing the backflow phenomenon that occurs in that area. Thus, even if there was no difference between the lines by a first look, they presented a slightly different thickness that might affect the properties of the flashed layers.

It is worth noting that a direct thickness measurement using conventional profilometry techniques was impossible to perform due to the flexible nature of the substrate and the extreme sensitivity of the profilometer head to curved surfaces. This prevented to obtained precise information about the layer's thickness. However, further analysis will make possible to evaluate the deposition in cross-section, allowing to estimate the dimension of the deposited film.
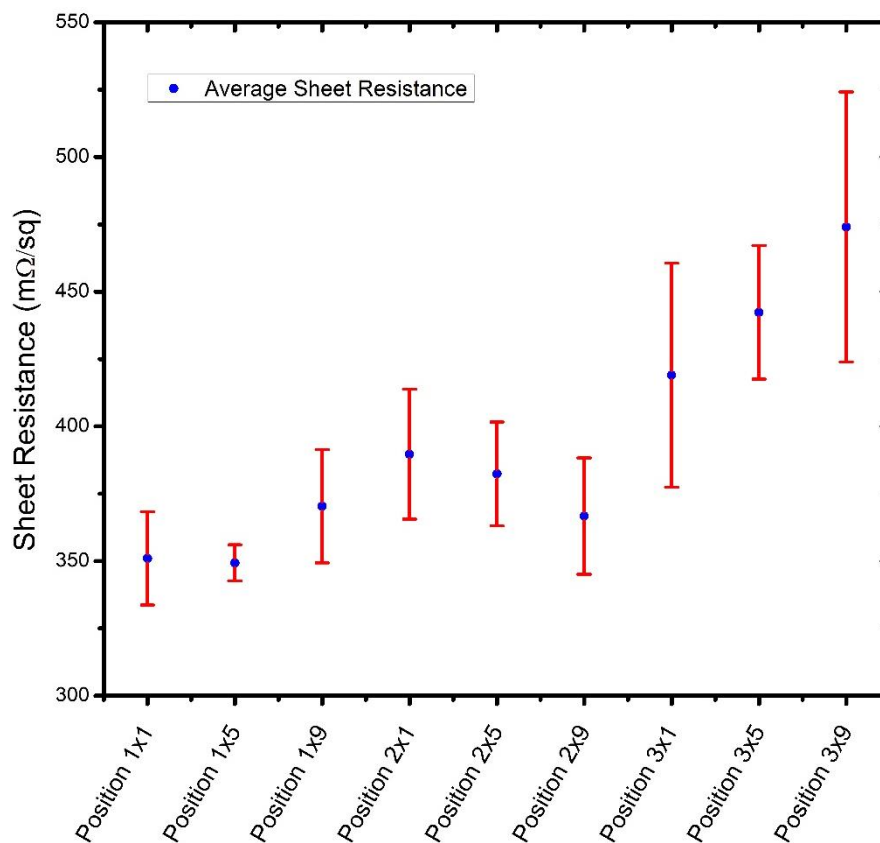
Figure 3.10. *Sheet resistance related to each position investigated: the value is averaged over the local measurements (3 for each line taken along the entire stripe) and the error on the measurement is also reported (error bars are ± one standard deviation).*

Furthermore, each line, which had been investigated by the spectroscopy analysis, was processed with intense pulse light applying a voltage of 2.7 kV for a 2000 µs pulse width: the aim was to understand the effect of such variations in deposition on the final metallic copper films. Notably, no difference in mechanical behavior was observed among the tested lines, which all show good stability even after a rough bending test. Only the sheet resistance showed a slightly variation, with lower conductivity for the third row stripes: the thinner layer probably resulted in a high layer resistance.

In **Figure 3.10** the average sheet resistance values for each line are reported, giving an order of magnitude about the sheet resistance variance over all the samples. The discrepancy was not too high, but in order to avoid significant inconvenient during data elaboration, it was decided for further depositions to coat only on the area covered by the first and the second row, where the results had been more uniform.

3.5.2 Flash Processing Uniformity

It is known that the light intensity during the pulse varies not only with the distance from the lamp window, but also along the perpendicular plane with a 100% intensity at the center of the support, as previously reported. So, it was necessary to understand how a different incidental energy might have affected the copper oxide reaction and the sintering mechanism over a larger area and not only for a simple 3 by 0.5 cm line, placed under the focus of the lamp. This may have given information about the possibility to create a more complex pattern to apply for a real application, which can easily cover a surface of 10x10 cm.

With respect to the pattern deposited for the 3D coater, a similar approach was applied also concerning flash processing uniformity, as shown in **Figure 3.8**: three rows for nine lines each, but in this case the pattern was kept large enough to understand the flashing mechanism over a bigger patterning. Instead, to process each line by itself, the three rows were processed all together. It was possible to evaluate not only the focused lamp range but also the outer area, having information about the size that a single pattern can reach for a single application, maintaining high standards. The target was to get good mechanical and electrical properties as obtained for the single stripe under a single intense light pulse. For this aim, the standard setting in order to obtain a sintered copper layer was applied (2.7 kV and 2000 µs for voltage and pulse width, respectively).

As expected, the result after one pulse was not homogeneous, providing uniform copper films only in the central area while the external lines remained partially sintered or even unreacted. The decreased light intensity in the outer circles leaded to less energy delivered to the copper oxide nanoparticle layers, indicating that it was not enough in order to start the reaction and the sintering process. Moreover, the patterning showed a sort of transition,

following the decreasing light intensity along the radius, from the center to the edge. While the inner films were completely sintered, the next lines resulted only partially sintered but even reacted, showing a different coloration from the original deposition, and tending to be yellowish. However, the reaction couldn't affect the outer stripes, which did not present any visible sign of reaction from CuO to Cu. This had to be further investigated due to the possibility to incur in more than one reactive step, as previously achieved: a multiple step reaction could involve an enhanced control of the mechanism, leading to better results because the finer variation of the process conditions.

An optimal result was reached with the standard flashing parameters, but at two pulses processing: the uniformity in terms of metal copper layer was reached in most of the patterning and only at the edge of the substrate the reaction did not occur, as shown in **Figure 3.11**. The lines look uniform along all the deposition, not showing any difference between each other.
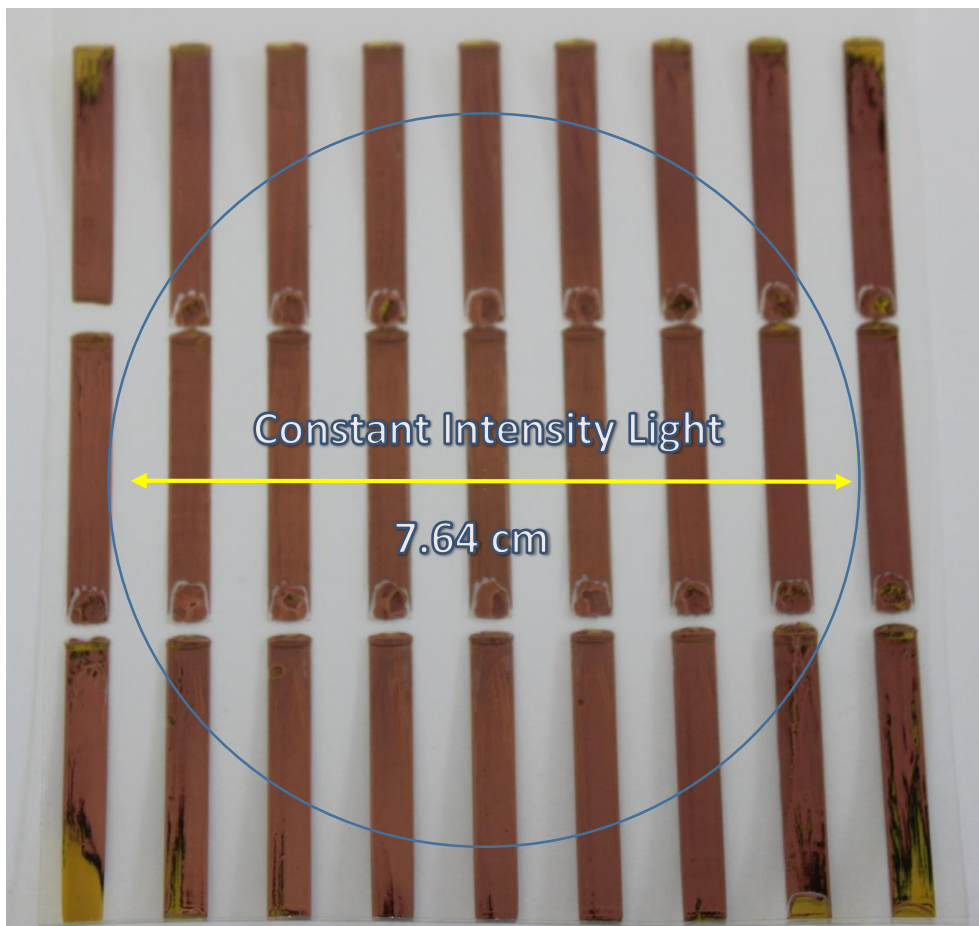
Figure 3.11. *Flash processing of a pattern 9 cm wide demonstrating that is possible to obtain a complete copper formation and sintered structure outer than the limit of relatively constant light intensity estimated by the production company.*

However, even if the optical quality may have been similar, it was important to understand if the electrical properties were similar as well. As a matter of fact, a different light intensity might have influenced the sintering process that could have been less efficient for the outer lines. The reaction took place, so the conditions were sufficient to induce sintering, but at lower lamp energies (that is at higher lateral distances from the lamp focus) the nanoparticles might have sintered only at the surface. For this purpose, a resistance analysis was performed and the relative sheet resistance was obtained for significant samples. **Figure 3.12** shows the average sheet resistance for the evaluated layers: it has to be considered from the 3D coater investigations that the third row usually shows thinner films, with the consequence of a higher resistance. This explains why the samples belonging to the last row were less conductive with respect to the others.
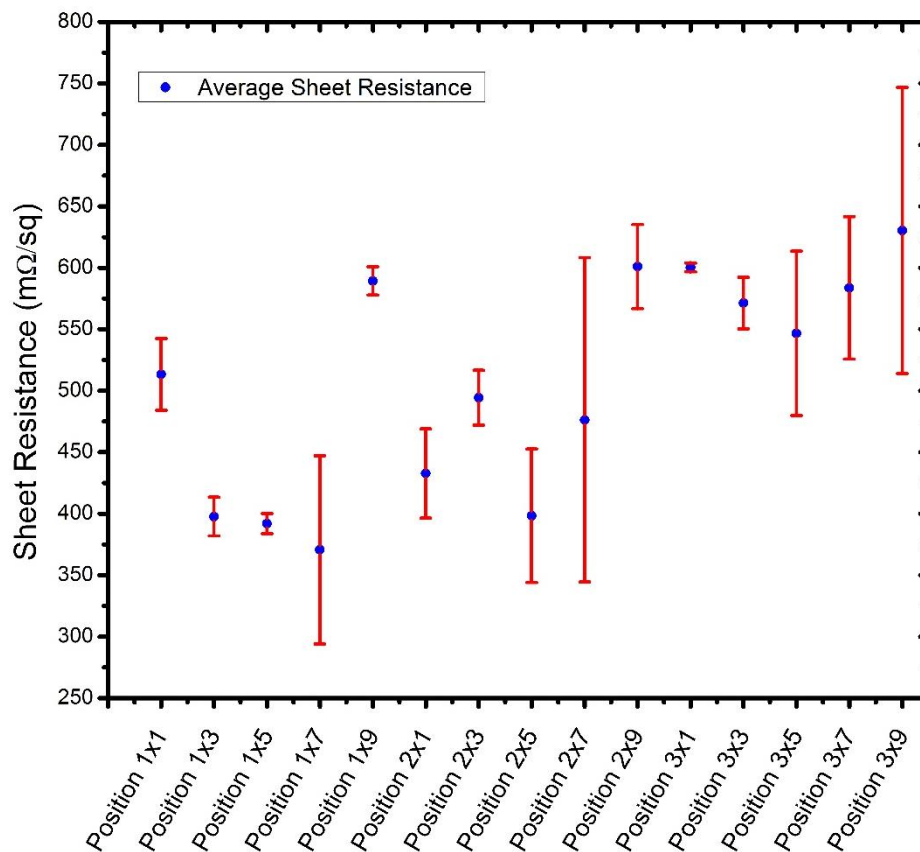
Figure 3.12. *Sheet resistance related to each position investigated: the value is averaged over the local measurements (3 for each line taken along the entire stripe) and the error on the measurement is also reported (error bars are ± one standard deviation).*

Based on this consideration, the flash lamp can easily process a larger pattern with an 8 cm diameter. This allows not only to investigate a single stripe, understanding the mechanism involved, but also to create a more complex pattern without any difficulty, which can be part of a real application. That enables flash sintering to move away from a simple laboratory scale and reach the industrial large-area manufacturing. It has been demonstrated not only as an experimental technique, but a reliable technology that can be applied in a real manufacturing process. Moreover, it can introduce several advantages such as room temperature processing and the capability to use plastic foils, becoming one of the most prominent technique for flexible printed devices. Based on these considerations, flash sintering is going to be a successful R2R technology.

3.6 Flash Processing Investigation

In the previous paragraph §3.5.2, it has been reported how a lower amount of energy supply to the copper oxide nanoparticle film might have different effects on its chemical and mechanical structure, leading not to a sintered layer but to an intermediate step. This was found quite casually due to the reduction on light intensity from the center to the edge of the lamp footprint, however it was further investigated, obtaining a depth comprehension of the phenomenon that occurs.

A slightly variation of the process conditions can improve several properties, both mechanical and electrical, as well as stability to oxidation. For example, a slow drying process may reduce the solvent content in the final layer: different flashing steps take place in order to gradually vary the supplied energy, reaching the conditions for solvent evaporation, but not to complete the copper reduction. With the last step, more energy is given to the system achieving a continuous metal copper film. In this way, then nanoparticles can pack more closely to each other creating a homogenous layer before sintering. The properties may quickly improve: the solvent and the organic molecules present in the ink are highly insulating and can create a barrier between neighboring nanoparticles; therefore, the removal of such organic compounds may improve the conductivity. Moreover, if the nanoparticles already create a continuous and dense layer, when they melt during the high intensity flash, they easily reach the percolation [41].

Obtaining a fine control of the reaction enables to understand the basilar mechanisms involved and increases the capability to choose the right path in order to optimize the film's properties. With this in mind, different flash processing conditions were applied trying to investigate the reaction mechanism and possible different steps.

3.6.1 *Effect of Flash Energy*

Flash process investigation was based on the knowledge that the reaction involves a thermal reduction of the copper oxide nanoparticles to form metallic copper. Thus, the energy supplied cannot decrease under a certain level because the reaction does not take place. For this reason, similar considerations assumed in the preliminary analysis were taken also in this case: considering a single pulse processing, the pulse width was fixed at the highest value possible, 2000 µs, varying the voltage within its possible range, between 1.95 kV and 3 kV. Increasing the voltage keeping all the other parameters constant allowed to slightly increase the energy delivered on the sample, analyzing the behavior of nanoparticle when a higher heat was generated.

This systematic approach led to very important results. At low energies, no reaction was observed, with the copper oxide film retaining the dark brown color of the as deposited coatings. But when the energy reached a threshold value, the nanoparticle started to react, changing the color to yellowish. Part of the solvent and stabilizer content evaporated, demonstrated by the hydrocarbon vapors that were generated by the flash processing. Increasing the power, the nanoparticle reacted further, leading to an intermediate state, where the layer showed a dark green color coming from a partial conversion to copper, as it will be further discussed in §3.6.2.2 . Treating the films at high level energy, a complete reduction of the nanoparticle was achieved, as well as their sintering, as previously observed. Increasing the voltage further, too much energy was supplied and complete delamination of the coatings from the substrate occurred.

Table 3.2. *Optical aspect and sheet resistance for the samples flashed with one 2000 µs light pulse at different voltages. The electrical energy supplied to the lamp is also indicated.*

Stage	Pulse Width (µs)	Voltage (kV)	Electrical Energy (J)	Optical Aspect	Sheet Resistance (mΩ/□)
1		1.95	665.51	Dark-Brown	Non Cond.
2		2.10	789.18	Dark-Brown	Non Cond.
3		2.30	972.85	Yellowish	Non Cond.
4	2000	2.50	1178.52	Dark-Green	Non Cond.
5		2.70	1406.73	Copper	380
6		2.90	1658.02	Light-Copper	Damaged
7		3.00	1792.47	Light-Copper	Damaged

Table 3.2 reports the different parameters involved, calculating the relative electrical energy delivered by the system in Joule, estimated by **Equation 2.11**. Considerations about the optical aspect are also made, as well as the main property, the sheet resistance.

This investigation was conducted for many samples deposited with the optimized conditions for ink-jet and slot-die printing described before: for the former the 20 μm and 25 μm drop spacing and for the latter the solutions diluted at 50% and 75% in volume of ethanol. Each deposition showed the same behavior: similar transitions appeared, more or less marked based on the nanoparticle content. This was an additional clue that the reaction might have had not only one step but also an intermediate level, represented by a partial reduction to copper (II) oxide to copper (I) oxide (Cu_2O).

This is demonstrated by **Figure 3.13**, where the reaction scale for different kind of deposition is showed. For each sequence, a transition from brownish copper oxide to
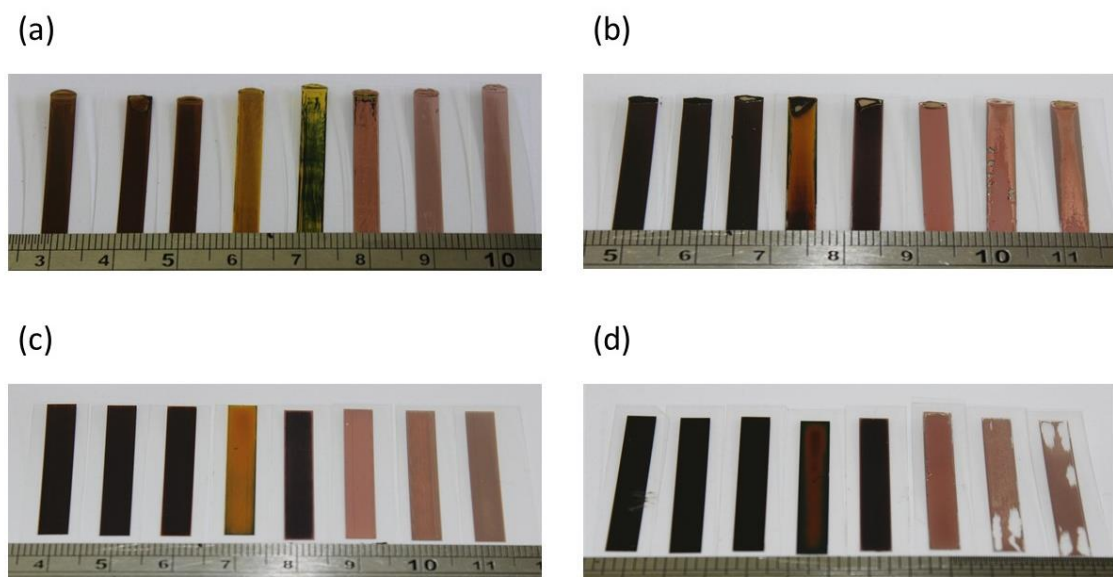
Figure 3.13. *The energy variation is illustrated for various types of deposition: (a) slot-die coating with ink diluted at 75% in volume of ethanol; (b) slot-die coating with ink diluted at 50% in volume of ethanol; (c) inkjet printing with 25 μm drop spacing; (d) inkjet printing with 20 μm drop spacing. In each panel, from left to right the samples have been processed from 1.95 kV to 3.0 kV, respectively.*

sintered metal nanoparticle can be observed, passing through a yellowish state and a dark green one. The fact that the intermediate states are more evident in some samples than others is due to their respective thickness.

A quick and rough mechanical test was also performed in order to evaluate the structural

stability after bending. Even if the inkjet printing depositions were characterized by optimal electrical properties, they tended to easily delaminate, interrupting the film continuity and exponentially increasing the resistance. This is obviously not ideal for a working device and further solutions to improve the stability are necessary, such as encapsulation. Conversely, the slot-die depositions are characterized by a higher stability: because of their higher solvent content of the slot-die inks the deposited layers are thinner and smoother and they form a more uniform interface with the underlying substrate which helps avoiding delamination.

3.6.2 Film Characterization

The different stages that occurred during the flash processing investigation were analyzed: in order to understand the possible transitions in terms of chemical composition and nanoparticle structure, several characterizations were performed, before and after the flash light exposure. Most of the characterizations were performed only for the solution deposited with slot-die and diluted at 75% in volume of ethanol, if it is not reported differently, reducing the amount of analysis to be performed. This was possible considering the similar transitions showed by both slot-die and inkjet printed stripes.

3.6.2.1 <u>Visible Transmission Analysis</u>

The transmission analysis enabled to characterize indirectly the copper nanoparticle layers in both qualitative and quantitative way, giving not only information about the layer composition but also roughly about its thickness, allowing a comparison between the different depositions. It is based on the absorption spectrum: every material absorbs in a defined range of wavelength, depending on its composition and structure. The transmission analysis evaluates the range of wavelengths that is not absorbed by the sample, giving an inverse spectrum with respect to the one obtained in absorption. If the absorption occurs in specific wavelength, its intensity is determined by the concentration of the absorbing species and their absorption coefficient. Considering the same material and a defined light intensity in input, the thicker is the layer, the lower is the light intensity in output, as defined by the Beer-Lambert law as following (**Equation 3.1**):

$$\frac{I_1}{I_0} = T = 10^{-A} \quad . \tag{3.1}$$

Where I_1 and I_0 are respectively the intensity of the transmitted and the incidental light, T is their ratio in percentage and A is the absorbance, defined in **Equation 3.2**:

$$A = k_\lambda \cdot l \quad . \tag{3.2}$$

Where k_λ is the copper attenuation coefficient in m^{-1} and l is the thickness of the sample analyzed in m. Because the substrate dimension is still the same in every analysis, different spectra are given by different film's thicknesses. In the further analysis, the wavelengths range between 300 and 1200 nm was investigated.

As previously described, the mass of ink deposited on the substrate had influenced the transitional steps during flash processing investigation. This could be evaluated with a transmission analysis that enables to compare the layers obtained with same deposition technique but with different solvent content or different inkjet printing resolution. An increased solution deposition rate generates a thicker film, leading to a higher density for unit of area: the transmitted light so decrease its intensity in relation with the nanoparticle content. **Figure 3.14** compares the slot-die and inkjet printing deposition at different thicknesses, the former obtained with a different solvent dilution, the latter with a different density of droplet per surface unit (dpi). In the **Figure 3.14a**, the transmission spectra for the slot-die coated samples are presented: the range of absorption is similar but the intensity varies with the solvent content. At high solvent contents, the overall transmission is higher. This is determined by the lower nanoparticle content that leads to a smaller absorption of the incidental beam. Therefore, the samples are thinner. This is also proved by the comparison of the inkjet printing spectra in **Figure 3.14b**. In this case the ink formulation does not change and what differs is only the nanoparticle density, due to the different droplets deposition per unit of area. As expected, the films absorb in the same range and, similarly to the previous layers, a smaller solid content leads a higher transmitted light.
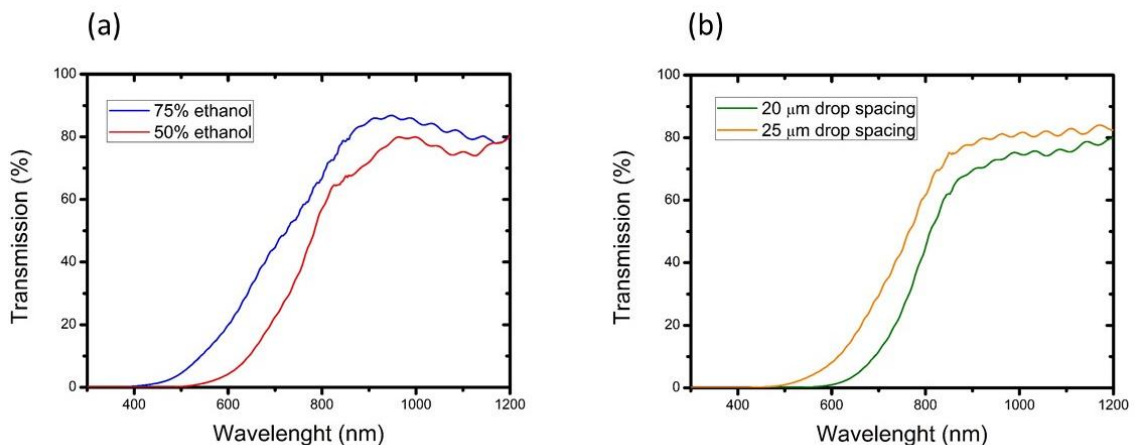
Figure 3.14. *Comparison between the transmission spectra of films deposited with different settings but same deposition technique: (a) slot-die coating with different solvent dilution; (b) inkjet printing with different drop spacing.*

Transmission characterizations were also performed for all the flashed sequence, in order to prove the different composition and structure that affected the layers in various conditions.
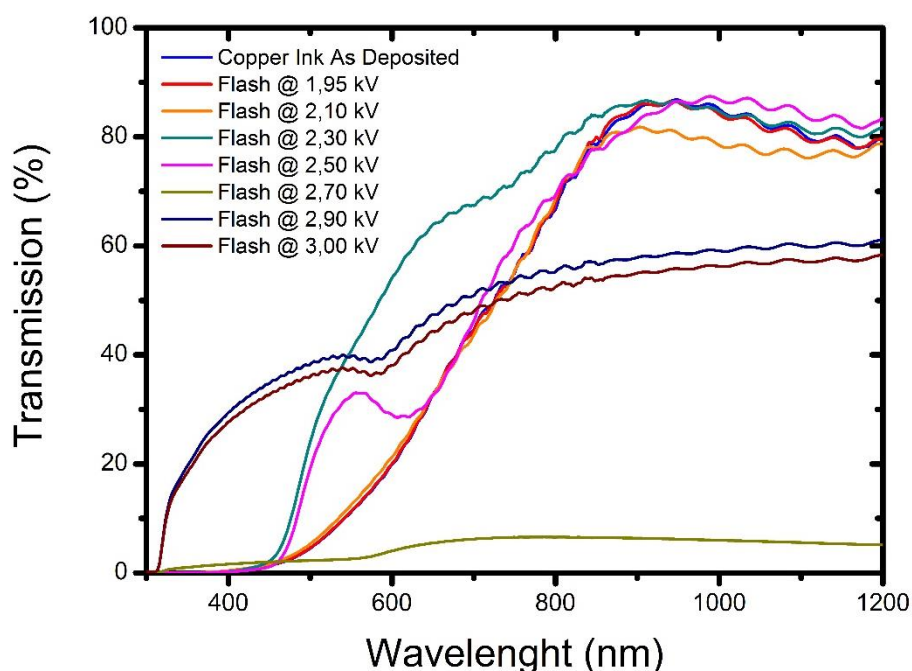
Figure 3.15. *The transmission spectra of the samples processed with different flashing energies.*

Figure 3.15 demonstrates the particular variations that occurred when an increasing flashing power was supplied. As previously described, at the initial stages the energy was not enough to generate any sort of reaction, indicated by the similar spectra until 2.1 kV. When the power reached a threshold value, defined by 2.3 kV of voltage, the layer radically changed its composition and structure, showing a higher transmission. As a matter of fact, the absorption range is similar but the absorption intensity is much smaller. This is related to the film changing from a brownish state to a yellowish condition, probably due to slightly chemical variations, maybe a partial oxidation or a different structure. When the power was further increased the copper layer showed a distinctive state, totally different from the previous one, characterized by a dark green coloration. This nature derived from the presence of plasmonic nanoparticles, as will be confirmed later. By definition, a localized plasmon is a particular condition when metal nanoparticle electrons density can couple with electromagnetic radiation with wavelengths that are much larger with respect

to the nanoparticle size. As a matter of fact, a specific light wavelength can drive the conduction electrons in the metal to collectively oscillate, leading to a phenomenon called surface plasmon resonance. When it occurs, distinctive absorption peaks appear, which are related to the specific metal, the dielectric properties of the environment and other factors. This is demonstrated by the spectrum of the sample exposed to a flash of 2.5 kV, which shows a peak around 550 nm.
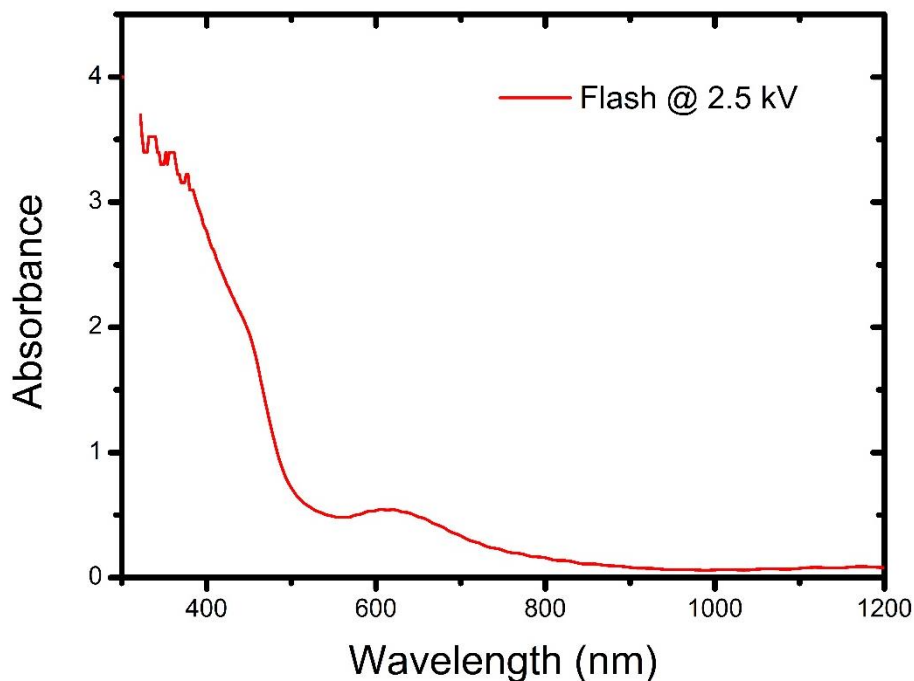
Figure 3.16. *Absorption spectrum of the film processed at 2.5 kV showing an absorption peak ascribed to a surface plasmon resonance.*

This can be further explained by **Figure 3.16**, where the relative absorption spectrum is presented.

Continuing with the flashed sequence, it is confirmed that at 2.7 kV the full sintering was reached, demonstrated by a practically flat transmission spectrum, coming from the highly reflective Cu film. It also showed that higher power leaded to delamination because the transmittance is relative high along all the wavelengths range.

3.6.2.2 FTIR Analysis

The Fourier Transformation Infrared analysis (FTIR) is a spectroscopic technique that is

focused on the infrared spectrum, which uses a Fourier transformation for data elaboration, giving in output an absorbance spectrum of the sample. The low energy associated with the infrared spectrum is absorbed by the molecular bonds: different chemical bonds have specific vibrational frequencies that when probed by IR radiation can provide a "chemical signature" of molecules and compounds, allowing to identify the different species present in the sample. Typical vibrational modes are for example, stretching, bending, rocking, scissoring, and twisting. A single chemical bond can have different vibrational modes at different frequencies. For this reason, samples composed of several different materials have complex infrared absorption spectra, which make single component identification challenging.
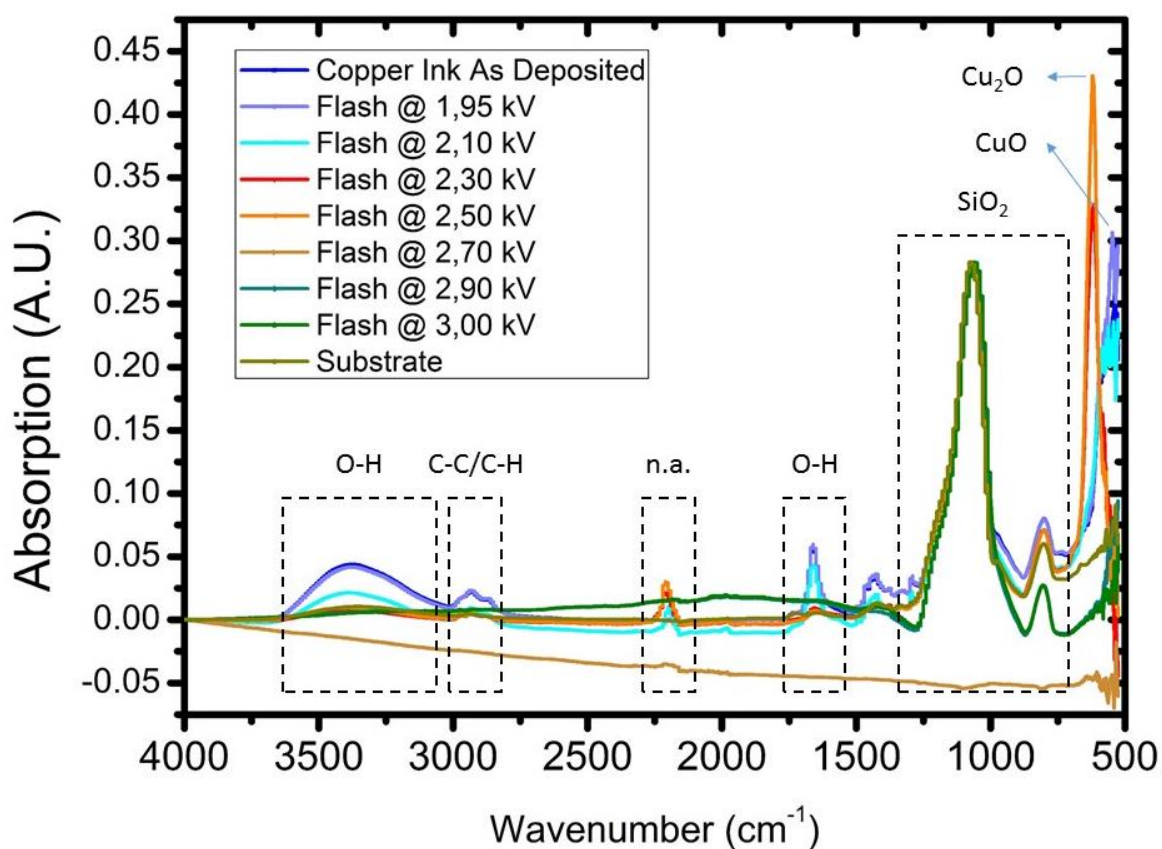
Figure 3.17. *FTIR spectra of the samples processed with a single flash with increasing applied voltage. Frequency regions of significant peaks are highlighted.*

In **Figure 3.17** the spectra of all the flashed layers sequence at different energy are reported: different transitions can be observed, suggesting that several reactions take place

during flash processing. It needs to be remembered that the ink formulation contains some stabilizers, as well as reduction agents that accelerate the copper oxide reaction. Thus, is quite possible that transformation of different compounds may occur.

The most important variations that can be observed are placed at 540 and 620 cm^{-1}. The first absorption represents the CuO molecular vibration ([42]) and it characterizes the spectra until the layer flashed at 2.1 kV, in line with the common behavior observed in **Figure 3.13**. But at 2.3 kV the optical aspect changes, as demonstrate by the peak at 620 cm^{-1}, which refers to the presence of Cu_2O ([42]). Finally, it is precisely proved that the transition had occurred was an intermediate oxidation state: the copper nanoparticle stepped from the first oxidation level to a second one, before reducing completely and sintering in a homogenous layer.

The substrate is a PET plastic foil coated with a porous layer that makes more stable the copper film when sintered. The porous surface is composed of porous silica. This is confirmed by the unaltered peaks at 1070 cm^{-1} with a shoulder at 1200 cm^{-1}, and an additional peak at 810 which refer to the stretching of the Si-O-Si chain. They pass through all over the flashing sequence without changing their shape or intensity, so they are not affected by the photothermic mechanism: obviously these peaks can't be seen with a metal film because it does not absorb in infrared. Therefore the property of the substrate are not involved in the flash processing, but only supply mechanical support to the copper layer ([43]) ([44]).

The copper oxide nanoparticle are suspended in an aqueous solution, so the ink must contain a water percentage that may reflect the presence of O-H bonds, as showed in the wavenumbers range of 3000-3500 cm^{-1}. Also metal oxide nanoparticles when dispersed in water show a certain amount of hydroxyl groups at their surfaces, which may contribute to such absorption. This absorption derives from the bending vibration of O-H group, which can be isolated or partially involved in hydrogen bonds, proving the presence of water ([45]). Peaks at 1650 and 1730 cm^{-1} are be also related to the H-O-H bond vibration, as reported in particular references ([43]), even if they may also refer to other compounds, such as the scissoring mode of the NH_2 group. It can be observed that overall trend involves a decrease of these peaks intensity at higher flashing power: it may be explained by the water evaporation due to the high local temperature, and also to de-hydroxylation of the CuO surface

However, the previous considerations may be also associated to the high content of ethanol, used to dilute the original formulation at 75% in volume of solvent. The evident intensity related to the O-H group might derive from the joined absorption of water and the organic compound. Furthermore, ethanol is highly volatile and very sensitive to the raising temperature, so it must follow the same evaporation process that affects the water while the power is increased. For this reason it is not possible to decouple the two

components. In addition to the peaks previously defined for water, the ethanol absorption occurs also in the range 1250-1500 cm^{-1}, where it decreases along the flash processing, reflecting the ethanol phase transformation from liquid to vapor at higher temperature [46]. While the C-O stretching can't be recognized because overlapped by the silica absorption, the solvent presence is also proved by the three peaks between 2800-3000 cm^{-1}, which involves the particular C-C and C-H stretching modes [43] [47]. Moreover, the peak at 1650 cm^{-1} may also refer to the scissoring vibration of amines, which could be part of reducing agents [48]. This in line with the absorption at 1480 cm^{-1}, which may involve different compounds, such as aldehyde or –COOH carboxylic group stretching. However the ink formulation is protected and it wasn't provided by the company, therefore the exact components couldn't be identified. As a matter of fact, while these peaks tend to disappear, other kinds of absorption take place. Some reagents may be involved in complex chemical reactions involving subsequent transformation steps before thermal decomposition. This is demonstrated by the absorption peaks that rise up with the Cu$_2$O at 2.3 kV, at 2190 cm^{-1} and 1580 cm^{-1}: several candidates are possible, for example isocyanate or amides, but also in this case a precise consideration is not possible because there are no references about the exact ink formulation.

Even if part of the absorption peaks cannot be uniquely associated, the FTIR analysis allowed showing the particular mechanism that occurred for the metal layer formation, deeply explaining the process that characterized the ink reaction.

3.6.2.3 <u>XRD Analysis</u>

The X-ray crystallography (XRD) analysis enabled to precisely demonstrate the intermediate transition from CuO to Cu$_2$O, before the complete reduction to Cu. This technique is able to recognize the atomic and molecular structure of a crystal by an incident x-ray beam. This is diffracted by the crystalline lattice, providing an output spectrum that is characteristic of a particular crystal.

Through XRD analysis it was possible to understand how the reaction occurred, giving the exact proportion of every single phase along the flash sequence. For this reason, a finer control on the flashing voltage was adopted, using increments of 0.1 kV to precisely map out the chemical and structural transformations. **Table 3.3** reports the electrical power scale that was applied, including a quick optical analysis. The additional steps were characterized by a mix of the main phases. So, it was so possible to observe the transition involving CuO and Cu$_2$O, as well as the reaction from Cu$_2$O to metal copper. It was also realized how at the lowest and highest conditions the chemical structure did not change, limiting the reaction window in the range of 2.1 kV and 2.7 kV.

Table 3.3. *Optical aspect and sheet resistance for the samples flashed with one 2000 μs light pulse at different voltages. The electrical energy supplied to the lamp is also indicated.*

Stage	Pulse Width (μs)	Voltage (kV)	Electrical Power (J)	Optical Aspect
1		1.95	665.51	Dark-Brown
2		2.10	789.18	Dark-Brown
3		2.20	878.31	Dark-Brown
4		2.30	972.85	Yellowish
5	2000	2.40	1072.90	Yellowish
6		2.50	1178.52	Dark-Green
7		2.60	1289.77	Copper
8		2.70	1406.73	Copper
9		2.90	1658.02	Light-Copper
10		3.00	1792.47	Light-Copper

Figure 3.18 shows the complete reaction from the CuO to Cu, highlighting the variation of the single phase through the different steps.

It can be seen how the copper (II) oxide concentration decreases when the energy delivered is increased: the intensity of the two relative peaks reduces, meaning that the CuO is decomposing. In the meantime, the Cu_2O formation takes place. At 2.3 kV the first reactive step is complete, demonstrated by the absence of CuO relative peaks. While the distinction between the two oxide phases seems really clear, the transition from Cu_2O to Cu is not so defined. Starting at the 2.4 kV step, the copper oxide (I) concentration progressively decreases, leaving space to small concentrations of metal copper: the presence of Cu slowly increases, and it is complete at 2.6 kV, when only the Cu peak remains, and no other variations can be observed.

Analyzing the intensity of each peak, the phase concentration can be estimated: the ratio between each intensity gives an idea about the relation that occurs within the different components, enabling to determine the phase percentage in every step. In **Figure 3.19**, the percentage variation of each phase is reported as a function of the voltage: the experimental points are not fitted by a real equation but they are joined by a line that is a guide for the eyes. It can be observed that the Cu_2O does not appear as a single phase but it coexists with either a small amount of CuO (at 2.3 kV) or a small amount of Cu (at 2.4 kV), indicating a very small window for the presence of just Cu_2O, possibly located around 2.3-

2.5 kV. In the reactive window, the reaction was very sensitive to the temperature, because small variations on the voltage leaded to changes in the nanoparticle structure. The lowest and the highest conditions are reported as well, demonstrating that in these ranges the overall chemical compositions was not affected by any sort of transition.
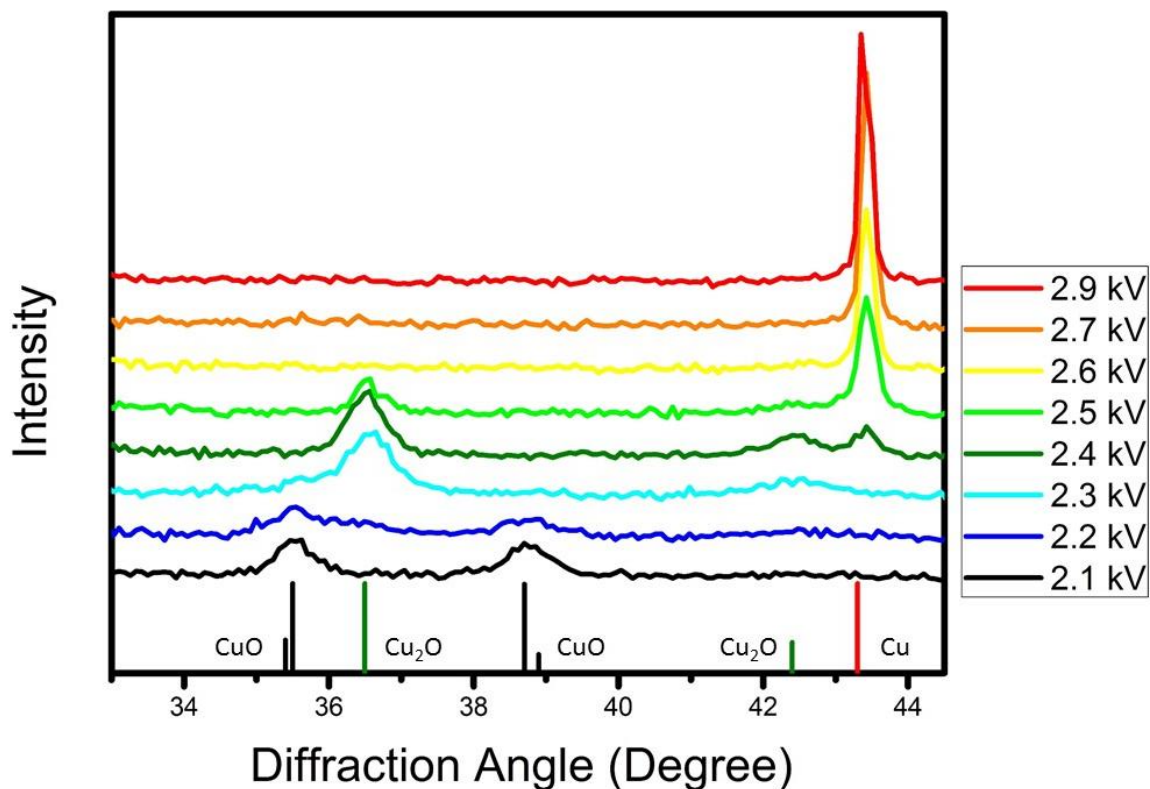
Figure 3.18. *XRD patterns for the samples processed with one single flash with voltage in the 2.1-2.7 kV window. It can be observed the intensity variation for each phase. Predicted diffraction peaks for CuO, Cu2O and Cu have been assigned according to ICDD No. 48-1548, ICDD No. 77-0199 and ICDD No. 04-0836, respectively.*
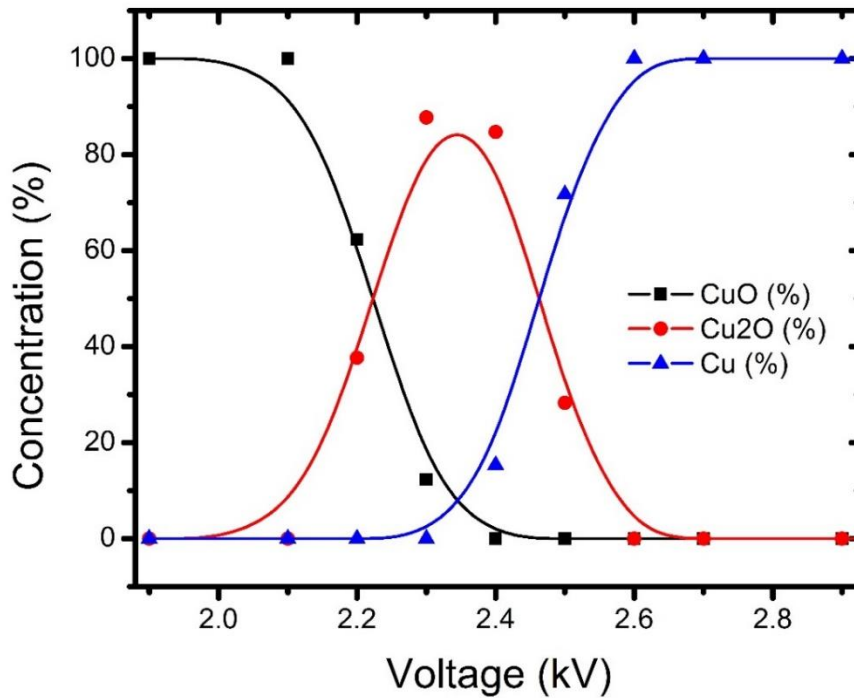
Figure 3.19. *Concentration of each phase as calculated from XRD data reported as a function of the applied voltage.*

XRD analysis was a powerful tool that enabled us to deeply understand the mechanism involved: it did not only prove without any uncertainty the existence of an intermediate reaction, confirming the results previously obtained, but also it gave an indication of the relative amount of each phase at every step of the flash processing.

3.6.2.4 SEM Analysis

The copper electrodes are conductive not only because of the copper oxide reduction, but also because the nanoparticle neck and sinter, creating a uniform and continuous layer that enables electrons to travel across the entire sample. As a first approximation, the denser and more percolated the sample is, the lower the electrical resistance will be. Scanning Electron Microscope (SEM) analysis is able to image the layer surface, scanning the film with a focused beam of electrons. The advantage of this technique with respect to the conventional optical analysis is the capability to achieve a resolution lower than 10 nm. It can be a useful tool in order to understand the nanoparticle structure. Moreover, the evaluation of the thickness with conventional methods was hard to obtain due to the

flexible nature of the substrate, which influenced the profile analysis. Thus, the SEM characterization was suitable also for investigations in cross-section, providing information about the film dimension.

(a)   (b)

(c)   (d)

(e)   (f)

(g)   (h)
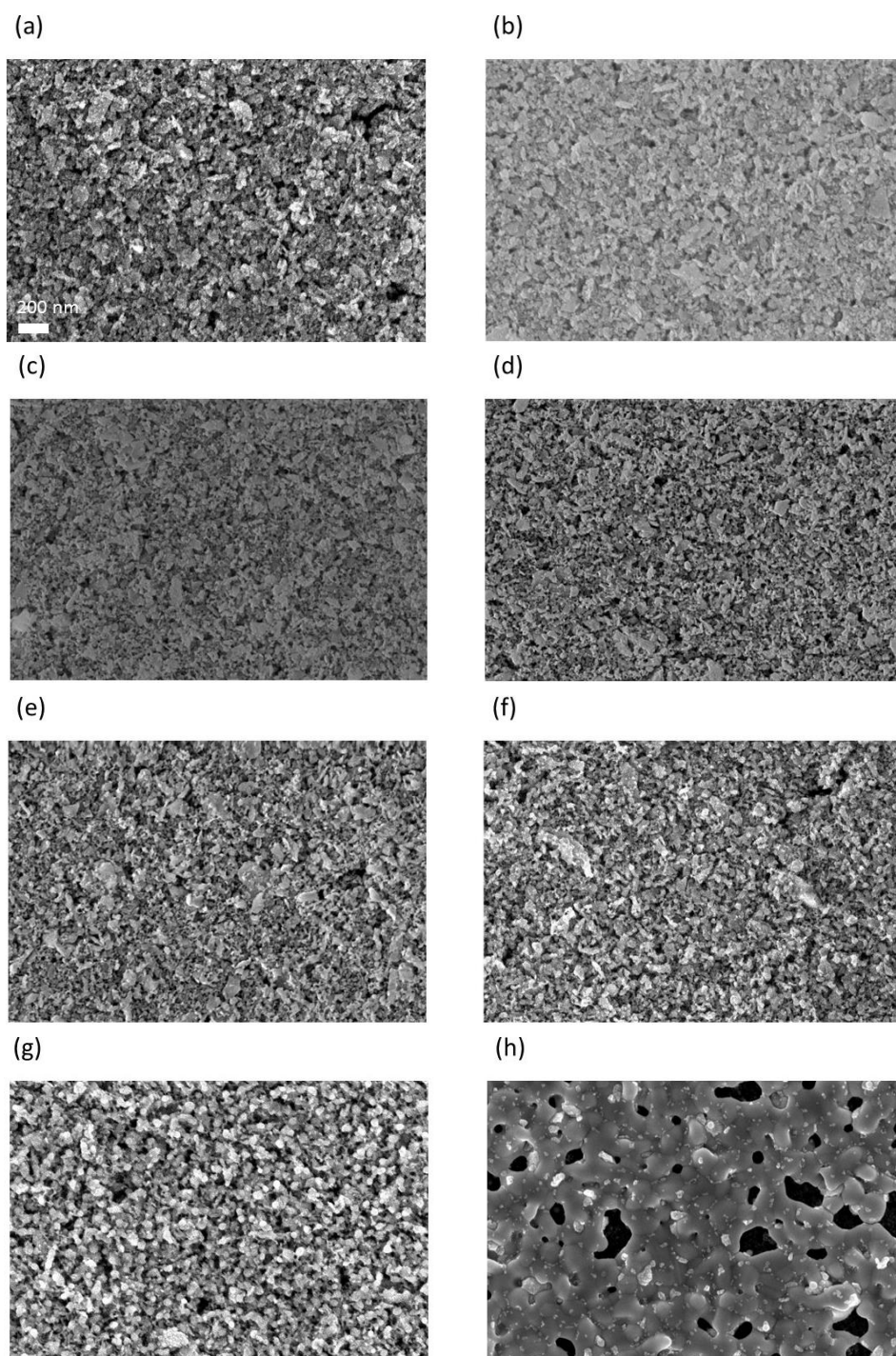
Figure 3.20. *The SEM analysis of the surfaces of the films treated under different conditions: (a) as deposited; (b) 2.1 kV; (c) 2.2 kV; (d) 2.3 kV; (e) 2.4 kV; (f) 2.5 kV; (g) 2.6 kV; (h) 2.7 kV. The scale bar applies to all panels.*

SEM analysis was performed in order to understand the surface evolution of the samples flashed at different conditions. In **Figure 3.20**, the film surface evolution over the entire flash range is illustrated. **Figure 3.20a** shows the surface of the as-deposited film: a highly porous structure with polydisperse particles can be observed. This morphology is retained in samples flashed at low energies, which also show a slight increase in porosity possibly due to solvent evaporation and removal of organic compounds that occurs in these steps (**Figure 3.20b-d**). In **Figure 3.20e** and **Figure 3.20f**, a change in the nanoparticle shape occurs: it is possible to observe some spherical particles as well as faceted, irregular particles. This phenomenon is consistent with the XRD analysis, which shows that metallic copper starts to form and coexists with the oxide phase. This aspect is even more evident in **Figure 3.20g**, where the film treated at 2.6 kV is shown: the entire surface is covered by the spherical nanoparticles, forming a copper layer. A further confirmation of this comes from the color of the samples, which have the typical bulk copper appearance (see **Figure 3.7**). However, the conditions are not sufficient to sinter the solid particles, so the structure is not continuous, and does not show electrical conductivity. The desired film is achieved in **Figure 3.20h**: the nanoparticle are not only reacted (from CuO to Cu), but also sintered, creating a uniform connection between each other. Such films are highly conductive, as presented in §3.4.2.

Figure 3.21 shows a higher magnification image of the sample flashed at 2.7 kV: it is possible to note that the nanoparticle have partially lost their spherical shape, and fused with each other to create a continuous copper film. The average nanoparticle diameter was estimated to be around 120-150 nm.
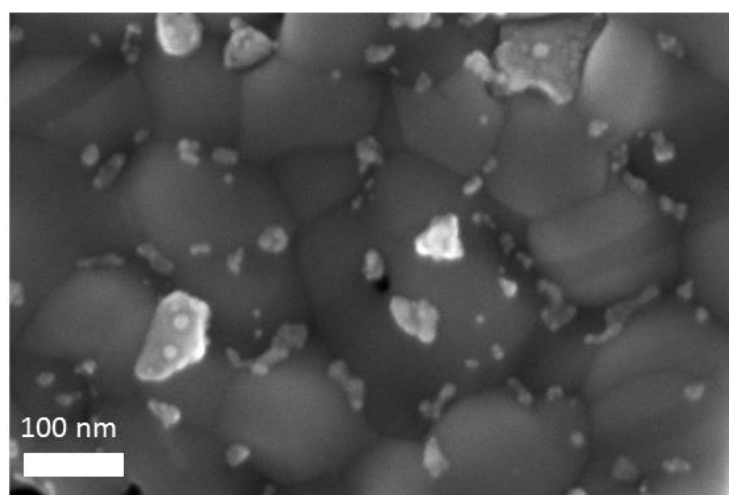
Figure 3.21. *High resolution SEM image showing a fully sintered copper film.*

It is very interesting to compare the initial structure with the final one. **Figure 3.22** highlights the different degree of interaction that exists within the copper particle before and after the flash processing. The overall structure evolves from separate nanoparticles within a porous organic matrix (**Figure3.22a**) to a dried, inorganic and percolated layer. As a matter of fact, the chemical nature changes from copper oxide to metal nanoparticle, which are able to melt and sinter. This can be observed in **Figure 3.22b** where the morphology reflects a single uniform metal layer.
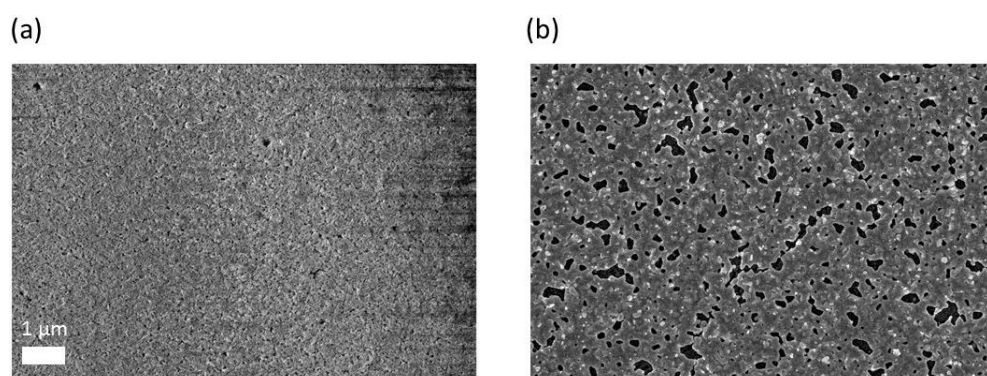
Figure 3.22. *Comparison at lower resolution between the surface of a layer as deposited and the film processed at 2.7 kV: it can be observed the change in the structure due to the intense pulse light effect. The scale bar applies to both panels.*

As the solvent evaporation occurs and as the particles sinter reducing the overall porosity, the thickness must change. In **Figure 3.23**, the layer cross-section before and after the intense pulse light can be evaluated. The average thickness in **Figure 3.23a** is estimated in 570 nm, while in **Figure 3.23b** is reduced to 210 nm, comparable with the nanoparticle size. This confirms that during the flash processing all the volatile components are vaporized and only the copper particles characterize the layer thickness.

The thickness analysis enables to characterize also the film properties. As a matter of fact, the resistance is the ability of the material to oppose to the passage of an electric current and it is a local property, which means it changes from sample to sample, based on their physical characteristic, especially on the dimension. However, the resistivity is a property that depends only on the material. A relation exists between the sheet resistance and the resistivity, which is shown in **Equation 3.3**:

$$R = R_S \cdot t_S \quad . \tag{3.3}$$

Where R is the resistivity in $\Omega \cdot$cm, R_s is the sheet resistance in $\Omega/\square$ and t_s is the thickness of the layer in cm.

(a) (b)
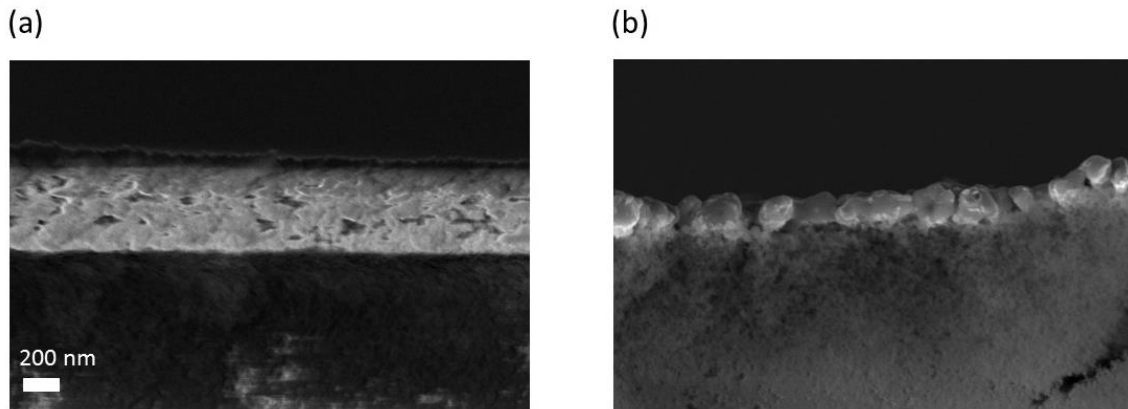
Figure 3.23. *The comparison between the thickness of a film as deposited (a) with a layer flashed at 2.7 kV and 2000 µs. The scale bar is common in both images.*

Considering an average sheet resistance of 400 $\mu\Omega/\square$ as an order of magnitude, in addition to the thickness previously reported, the resistivity for the copper electrodes obtained by depositing through slot-die a solution diluted at 75% in volume of ethanol is around 8.4 $\mu\Omega \cdot$cm. The most performing samples prepared from a slot-die process achieved resistivity values of 7.35 $\mu\Omega \cdot$cm (sheet resistance 350 $\mu\Omega/\square$). The relative conductivity can be calculated as $1.19 \cdot 10^7$ S/m for the average result and in $1.36 \cdot 10^7$ S/m for the most performing electrode, respectively achieving 20% and 33% of the bulk copper conductivity, defined as $5.96 \cdot 10^7$ S/m.

Summary

In the chapter the printing and flash sintering of copper oxide inks was described. Under highly optimized conditions, the copper oxide could be converted through to metallic copper films that exhibited bulk conductivities about 80% lower than that of bulk copper. In the following chapter, investigations into the structural and environmental stability of such films will be presented, highlighting the need for multi-layer deposition.

Chapter 4

Multilayer Depositions and Stability Tests

After thoroughly investigating the flash processing conditions, we now focus our attention to the stability of the copper electrodes. Various tests were performed analyzing the effect of different conditions such as time, environment and mechanical stress. The aim was to explore the performance of the copper layers according to the preparation conditions and to understand their stability.

4.1 Effects of multistep flash processing on copper electrodes

From the results presented in Chapter 3, we know that the reaction proceeds in different steps before obtaining the sintered metal copper layers. The final material can be obtained following two main different reaction paths: in one way the energy supplied during the light pulse is enough to carry the copper (II) oxide directly to the metallic phase (1 step flash). In the other, it is possible to stabilize the Cu_2O with a first flash at low intensity, and then complete the reaction to metallic Cu with a second flash (2 steps). In a two steps process the residual solvent is most likely removed during the first flash, leaving more inorganic material that will have enhanced sintering properties. However, this intermediate transition may consume most of the reducing agents, lowering the sintering ability of the printed layer.

With this in mind, the stability of Cu electrodes sintered using both processes were investigated, focusing on the optical and electrical properties. The samples were analyzed in both inert gas (nitrogen) and ambient conditions (air, 25% humidity). In order to understand differences between the two coating techniques in terms of metal layer formation and solvent evaporation, the more stable depositions as reported in § 4.3.2 were studied. However, in order to reduce the amount of samples, only the ink formulation diluted at 75% in volume of ethanol was considered in the further analysis, if it is not differently reported

Table 4.1. *Total electrical energy applied for the two approaches.*

Number of Pulses	Pulse Width (µs)	Voltage per Pulse (kV)	Total Electrical Energy (J)
1		2.7	1406.73
2	2000	2.3	2379.58
		2.7	

Table 4.1 presents the data obtained for samples prepared using the two approaches: it introduces the single or double steps, the settings related and the amount of energy delivered, calculated by Equation 2.8 and considering the steps sequence.

In **Figure 4.1** the different electrodes are illustrated just after the flash processing. In terms of metal copper layer formation, no differences can be observed by visually analyzing the samples: the films are fully converted to Cu, showing uniformity along the entire film.
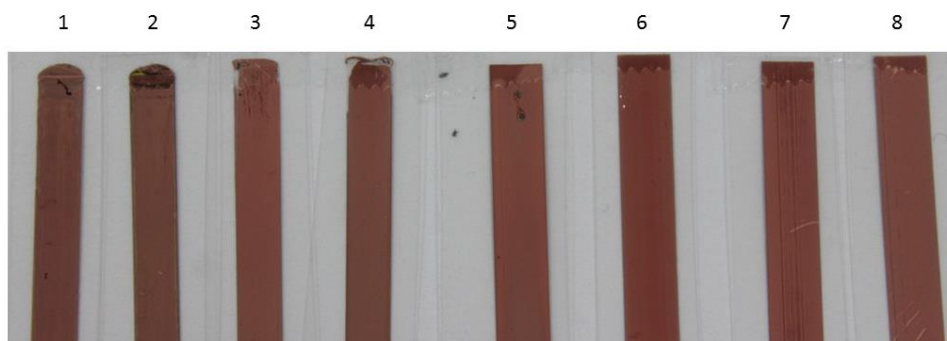
Figure 4.1. *The copper electrodes obtained with two different approaches. Slot-die coating 75% solvent dilution: (1) 1 step, (2) 2 steps. Slot-die coating 50% solvent dilution: (3) 1 step, (4) 2 steps. Inkjet printing 20 µm drop spacing: (5) 1 step, (6) 2 steps. Inkjet printing 25 µm: (7) 1 step, (8) 2 steps.*

Further evidence of this uniformity came from the SEM analysis: two samples are compared in **Figure 4.2**, referring to a different flash processing approach. **Figure 4.2a** illustrates a sample where a one-step approach was followed, while on in **Figure 4.2b** two flashing steps were applied the film. However, there are no main differences between the two structures.

(a) (b)
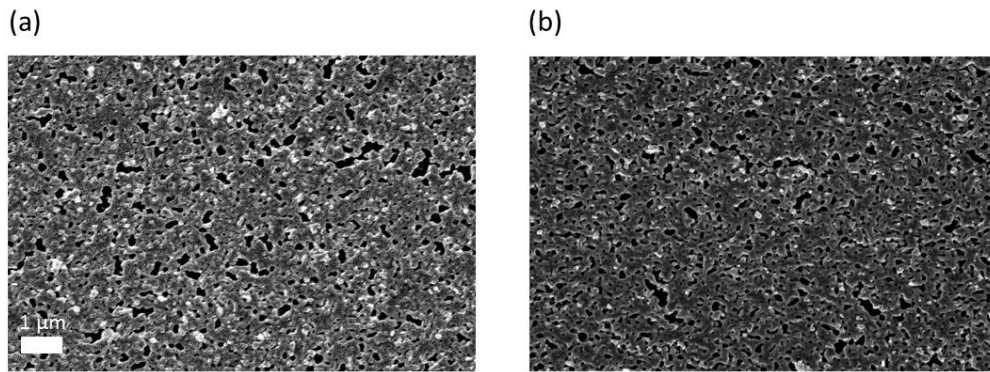
Figure 4.2. *The comparison between SEM images of two surfaces: (a) surface of a sample processed with one-step approach; (b) surface of a sample processed with two-step approach.*

The stability in inert environment was analyzed. Sheet resistance measurements were taken at different temporal intervals across 20 days, in order to evaluate possible variations in time. The electrical conductivity was not affected by any sort of reaction or film instability, due to the constant sheet resistance measured in the time range. The electrodes did not also show any difference in optical aspect, confirming what was demonstrated by the electrical analysis.

(a)

(b)
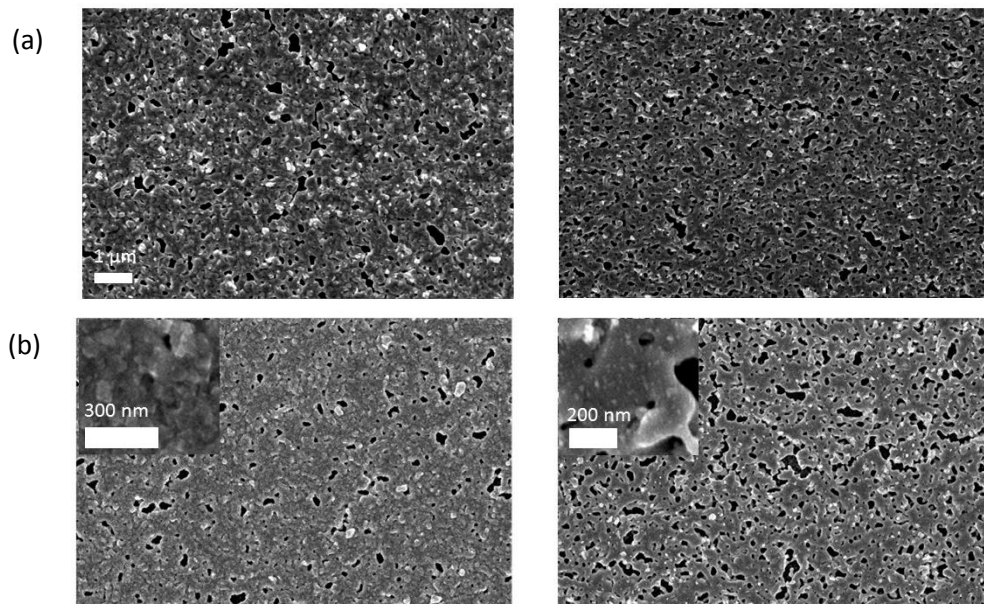
Figure 4.3. *Comparison between the surfaces of the samples treated in (a) nitrogen environment (one-step on the left and two-steps approach on the right); and (b) the ones of the electrodes exposed to oxygen (one-step approach on the left and two-steps process on the right). The scale bar is applied to all the main panels. In (b) a higher resolution of the surfaces is also reported.*

Obviously the presence of oxygen in the environment may affect the electrode, causing partial oxidation of Cu and therefore a detrimental effect on the electrode performances. The oxygen exposure could have been the key to understand a better approach than the other in terms of structural stability. For this reason stability tests in air were conducted. The SEM images of surfaces of copper electrodes are illustrated in **Figure 4.3**. The samples were obtained with the two different approaches and exposed to air and nitrogen. The layers that had been exposed to oxygen show a more wrinkled surface (**Figure 4.3a**) than the nitrogen counterparts, as shown in **Figure 4.3b**.

Moreover, the one-step flash processing sample is characterized by a higher oxidation rate of the surface, as it can be observed in **Figure 4.3b** (boxes). This is also confirmed by the optical aspect. As a matter of fact, after some days, the samples left in air started to visually look differently. The samples processed with the one pulse sequence seemed to react, showing a greenish color, due to re-oxidation of the copper, as shown in **Figure 4.4**.

Figure 4.4. *Samples exposed to oxygen: comparison between a one-step approach (top) and a two-steps process (down).*

However, even if an oxidized surface had been formed and the samples exposed to oxygen looked differently, it did not affect the electrical properties, which remain quite constant in the short period after the pulsed light exposure. Perhaps, this is due to the formation of a superficial oxidized layer that prevent the underneath layer to react. However, further in-time analysis will be treated more specifically.

After this investigation, a better processing did not really come out because no deep variations affected the electrodes in both approaches. Thus, in order to minimize the energy consumption, a single light pulse treatment was adopted as standard.

4.2 Multilayer Approach

A one layer deposition has been the only standard used until now. However, a multilayer approach could lead to a more stable flashed film, improving not only the mechanical, but also the electrical properties. As a matter of fact, the one-layer copper electrodes showed a very good conductivity, but they did not reach the values for bulk copper. Moreover, when bent, the structure did not sustain any kind of stress, leading to cracked film or delamination.

We hypothesized that adding more layers will help achieve a denser film that can show improved electrical and mechanical properties. The mechanical properties are directly related to the film thickness, to its morphology and to the residual stresses that remain in the film after the sintering process. These depend on many factors such as the deposition process, the equivalent temperature reached during sintering the mismatch in coefficient of thermal expansion between the film and the substrate. Furthermore, the electrical properties are related to the thickness and the morphology of the films: in fact, thicker and denser films have on average a lower sheet resistance because of the reduced amounts of defects, pores and grain boundaries that are detrimental for achieving high conductivity.

4.2.1 Multilayer Deposition

In order to obtain a multilayer electrode, two different approaches were adopted. First, two layers were coated on top of each other with just an air drying step between the first and the second deposition. Even if thick films were obtained, the samples showed poor adhesion and delamination problems during the sintering steps. As a matter of fact, when the sample is processed, only the superficial part is affected by high light intensity, due to the dark-brown color that absorbs most of the energy, while the underneath material receives only part of the emitted light. Thus, when the entire structure is flash processed, a non-optimal mechanism may be achieved: while the exposed surface could reach the sintering mechanism, the underlying material may be interested by a lower temperature, leading only to the solvent evaporation. Therefore, even if a superficial copper layer is formed, the solvent acts from below, leading to an intolerable stress for the electrode. Referring to the optimal settings considered in §3.4.2, a second layer deposition as defined so far showed the same issue for every technique.

The second approach was focused on the reduction of the stress mismatch between the two layers. As a matter of fact, processing the first layer with the pulsed light before the second deposition could have improved its stability, reducing the residual stress between it and the substrate, as well as between the two layers. With this in mind, an optimized sequence was performed, involving the following steps: i) deposition of the first layer with the optimal setting; ii) flash processing with a single light pulse; iii) deposition of a second

layer over the first one in the same conditions; iv) flash processing of the second layer. Even if the single layer did not show any problem, dealing with a process optimized in the previous sections, the results for the second deposition after the flash exposure were totally different. As a matter of fact, the same issue involved in the first approach, occurred also in this procedure: for most of the deposition the copper layer just delaminated, involving the entire film or part of it. As happened for the solution diluted up to 50% in volume of ethanol: in this case, only some spots were interested, but they were sufficient to make the electrodes not suitable for any sort of application, as shown in **Figure 4.5**.
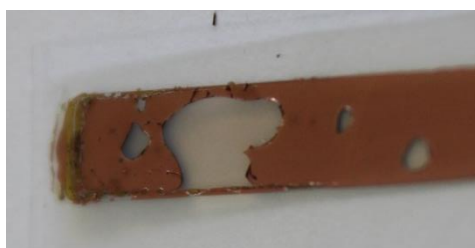
Figure 4.5. *Delaminated electrode after flash processing.*

The delamination process might be explained by a simple consideration: the higher solid content leaded to a thicker film, so the stress incurred during the copper film formation was too high, generating cracks in the structure.

Only the formulation with the highest solvent content showed an optimal stability, enabling a double-layer structure. This phenomena may be explained by different factors: the lower solid particle leaded to a thinner layer, where the residual stress in both step was low enough to not generate cracks. It has to be understood that the intense light exposure is a very fast process, which enables the formation of metal films in millisecond; so, the stresses that can affect the copper film are expected to be high due to the extremely fast temperature variation that occurs in this technique. A lower nanoparticle content may be only partially affected by the strain generation with respect a ticker layer. Furthermore, the second layer is deposited and flashed over an already sintered and stabilized copper film: the further deposition makes the overall electrodes more even, covering the structural defects of the underlying film and creating a very strong interphase. The more complex interconnections between the two depositions related to a thinner layer enhanced the stability of the final electrodes. Conversely, when the overall film is too thick, the interphase is less important and the residual stress becomes the main factor that leads to

delamination.

With this optimized procedure, it was possible to obtain multilayered, sintered films with up to 3 printed layers. **Table 4.2** summarizes the details and the results for the samples prepared with such multilayer approach. The energy supplied over the entire process, the relative sheet resistance and a rough stability analysis are described for single, double and triple layers.

Table 4.2. *Description of the main flash process parameters and main properties for one, two and three layers electrodes.*

Number of Layers	Setting for Single Pulse (μs, kV)	Total Electrical Energy Supplied (J)	Average Sheet Resistance (mΩ/□)	Rough Stability
1	2000 μs 2.7 kV	1406.73	400	Unstable
2		2813.46	170	Stable
3		4220.19	155	Stable

As expected, the double layer improved the electrode properties: the sheet resistance was roughly half of the one measured for the single layer. Furthermore, the stability increased because no cracks could be seen after a quick manual bending test, in contrast with the results obtained for the single deposition. However, for the triple layer the overall properties did not change enough to justify the extra processing step, in terms of solid and organic content deposited and energy consumption.

4.2.1.1 SEM Analysis

As the second layer improved the properties of the copper electrodes, a SEM analysis was performed in order to understand the reason of this enhancement.

In **Figure 4.6**, the single layer, the double and the triple layer surfaces are compared: it is possible to observe a higher level of percolation in the latter films (**Figure 4.6b, c**), which covers more uniformly the substrate. On the contrary, the former is more porous, with bigger gaps between Cu grains, as showed in **Figure 4.6a**.

This probably explains why the sheet resistance and the mechanical stability are drastically improved in the multilayer structures. However, the differences between them are not so evident, which can explain the similar properties, both mechanical and electrical ones. As a matter of fact, it can be observed in the higher resolution of the triple layer surface that a morphology similar to the one of the single layer exists: the third layer might have been

deposited over a denser film, not permeating the underlying material as the double configuration did. It can reasonably explain why the properties were not enhanced between the multilayer depositions: the denser structure assumed a more important role with respect the superficial film in terms of mechanical and electrical behavior.
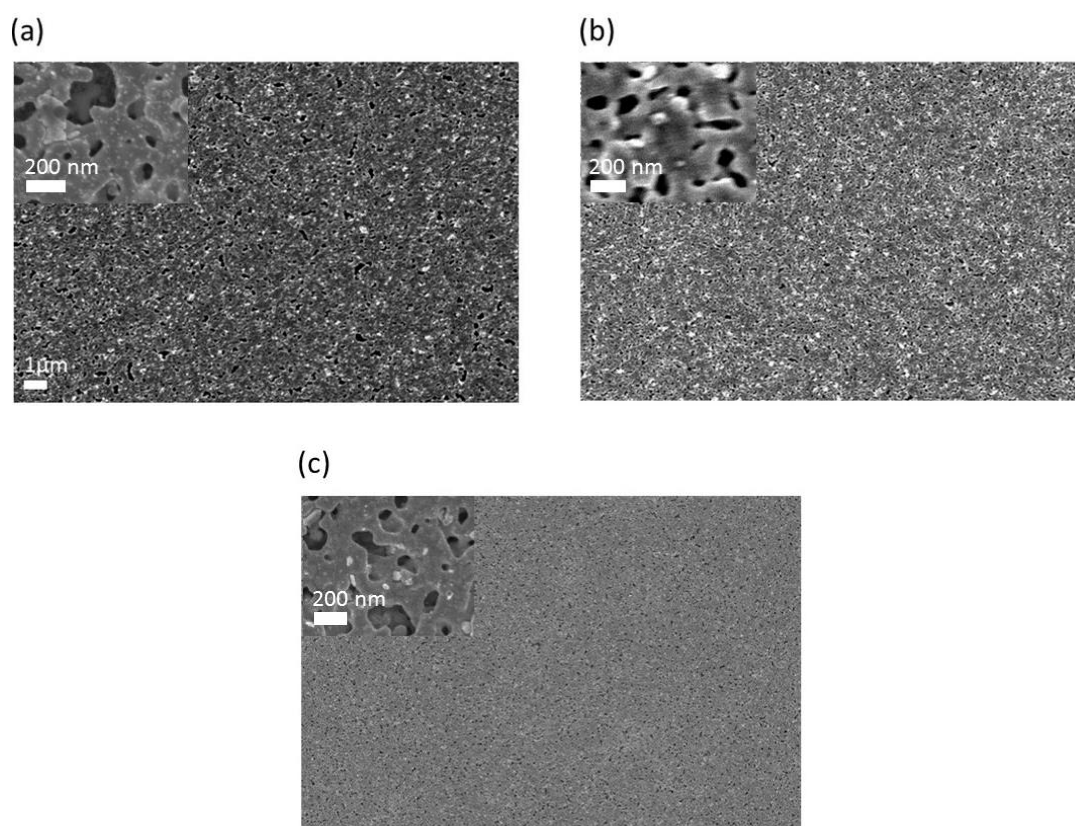
Figure 4.6. *The one, two and three layers structures are compared. They present different levels of porosity. The scale bars in the main figure is applied to all the main panels.*

From the SEM cross-section analysis of samples showed in **Figure 4.7,** it was possible to evaluate the thickness of the various samples. These were found to be 570, 210, 380 and 510 nm for the as deposited, one, two and three layered films, respectively. A comparison between the samples highlights their different morphology: the double and the triple layers show a denser, more interconnected structure. For these reasons both the electrical and the mechanical properties are enhanced.
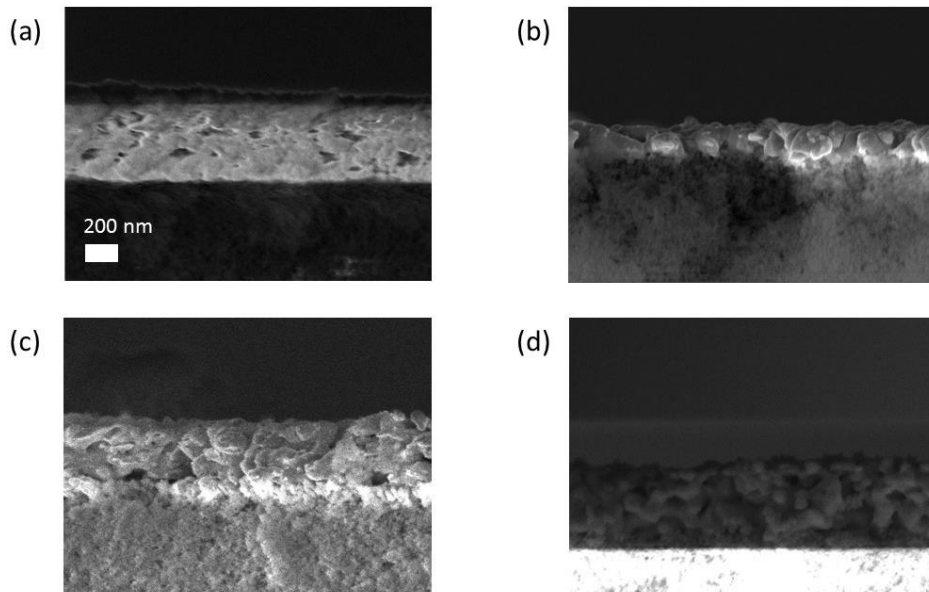
Figure 4.7. *Comparison between the thicknesses of different samples: as deposited (a); one layer flashed (b); double layer flashed (c) and triple layer flashed (d).*

Again, the cross-section analysis enables the sheet resistance, which is a surface measurement and depends on the thickness, to be related to the resistivity, which is a property of the material. Considering the sheet resistance values previously estimated and the thicknesses evaluated from the SEM images, the resistivity can be calculated through **Equation 3.1**. For the double layer the average sheet resistance is 170 mΩ/□, which multiplied for the average thickness, estimated in 380 nm, gives a resistivity of 6.46 μΩ·cm. This is slightly lower than the one of the single layer (6.8 μΩ·cm). The triple layer is instead characterized by 510 nm thickness, giving a resistivity of 7.65 μΩ·cm, comparable with the value obtained for one layer. Thus, the conductivity was $1.54 \cdot 10^7$ S/m for the double layer and $1.47 \cdot 10^7$ S/m for the triple, achieving 25% and 24% of the bulk copper conductivity, respectively.

The most performing sample is a double layer showing a sheet resistance of ~160 mΩ/□, achieving a conductivity of $1.64 \cdot 10^7$ S/m, which is 27.5% of the bulk copper conductivity. This result is compared in **Table 4.3** with outcomes of different works. Even if various techniques were used to deposit the starting material, in every case a flash processing of the sample is considered, allowing a comparison of the main parameters. Where possible, the sheet resistance values, thicknesses and resistivities are provided. Furthermore, the substrate where the material was deposited is indicated in order to give the tools to compare

the results obtained in different works for copper electrodes fabrication ([49-50]) ([51-52]) ([27, 40]) ([39])

Table 4.3. *Comparison between deposition technique, material, substrate, flashing conditions and copper electrodes properties of different works.*

Deposition Technique	Starting Material	Substrate	IPL	Film's Thickness	R_s (mΩ/□)	R (µΩ·cm)	Ref.
Mask Printing	Cu Formate [Cu(HCOO)$_2$]	Glass	230 V 1,4 ms 2.69 J/cm^2	650 nm	-	56	([49])
Spin Coating	CuO NPs	PI	1 Pulse 10 ms 12.5 J/cm^2	-	72	-	([50])
Spray Coating	Cu(NO$_3$)$_2$ to form CuO/Cu$_2$O	PET	1 Pulse 22.4 J/cm^2 2 ms	8 µm	120	96	([51])
Three roll Milling	Cu NPs + 5% Cu NWs	PI	1 Pulse 10 ms 12.5 J/cm^2	10 µm	-	22.77	([27])
Doctor Blading	Cu NPs 50% + Cu µPs	PI	1 Pulse 10 ms 12.5 J/cm^2	20 µm	-	80	([40])
Inkjet printing	CuO NPs (Metalon®)	PET	40 Pulses 0.58-1.5 ms	580-670 nm	150	9	([39])
Inkjet Printing	CuO NPs (Metalon®)	PET (Novele™)	3 Pulses 7.48 J/cm^2 10 ms	420 nm	121	5.5	([52])
Inkjet Printing	CuO NPs (Metalon®)	PET (Novele™)	1 Pulse 2 ms 2700 V	-	90	-	This work
Slot-Die	CuO NPs (Metalon®)	PET (Novele™)	1 Pulse 2 ms 2700 V	380 nm	160	6.1	This work

It can be observed that the slot-die coating achieved results comparable with the ones obtained with the inkjet printing, a technique with a higher deposition resolution and for which the ink is optimized (also in the case of best resistivity for inkjet printing, 5.54 µΩ·cm). Furthermore, it shows considerably better results if compared with other types of deposition. Moreover in this work, a slightly lower value of sheet resistance with the inkjet printing was achieved with respect to similar works.

4.3 Performance of Copper Electrodes

In the previous section, we demonstrated that an oxidant environment could affect the performances of the electrodes, because copper nanoparticles tend to oxidize when exposed to an atmosphere containing oxygen.

To better understand the variations on sheet resistance due to the oxidation process, tests on copper electrodes exposed at different atmospheres for different times were conducted. In order to achieve reliable measurements and avoid damaging the Cu electrodes, Silver contact pads were deposited by vacuum deposition at the edges of the copper line, as shown in **Figure 4.8**. Silver was chosen because it has a higher conductivity than copper and it is more resistant to oxidation. These silver pads provide optimal contact points for resistance measurements, while the Cu electrode is not damaged.

Figure 4.8. *The configuration of the sample utilized for evaluating the performance of the copper electrodes. The non-covered part is 5 cm long, while the silver edges are around 1.5-2 cm large.*

In addition to environmental stability, one of the most important characteristics for a flexible device is the capability to bend without losing functionality. For these reasons, we tested the sintered copper lines for different bending conditions. For proper measurement, the same silver contact pads shown in **Figure 4.8** were used.

For the performances evaluation, only the copper electrodes deposited with 75% in volume of ethanol was utilized, due to the fact that was possible to achieve a double layer structure without any problem with this kind of formulation.

4.3.1 Stability Tests

The stability tests were performed both in air at ambient conditions and in a nitrogen-filled glove box, with the latter mimicking the condition of an encapsulated system. In fact the nitrogen environment does not allow atmospheric agents such as oxygen and moisture to attack the electrode surface, altering is chemical nature. Similar situations have been previously reported, but in this case a better characterization of the surrounding environment was performed: temperature and relative humidity were reported for each air measurement, as well as moisture and oxygen traces for the measurements performed in nitrogen. In this way, a possible resistance variation can be explained by relation to environment changes.

Single and double layer were analyzed, investigating the different properties that can be achieved with the thicker, denser and more conductive coatings. The resistance variation for such samples exposed to the two environments for several days is reported in **Table 4.4**.

Table 4.4. *The resistance variation over 21 days is reported for single layer (1L) and double layer (2L) in nitrogen and air, considering the main environment properties.*

	Nitrogen				Air			
Day	**1L (Ω)**	**2L (Ω)**	**H_2O/O_2 (ppm)**	**Temperature (°C)**	**1L (Ω)**	**2L (Ω)**	**Relative Humidity (%)**	**Temperature (°C)**
1	6.3	2.2	0.3/3.66	26.9	5.4	2.2	36.5	20.2
2	6.3	2.2	0.2/2.89	26.8	5.4	2.4	46	22
3	6.4	2.3	0.3/5.47	27.8	5.6	2.5	47.6	22.2
4	6.3	2.2	0.2/4.00	29.5	5.5	2.5	46.6	22.7
5	6.3	2.4	0.2/2.63	26.6	5.5	2.5	36	22.2
9	6.5	2.4	0.15/3.35	24.5	5.7	2.5	50	20.6
10	6.4	2.4	0.2/2.85	30.8	5.9	2.6	41.4	21.5
12	6.4	2.5	0.2/2.4	27.4	6.1	2.6	35.8	22.9
21	6.4	2.5	0.2/3.3	25.2	6.6	2.6	44.1	21.9

There is a negligible resistance variation in time for all electrodes, especially when kept under nitrogen atmosphere. A slight increase in resistance is observed for the samples

exposed to air, as expected, but the resistance increased only by ~20%. This is a very good result, considering the high reactivity of nano-sized copper with oxygen. We therefore demonstrated good stability of our printed electrode in air without any type of encapsulation. If some oxidation occurs, it might be only superficial and it does not affect the bulk of the sintered films. Long term stability tests are still in progress at this time.

4.3.2 Bending Tests

Bending tests were performed using a similar approach to that used in the previous section. Inert and oxidant environments were tested, as well as single and double layer films. This investigation is of paramount importance for a flexible device, which is designed to reach a certain bending angle without changing its properties.

There are two types of stress that can be generated within the copper electrodes, depending on the type of bending test that is performed. In the outer bending test the sample is bent in a convex shape (∩), inducing a tensile strain on the copper film. Differently, in the inner bending test the sample is bent in a concave shape (∪), generating a compressive stress. Obviously, the nature of the strain is different, leading to opposite response by the layer, but the nominal bending strain ε of the film can be calculated in both cases by the following **Equation 4.1** ([53]):

$$\varepsilon \cong \frac{h_f + h_s}{2r} \ .$$
(4.1)

Where h_f and h_s are the respective thicknesses of the film and the substrate in mm, and r the bending radius in mm.

The tests were performed manually, keeping both the curvature radius constant. A standard was defined: a fixed post with a known bending radius of 2.5 mm was used as a rigid support around which the copper electrodes were bent. The substrate was curved until the edges were parallel. The bending frequency was also kept constant, with a bending cycle every 2 second, while the resistance was measured every 5 cycles in order to obtain enough experimental points for a total of 100 cycles. We used only the outer bending test condition, which generates a tensile strain. An inner bending test would have required to place the layer surface in contact with the rigid support, with the consequence of possible scratch and friction problems, which will have affected the resistance measurements.

In **Figure 4.9**, the resistance variation calculated as R/R_0, where R is the experimental value (in Ω) after a specific number of cycles and R_0 is the initial resistance (in Ω), is reported as a function of the bending cycles. A comparison between nitrogen and air environment was performed for the single layer (**Figure 4.9a**), as well as for the double one (**Figure 4.9b**), in order to evaluate the response of different structures and different

environments under a bending test.

The fact that the curvature radius and the bending frequency were kept constant for all conditions, and considering the thickness for the same type of deposition (single or double layer) constant, enabled to compare the effect of different environments on the electrode resistance during a bending test. Based on the previous considerations, the bending strain for similar films was roughly constant in both situations, estimated in 0.068 for the single layer and 0.088 for the double layer.
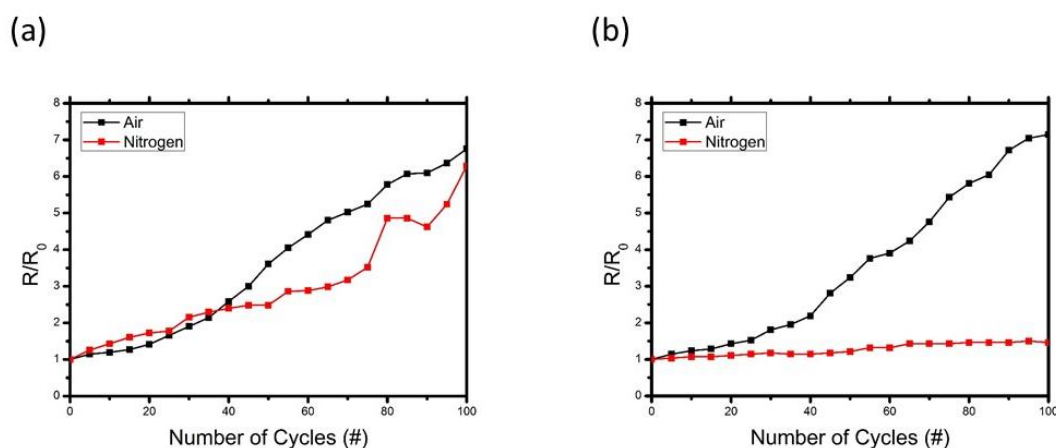
Figure 4.9. *The behavior of a single layer (a) and a double layer (b) under bending tests in different environments.*

The single layer shows a similar trend in both air and nitrogen atmosphere: the oxidant environments did not affect in particular way the electrical properties of the copper film, which are mainly affected by the mechanical stresses induced by the bending tests.

Differently, the resistance of the double layer remained practically constant in nitrogen atmosphere, while in air a six-fold increase in resistance was observed. In this case, the oxygen might have assumed an important role, causing the oxidation not only of the surface but also of the bulk of the electrode. Further analyses are in progress in order to understand such behavior. The double layer bent in a nitrogen environment showed a resistance variation of only 18%, comparable with other studies, where a thicker film (10μm) and a larger radius (7 mm) were investigated, involving a lower stress ([27]).

4.3.2.1 SEM Analysis

Once more, the SEM analysis can firmly support the results previously obtained. An investigation of electrodes' surface was performed before and after the bending test, in

order to study the structure variations due to the application of a tensile stress. **Figure 4.10** illustrates the comparison between the two different situations of a single layer electrode. It can be observed that a cracking process occurred during the bending test (**Figure 4.10b**): this loss of integrity of the electrode explains the reduction on conductivity that was observed.
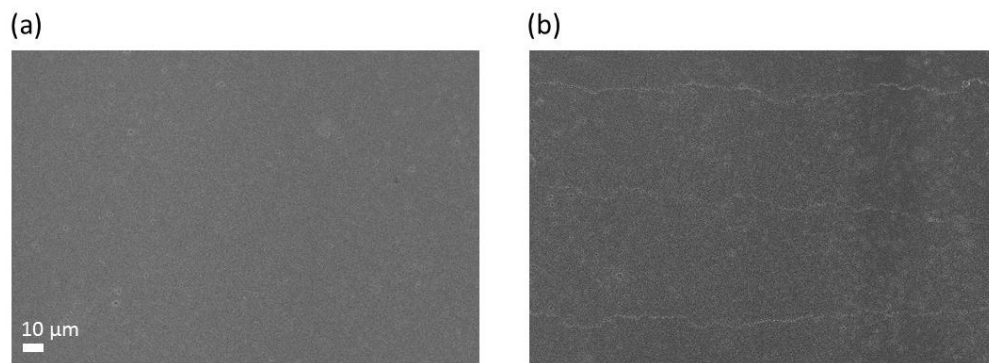
Figure 4.10. *The surfaces of a single layer before bending test (a) and after (b) are illustrated.*
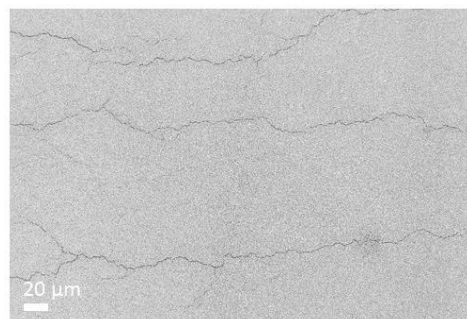
Figure 4.11. *The surfaces of a double layer after bending test is reported.*

Similarly, in **Figure 4.11**, the SEM images of the double layer after bending is shown: the structure is not uniform, characterized by multiple cracks that surely influenced the average resistance, leading to a reduced conductivity. The uniformity was in fact compromised.

However, while in the single layer the cracks are all parallel between each other and orthogonal to the electrode axis, in the double deposition the cracks are branched. This difference on the cracked structures may explain the different behavior during the bending

test. While the one-layer film is characterized by continuous cracks, which traverse the entire width of the electrode, in the double layer the branched morphology of the cracks allows continuous copper pathways to exist across the entire electrode, affording a more stable configuration.

Thus, in the single layer the conductivity has been reduced by mechanical discontinuity, not allowing the electric current to find a proper path along the entire electrode. This process is partially independent from the oxidant environment and the similar behavior in both situations is justified. In the double layer, the electric current could pass properly through the electrode, but because of the more complex cracked structure a larger exposed inner surface made the sample more susceptible to oxidation. This explains the different trend in nitrogen and air for the two layered copper electrodes.

Summary

In this chapter we explored the deposition of multi-layered films to achieve thickness controlled copper electrodes. These were assessed under different environmental and bending conditions. It was found that a bi-layered structure fabricated by the deposition of a single copper oxide layer, which was flashed, and this process repeated, provided the optimal conditions for conductivity, environmental stability and structural stability.

Chapter 5

Conclusion

In this thesis the depositions of copper oxide nanoparticle inks on plastic substrates has been successfully developed and thoroughly investigated. Furthermore, great outcomes derived from the intense pulsed light process necessary to reduce the copper oxide to metallic copper and allow the nanoparticle to melt and sinter, creating high performance copper electrode.

The investigation started from the optimization of the two coating techniques used to deposit the nanoparticle solution: while this process was fairly easy for the inkjet printing, because the ink is especially designed for this technology, it resulted challenging for the slot-die coating. The optimal deposition was achieved with a dilution in ethanol up to 75% in volume of the original ink. This allowed to avoid clogging problems and aggregation of nanoparticles due to a high solid content, and also to reduce the viscosity for a more uniform deposition. This success is magnified by the absence of experimental studies performed for nanoparticle inks associated to a slot-die deposition. The capability to print with high reliability multiple stripes of copper oxide films is a great achievement for slot-die technology.

The intense pulsed light process was a fundamental part in the fabrication of copper electrodes and so most of the efforts were directed towards its understanding in order to develop a deep knowledge of this mechanism. Several studies were conducted investigating the effects of different light intensities on the chemical nature and morphological structure of the deposited films. The different steps occurring during the light-induced transformation of copper oxide to metallic copper were successfully isolated and fully characterized. Many different analyses were performed in order to understand this mechanism: the CuO nanoparticle did not show any kind of transformation if exposed to low energy light pulses; however, for an intermediate light intensity, CuO was partially reduced to Cu_2O. The final transition to Cu was possible only increasing the energy supplied to the films. It is also interesting to observe that precise pulse conditions were identified where only the chemical reduction to Cu but not the sintering occurred. Visible transmission, FTIR, XRD and SEM analysis enabled to verify the excellent control of the reaction.

At 2.7 kV and 2000 μs (flash sintering parameters), corresponding to a supplied electrical energy of ~1400 J, fully sintered copper electrodes were achieved. The sheet resistances that characterized the copper films varied along the different solutions deposited: for slot-die the most performing values obtained were 350 mΩ/□ and 165 mΩ/□, for solution diluted up to 75% and 50% in volume of ethanol respectively. With the inkjet printing, a sheet resistance similar to the one achieved by the ink production company was obtained, with a lowest value of 90 mΩ/□.

However, in order to enhance the overall properties, a multilayer approach was also developed. The idea was to increase the conductivity and the mechanical properties of the electrodes by achieving a denser coating. However, a multilayer structure was possible only with the ink formulation diluted at 75% in volume of solvent and deposited with slot-die: the double layer electrode was proven to be the most performing in terms of properties and in terms of material and energy consumption.

Stability tests were performed in order to verify this concept: in-time investigations were conducted in air and nitrogen. This enabled to demonstrate an optimal stability of the copper films not only in nitrogen environments, which mimic an encapsulation process, but also in air, considering the tendency of copper to oxidize. Moreover, bending tests were performed in similar conditions with a bending radius of 2.5 mm over a 100 cycles, highlighting an optimal stability to bending stresses as well. Eventually, even if the double layer structure as obtained showed higher conductivity, it was characterized by a better mechanical stability, leading to superior overall behavior.

The best electrode showed a resistivity of 6.1 μΩ·cm, which leaded to a conductivity of $1.64 \cdot 10^7$ S/m achieving 27.5% of the bulk copper conductivity. Moreover, it was characterized by a resistance variation of only ~20% in nitrogen within 20 days, , while the resistance increase was only of 18% during the bending test in nitrogen.

Based in these results, additional investigation may be introduced: the deposition with slot-die could be modified using different dilutions or formulations, in order to understand if there is a possibility to further improve the deposition process. Moreover, a better knowledge of the phenomena involved could help obtaining experimental relations between the several parameters: a connection between the ink pumped and the thickness of the film deposited might make the difference optimizing the electrode's properties.

Moreover, several investigations may be conducted also in the flash processing, trying to vary the energy not only through the voltage applied but also considering all the other parameters, such as pulse width, number of pulses and period between each pulse. This can help comprehending the effects on the deposited films in terms of solvent drying and nanoparticle transformation.

Eventually, the fabrication of a more complex device, involving other types of flexible applications such as OLEDs or solar cells, may be the final achievements that might close a cycle started with this thesis. The possibility to integrate in a real application the knowledge on the electrodes fabrication achieved in this work is not so far, as shown in **Figure 5.1**, where an advanced pattern is obtained with inkjet printing.

(a)   (b)
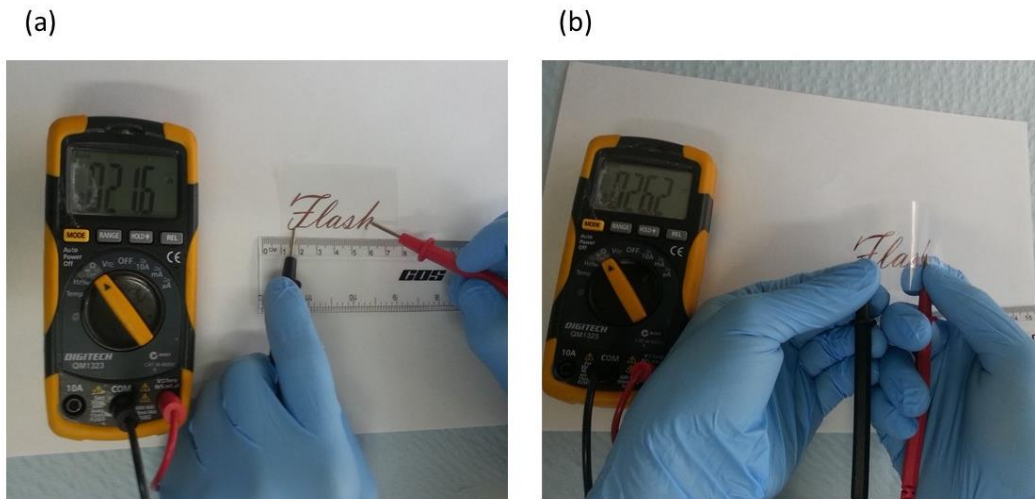
Figure 5.1. *Pattern obtained by inkjet printing and flashed with standard condition: (a) shows the electrical properties after flash processed and (b) demonstrates the capability to be still conductive also after bending.*

However, the possibility to modify the customized 3D printer changing the slot-die coating head with a needle head seems much more interesting, in order to obtain a finer patterning with respect to the technique adopted. In addition to minor mechanical changes, this solution may become very competitive with respect to inkjet technology, due to the simpler instrumentation and the less issues related to the ink deposition.

Nomenclature

A	$=$	Absorbance (-)
c	$=$	concentration of the solid material (g/cm^3)
c_i	$=$	heat capacity (J/K)
c_l	$=$	speed of light (m/s)
d	$=$	thickness of the film (cm)
E_λ	$=$	energy associated to a specific wavelength (J)
E	$=$	electrical energy related to the light pulse (J)
f	$=$	flow rate (cm^3/min)
f_p	$=$	proportionality factor (-)
g	$=$	gap distance (cm)
h	$=$	Planck constant (J·s)
h_f	$=$	film thickness in flash processing analysis (mm)
h_s	$=$	substrate thickness in flash processing analysis (mm)
I_0	$=$	intensity of incidental light (-)
I_1	$=$	intensity of transmitted light (-)
k	$=$	empirical constant (s)
k_i	$=$	thermal conductivity (W/m·K)
k_p	$=$	pick-out ratio (-)
k_λ	$=$	copper attenuation coefficient (1/m)
l	$=$	thickness of the sample (m)
l_s	$=$	syringe stroke value in printing software (mm)
l_0	$=$	syringe stroke (mm)
N_d	$=$	number of droplet delivered per unit of area (cm^{-2})
P	$=$	amount of ink dispensed by the printing software (µl)
R	$=$	resistivity (Ω·cm)
R_s	$=$	sheet resistance (Ω/□)
r	$=$	bending radius (mm)
S	$=$	web speed (cm/min)
T	$=$	transmittance (-)
T_g	$=$	glass transition temperature (°C)
T_{max}	$=$	maximum process temperature (°C)

t	=	light pulse time (μs)
t_p	=	duration of the flash process (μs)
t_S	=	thickness of the copper layer (cm)
V	=	voltage (V)
V_d	=	droplet volume (cm^3)
V_{screen}	=	theoretical paste volume of the screen (cm^3)
V_o	=	syringe volume (μl)
x_f	=	thickness of the film (cm)
x_i	=	thickness of a generic film (m)
x_s	=	thickness of the substrate (cm)

Greek Letters

α	=	empirical constant (-)
Δ	=	variation between the initial and the final state (-)
ε	=	nominal bending strain (-)
λ	=	wavelength (m)
ρ	=	density of material (g/cm^3)
τ_f	=	thermal equilibration time of the film (s)
τ_i	=	generical equilibration time (s)
τ_s	=	thermal equilibration time of the substrate (s)
ω	=	angular velocity (m/s)

Acronyms

BHJ	=	bulk-heterojunctions
CSIRO	=	Commonwealth Scientific and Industrial Research Organization
CVD	=	chemical vapor deposition
CTE	=	coefficient of thermal expansion
DMP	=	Dimatix Material Printer
DOD	=	drop-on-demand
FPCs	=	Flexible and Printed Circuits
FPEs	=	Flexible and Printed Electronics
FTIR	=	Fourier transmission infrared
GIZO	=	gallium indium zinc oxide

IPL	=	intense pulsed light
LCDs	=	liquid crystal displays
LPCVD	=	low-pressure chemical vapor deposition
OLEDs	=	organic light-emitting diodes
PC	=	poly carbonate
PCB	=	Printed Circuit Board
PCO	=	polycyclic olefin
PDMS	=	polydimethylxiloxone
PECVD	=	plasma-enhanced chemical vapor deposition
PEDOT:PSS	=	3, 4-polyethylenedioxythiopene-polystyrene sulfonic acid
PEN	=	polyethylene naphthalate
PES	=	polyethersulphone
PET	=	polyethylene terephthalate
PI	=	polyimide
R2R	=	Roll-to-roll
SEM	=	scanning electron microscope
SOG	=	spin on glass
TFTs	=	thin film transistors
UV	=	ultraviolet
XRD	=	X-ray diffraction

Bibliography

1.   www.flextech.org. (accessed 28/06/2015).
2.   www.semi.org. (accessed 24/06/2015).
3.   www.IDTechEx.org. (accessed 28/06/2015).
4.   Linz, T.; Kallmayer, C.; Aschenbrenner, R.; Reichl, H. In *Fully untegrated EKG shirt based on embroidered electrical interconnections with conductive yarn and miniaturized flexible electronics*, Wearable and Implantable Body Sensor Networks, 2006. BSN 2006. International Workshop on, 3-5 April 2006; 2006; pp 4 pp.-26.
5.   www.flexiblecircuit.com. (accessed 29/06/2015).
6.   www.allflexinc.com. (accessed 27/06/2015).
7.   Khan, S.; Lorenzelli, L.; Dahiya, R. S., Technologies for Printing Sensors and Electronics Over Large Flexible Substrates: A Review. *Sensors Journal, IEEE* **2015,** *15* (6), 3164-3185.
8.   Perelaer, J.; Smith, P. J.; Mager, D.; Soltman, D.; Volkman, S. K.; Subramanian, V.; Korvink, J. G.; Schubert, U. S., Printed electronics: the challenges involved in printing devices, interconnects, and contacts based on inorganic materials. *Journal of Materials Chemistry* **2010,** *20* (39), 8446-8453.
9.   Sun, Y.; Rogers, J. A., Inorganic Semiconductors for Flexible Electronics. *Advanced Materials* **2007,** *19* (15), 1897-1916.
10.   Kim, D. S.; Khan, A.; Rahman, K.; Khan, S.; Kim, H. C.; Choi, K. H., Drop-on-Demand Direct Printing of Colloidal Copper Nanoparticles by Electrohydrodynamic Atomization. *Materials and Manufacturing Processes* **2011,** *26* (9), 1196-1201.
11.   Chiang, C. K.; Fincher, C. R.; Park, Y. W.; Heeger, A. J.; Shirakawa, H.; Louis, E. J.; Gau, S. C.; MacDiarmid, A. G., Electrical Conductivity in Doped Polyacetylene. *Physical Review Letters* **1977,** *39* (17), 1098-1101.
12.   Choi, M.-C.; Kim, Y.; Ha, C.-S., Polymers for flexible displays: From material selection to device applications. *Progress in Polymer Science* **2008,** *33* (6), 581-630.
13.   Niu, X. Z.; Peng, S. L.; Liu, L. Y.; Wen, W. J.; Sheng, P., Characterizing and Patterning of PDMS-Based Conducting Composites. *Advanced Materials* **2007,** *19* (18), 2682-2686.
14.   Dahiya, R. S.; Adami, A.; Collini, C.; Lorenzelli, L., Fabrication of single crystal silicon micro-/nanostructures and transferring them to flexible substrates. *Microelectronic Engineering* **2012,** *98* (0), 502-507.
15.   Nomura, K.; Ohta, H.; Ueda, K.; Kamiya, T.; Hirano, M.; Hosono, H., Thin-Film Transistor Fabricated in Single-Crystalline Transparent Oxide Semiconductor. *Science* **2003,** *300* (5623), 1269-1272.
16.   Cheng, I. C.; Wagner, S., Overview of Flexible Electronics Technology. In *Flexible Electronics*, Wong, W.; Salleo, A., Eds. Springer US: 2009; Vol. 11, pp 1-28.
17.   Plichta, A.; Weber, A.; Habeck, A., Ultra Thin Flexible Glass Substrates. *MRS Online Proceedings Library* **2003,** *769*, null-null.
18.   Cheng, I. C.; Kattamis, A.; Long, K.; Sturm, J. C.; Wagner, S., Stress control for overlay registration in a-Si:H TFTs on flexible organic-polymer-foil substrates. *Journal of the Society for Information Display* **2005,** *13* (7), 563-568.
19.   Afentakis, T.; Hatalis, M.; Voutsas, A. T.; Hartzell, J., Design and fabrication of

high-performance polycrystalline silicon thin-film transistor circuits on flexible steel foils. *Electron Devices, IEEE Transactions on* **2006,** *53* (4), 815-822.

20.   Ma, E. Y.; Wagner, S., Amorphous silicon transistors on ultrathin steel foil substrates. *Applied Physics Letters* **1999,** *74* (18), 2661-2662.

21.   Steimle, J., Printed electronics for human-computer interaction. *interactions* **2015,** *22* (3), 72-75.

22.   Krebs, F. C., Fabrication and processing of polymer solar cells: A review of printing and coating techniques. *Solar Energy Materials and Solar Cells* **2009,** *93* (4), 394-412.

23.   Søndergaard, R.; Hösel, M.; Angmo, D.; Larsen-Olsen, T. T.; Krebs, F. C., Roll-to-roll fabrication of polymer solar cells. *Materials Today* **2012,** *15* (1–2), 36-49.

24.   https://www.novacentrix.com/sites/default/files/files/Metalon%20ICI-002HV%20data%20sheet%281%29.pdf. (accessed 29/06/2015).

25.   Park, B. K.; Kim, D.; Jeong, S.; Moon, J.; Kim, J. S., Direct writing of copper conductive patterns by ink-jet printing. *Thin Solid Films* **2007,** *515* (19), 7706-7711.

26.   Kim, D.; Moon, J., Highly Conductive Ink Jet Printed Films of Nanosilver Particles for Printable Electronics. *Electrochemical and Solid-State Letters* **2005,** *8* (11), J30-J33.

27.   Joo, S.-J.; Park, S.-H.; Moon, C.-J.; Kim, H.-S., A Highly Reliable Copper Nanowire/Nanoparticle Ink Pattern with High Conductivity on Flexible Substrate Prepared via a Flash Light-Sintering Technique. *ACS Applied Materials & Interfaces* **2015,** *7* (10), 5674-5684.

28.   Park, S.-H.; Kim, H.-S., Flash light sintering of nickel nanoparticles for printed electronics. *Thin Solid Films* **2014,** *550* (0), 575-581.

29.   Yung, K. C.; Gu, X.; Lee, C. P.; Choy, H. S., Ink-jet printing and camera flash sintering of silver tracks on different substrates. *Journal of Materials Processing Technology* **2010,** *210* (15), 2268-2272.

30.   Hong, S.; Lee, J.; Kang, H.; Lee, K., Slot-die coating parameters of the low-viscosity bulk-heterojunction materials used for polymer solarcells. *Solar Energy Materials and Solar Cells* **2013,** *112* (0), 27-35.

31.   Vak, D.; Hwang, K.; Faulks, A.; Jung, Y.-S.; Clark, N.; Kim, D.-Y.; Wilson, G. J.; Watkins, S. E., 3D Printer Based Slot-Die Coater as a Lab-to-Fab Translation Tool for Solution-Processed Solar Cells. *Advanced Energy Materials* **2015,** *5* (4), n/a-n/a.

32.   Shen, W.; Zhang, X.; Huang, Q.; Xu, Q.; Song, W., Preparation of solid silver nanoparticles for inkjet printed flexible electronics with high conductivity. *Nanoscale* **2014,** *6* (3), 1622-1628.

33.   Cui, X.; Boland, T., Human microvasculature fabrication using thermal inkjet printing technology. *Biomaterials* **2009,** *30* (31), 6221-6227.

34.   Setti, L.; Piana, C.; Bonazzi, S.; Ballarin, B.; Frascaro, D.; Fraleoni-Morgera, A.; Giuliani, S., Thermal Inkjet Technology for the Microdeposition of Biological Molecules as a Viable Route for the Realization of Biosensors. *Analytical Letters* **2004,** *37* (8), 1559-1570.

35.   Zhang, T.; Wang, X.; Li, T.; Guo, Q.; Yang, J., Fabrication of flexible copper-based electronics with high-resolution and high-conductivity on paper via inkjet printing. *Journal of Materials Chemistry C* **2014,** *2* (2), 286-294.

36.   Allen, M. L.; Aronniemi, M.; Mattila, T.; Alastalo, A.; Ojanperä, K.; Suhonen, M.; Seppä, H., Electrical sintering of nanoparticle structures. *Nanotechnology* **2008,** *19* (17), 175201.

37.   Abbel, R.; van Lammeren, T.; Hendriks, R.; Ploegmakers, J.; Rubingh, E. J.; Meinders, E. R.; Groen, W. A., Photonic flash sintering of silver nanoparticle inks: a fast and convenient method for the preparation of highly conductive structures on foil. *MRS*

Communications **2012,** *2* (04), 145-150.

38.   Schroder, K. A., Mechanisms of Photonic Curing™: Processing High Temperature Films on Low Temperature Substrates. *NSTI* **2011,** *Nanotech 2011 Vol. 2* 220 - 223.

39.   Paquet, C.; James, R.; Kell, A. J.; Mozenson, O.; Ferrigno, J.; Lafrenière, S.; Malenfant, P. R. L., Photosintering and electrical performance of CuO nanoparticle inks. *Organic Electronics* **2014,** *15* (8), 1836-1842.

40.   Joo, S.-J.; Hwang, H.-J.; Kim, H.-S., Highly conductive copper nano/microparticles ink via flash light sintering for printed electronics. *Nanotechnology* **2014,** *25* (26), 265601.

41.   Park, S.-H.; Jang, S.; Lee, D.-J.; Oh, J.; Kim, H.-S., Two-step flash light sintering process for crack-free inkjet-printed Ag films. *Journal of Micromechanics and Microengineering* **2013,** *23* (1), 015013.

42.   Papadimitropoulos, G.; Vourdas, N.; Vamvakas, V. E.; Davazoglou, D., Deposition and characterization of copper oxide thin films. *Journal of Physics: Conference Series* **2005,** *10* (1), 182.

43.   Innocenzi, P.; Falcaro, P.; Grosso, D.; Babonneau, F., Order−Disorder Transitions and Evolution of Silica Structure in Self-Assembled Mesostructured Silica Films Studied through FTIR Spectroscopy. *The Journal of Physical Chemistry B* **2003,** *107* (20), 4711-4717.

44.   Almeida, R. M.; Pantano, C. G., Structural investigation of silica gel films by infrared spectroscopy. *Journal of Applied Physics* **1990,** *68* (8), 4225-4232.

45.   Vallée, C.; Goullet, A.; Granier, A.; van der Lee, A.; Durand, J.; Marlière, C., Inorganic to organic crossover in thin films deposited from O2/TEOS plasmas. *Journal of Non-Crystalline Solids* **2000,** *272* (2–3), 163-173.

46.   Doroshenko, I.; Pogorelov, V.; Sablinskas, V., Infrared Absorption Spectra of Monohydric Alcohols. *Dataset Papers in Chemistry* **2013,** *2013*, 6.

47.   Kung, K. H. S.; Hayes, K. F., Fourier transform infrared spectroscopic study of the adsorption of cetyltrimethylammonium bromide and cetylpyridinium chloride on silica. *Langmuir* **1993,** *9* (1), 263-267.

48.   Maria Chong, A. S.; Zhao, X. S., Functionalization of SBA-15 with APTES and Characterization of Functionalized Materials. *The Journal of Physical Chemistry B* **2003,** *107* (46), 12650-12657.

49.   Araki, T.; Sugahara, T.; Jiu, J.; Nagao, S.; Nogi, M.; Koga, H.; Uchida, H.; Shinozaki, K.; Suganuma, K., Cu Salt Ink Formulation for Printed Electronics using Photonic Sintering. *Langmuir* **2013,** *29* (35), 11192-11197.

50.   Hwang, H.-J.; Chung, W.-H.; Kim, H.-S., In situ monitoring of flash-light sintering of copper nanoparticle ink for printed electronics. *Nanotechnology* **2012,** *23* (48), 485205.

51.   Dharmadasa, R.; Jha, M.; Amos, D. A.; Druffel, T., Room Temperature Synthesis of a Copper Ink for the Intense Pulsed Light Sintering of Conductive Copper Films. *ACS Applied Materials & Interfaces* **2013,** *5* (24), 13227-13234.

52.   Kang, H.; Sowade, E.; Baumann, R. R., Direct Intense Pulsed Light Sintering of Inkjet-Printed Copper Oxide Layers within Six Milliseconds. *ACS Applied Materials & Interfaces* **2014,** *6* (3), 1682-1687.

53.   Eun, K.; Chon, M.-W.; Yoo, T.-H.; Song, Y.-W.; Choa, S.-H., Electromechanical properties of printed copper ink film using a white flash light annealing process for flexible electronics. *Microelectronics Reliability* **2015,** *55* (5), 838-845.

Ringraziamenti

In questo ultimo sforzo voglio allontanarmi da quella che é stata la mia compagna di viaggio fino ad ora, la lingua inglese. Un pó per fatica, avendo appena affrontato un volo di 24 ore che mi ha riportato in patria dopo questa magnifica esperienza, ma soprattutto perché so che non riuscirei ad esprimere al meglio i miei ringraziamenti a quelle persone davvero speciali che mi hanno sostenuto in questo lungo viaggio. É stata un'esperienza fantastica, un'occasione non solo per vedere l'altra parte del mondo ma anche per conoscere, apprendere e imparare moltissime cose nuove, mettendo le basi per quello che saró un domani. Non c'é un ordine che posso dare nel ringraziare le molte persone che hanno preso parte insieme a me a questo progetto, perché tutte hanno avuto il loro ruolo fondamentale, se quindi ne daró uno é perché comunque da qualche parte dovró pur cominciare.

La prima persona cui tengo veramente ringraziare é Karla, una compagnia di viaggio ma soprattutto di vita, che mi ha sempre sostenuto e tirato avanti, anche nei momenti piú difficili e stressanti. A Lei che é sempre stata li a tirarmi su il morale ed incoraggiarmi, che ha condiviso con me le gioie e i dolori quotidiani di questa esperienza australiana.

Un sentito Grazie va anche ad Enrico, quello che piú di ogni altro in vita mia é stato un mentore per me, aiutandomi quotidianamente non solo ad affrontare questo progetto, ma dimostrandomi soprattutto come si possa dare tanto ad una persona senza ricevere niente in cambio. Una presenza costante, una persona fantastica, una Sicurezza. Un ringraziamento speciale va anche ai miei genitori, che mi hanno supportato moralmente e finanziariamente in questa esperienza, i quali per primi insieme a Karla hanno insistito per cercare la possibilitá di una Tesi in Australia. Come poi non ringraziare le persone che l'hanno resa realtá, il Prof Martucci e Jack (you can do it!), che insieme hanno preparato il terreno per questo magnifico progetto, o che l'hanno resa divertente, ricordando Joel.

Un grazie a tutte quelle persone che sono state una presenza costante e che nonostante i 10000 km di distanza non mi hanno mai fatto mancare il loro supporto. Loris, Luca, Ascanio, Alberto, Luca, Brombe, le chiamate whatsapp e quelle skype. Non dimenticheró mai le connessioni saltate! Con questa Tesi finiscono anche i miei 5 anni di universitá (si spera!) e quindi colgo l'occasione di salutare tutte quelle persone che li hanno condivisi con me, per intero o in parte, ma che hanno comunque lasciato un segno. Anita, Lucrezia, Dario, Zac.. e tanti mazzi di carte! Insomma ringrazio tutti quelli che hanno avuto a che fare con me, dicendo che ci sará sempre tempo per una birra insieme! Cheers, **Francesco**.